Global Reactor Effects on Homogenized Parameters for Nodal Diffusion Theory Analyses of Light Water Reactors

A Thesis
Presented to
The Academic Faculty

by

James Walter Malo

In Partial Fulfillment
of the Requirements for the Degree
Doctor of Philosophy
in Nuclear Engineering

Georgia Institute of Technology
March 1994

Global Reactor Effects on Homogenized Parameters for Nodal Diffusion Theory Analyses of Light Water Reactors

Date : 3/24/94

Approved:

James W. Malo

Dr. Weston M. Stacey Jr.
(Thesis Chairman)

Dr. Dale B. Lancaster
(Thesis Advisor)

Dr. Ronald E. Pevey

Dr. Henry C. Honeck

Dr. Farzad Rahnema

Dr. Chris K. Wang

DEDICATION

The author wishes to express sincere appreciation first and foremost to his family and friends. Without their encouragement, support and flattery, the thesis would have been a task rather than an enjoyment. The author thanks his mother and thoughts of his father. Gratitude is also given to the nephews and nieces, Andy, Sarah, Ben, and Marissa, for all their fun times, curious questions, and neverending laughter. Many thanks also to the authors brothers and their wives. The author also wishes to recognize all his long time friends, in particular, Brad Hall, Wayne McComb, Mo Duncan, and Rob McAlister for spurring on ideas. Thanks to the special friend in Jennifer James for her honesty and motivation.

Also for curious questions followed by long discussions, the author gives credit for much of this thesis to Dale Lancaster. The author is indebted to Dale and Westinghouse Savannah River Site (Ron Pevey, Courtney Apperson, and Mel Buckner) for providing and arranging funding for the thesis. The author also thanks Dr. Stacey for serving as a thesis advisor and chairman and his helpful comments on the thesis.

The author of this thesis wishes to recognize all authors who have taken the time and effort to publish their discoveries, thoughts, and ideas for all the world to critique. For the work in this thesis, this most definitely includes Allan F. Henry and his students.

BIOGRAPHICAL NOTE

James Walter Malo was born April 3, 1964 in Columbus, Georgia. He was raised in Upatoi, Georgia and graduated from Shaw High School in 1982. That year, he entered college at Columbus College for two years. Then he transferred to the Georgia Institute of Technology in 1984 and received his Bachelor of Science in Nuclear Engineering in June of 1987. He returned to Georgia Tech and earned his Master of Science Degree in Nuclear Engineering in September of 1989. Finally, in June of 1994, his academic career as a student ended when he was presented his Doctor of Philosophy degree.

TABLE OF CONTENTS

LIST OF TABLES

LIST OF ILLUSTRATIONS

SUMMARY

A method that makes it feasible to incorporate global reactor information into homogenized parameters used for nodal diffusion theory analyses was developed. Global reactor information can be used sucessfully to find homogenized parameters that are more accurate than infinite lattice homogenized parameters, but past approaches are expensive. An iterative method was developed that achieves the objective by using linear correlations to model changes in the homogenized parameters due to current-to-flux ratios from the nodal solution.

A numerical approach was used to analyze several one- and two-dimensional geometries. The one-dimensional analyses showed that the edge-to-average flux ratio from the lattice homogenization should be correlated rather than the flux discontinuity factor. Accurate flux discontinuity factors are then found from the edge-to-average flux ratio correlation. It was found that accurate correlations required a boundary condition, the shifted circle condition, that is uncommon to transport theory codes. This boundary condition allows a current to be created on a node boundary but other higher odd moments of the angular flux are equal to zero. It was demonstrated that this effect caused the scalar flux on the surface of a node to be more accurate than other transport theory

boundary conditions. The one-dimensional analyses also showed that linear correlations are sufficiently accurate to model the global reactor effects on the homogenized parameters.

Two-dimensional analyses of light water reactor assemblies demonstrated that the iterative procedure reduces the assembly power errors by a factor of two compared to using infinite lattice homogenized parameters without correlations. The analyses also confirmed that the method is independent of the flux approximation used in the nodal code and independent of the diffusion coefficients provided that reasonable diffusion coefficients are used. However, it was also shown that more accurate flux approximations and diffusion coefficients require only one or two adjustments to the homogenized parameters to achieve practical convergence on the homogenized parameters.

CHAPTER I

INTRODUCTION TO NODAL ANALYSIS

1.1 Development of Nodal Analysis Methods

During the 1980's, several nodal codes for the solution of the neutron diffusion equation developed into popular reactor analysis tools.[1,2,3,4] Lawrence reported that the accuracies of nodal codes are the same factor of ten as fine mesh finite difference calculations for the IAEA benchmark problems.[5] Despite their proven accuracy, there are some basic approximations in the nodal analysis routines.

Development of nodal codes began in the 1960's with the FLARE[6] code. The initial purposes of nodal codes were to serve as reactor simulators rather than detailed analysis tools. With this purpose in mind, a pin-by-pin analysis was not necessary so nodal codes modelled an entire fuel assembly as one node. The FLARE code used a one-and-a-half group model (no thermal leakage) and adjusted reactor parameters such as reflector albedos to fit actual operating experience. Due to these approximations, early nodal codes of the FLARE type could diverge from a solution in the limit of infinitely small mesh spacing. To avoid this problem, consistently formulated nodal codes[1,3,5] (or modern nodal codes) began emerging during the 1970's. These codes avoid the use of empirical parameters and reflector albedos and use higher ordered flux approximations.[5] This allows consistently formulated nodal codes to converge and yield accurate results in

the limit of an infinite number of spatial meshes. This is also a feature of finite difference equations. As the mesh spacing decreases, the Taylor series approximation for derivatives becomes more accurate.[7] A distinction between nodal diffusion theory and fine mesh finite difference is the transverse integrated procedure. In this procedure, the diffusion equation is integrated over the transverse directions to supply leakage terms. In essence, nodal diffusion equations are one-dimensional equations with known leakages in the transverse direction. Conversely, finite difference equations solve for fluxes in all surrounding nodes.

After consistently formulated nodal codes developed, the question remained how to generate homogenized reactor parameters from the heterogeneous node. Nodal codes model a large heterogeneous region of the reactor (often an entire fuel assembly) as a single homogeneous node by using equivalent homogenized parameters. The equivalent homogenized parameters are cross sections and diffusion coefficients that represent the region or node. Also included as homogenized parameters are heterogeneity factors or flux discontinuity factors which add freedom to the equation set to allow one solution method to give results equivalent to another solution method. Equivalent homogenized parameters are discussed in Section 1.2. In the late 1970's, Koebke provided the first homogenization technique capable of reproducing exact reference results. *Exact* refers to a known reference solution such as a heterogeneous transport theory solution. Koebke named this homogenization method equivalence theory[8,9] because it allowed a nodal

diffusion theory solution to yield equivalent results from a reference solution. Smith later developed a different approach called generalized equivalence theory.[10,11]

The global reactor calculation provides integral information concerning each node. This information is volume integrated reaction rates and fluxes and surface integrated currents of the node. However, in addition to integral results, a reactor analysis also needs to supply local parameters, such as individual fuel pin powers. Much work during the 1980's addressed this dehomogenization problem.[8,9,12,13,14] There are three ways to calculate local information. One method uses the surface integrated currents as boundary conditions to a detailed heterogeneous calculation. This method is accurate but also expensive. The second method is simply to combine global flux tilts in a node with a form function created during the homogenization process. The homogenization process renders detailed information about heterogeneities within the node. Specifically, an intranodal flux shape is available. The intranodal flux shape provides a form function for the power output of each pin in the node without accounting for the global flux shape in the node. This method is computationally cheap but also less accurate. It superimposes the x and y direction flux shapes in a node together as an approximation to the global flux shape for that node. This action often overpredicts the flux along the perimeter of the node and especially at the corners of the node. Another method uses global reactor information to approximate corner point fluxes for each node. Corner point fluxes eliminate the error of overpredicting the global flux shape along the perimeter of the node and as a result, reduce errors throughout the node. This method does not use the principle

of superposition to multiply the x and y direction flux shapes together, but uses a more analytic solution to obtain the global flux shape in the node. The method is both accurate and inexpensive.

In conclusion, nodal analyses consist of three distinct steps.[9] The homogenization process collapses each heterogeneous node into a set of equivalent homogenized parameters required by the nodal code. Then, the nodal code calculates integral results of a global reactor solution and lastly, the dehomogenization process finds local reactor characteristics. Since global reactor information is unavailable during the homogenization process, the homogenized parameters do not account for the effect that neighboring nodes have on them. There are several methods to include these interassembly effects into the homogenized parameters, however, methods previously developed are expensive and, as a result, are impractical to employ in the nodal analysis procedure. In this thesis, a method that is feasible for including interassembly effects to improve the accuracy of the homogenized parameters is presented. Also, it is shown that the improved homogenized parameters improve the accuracy of the global reactor solution.

1.2 Formally Exact Homogenization Schemes

In this section, we will assume that an exact solution (or reference solution) is available and can be used to find homogenized parameters. It is proven that traditional flux-weighted constants and an additional homogenization parameter are necessary to

reproduce integral results of the reference solution. This exercise serves to develop theory needed in calculating homogenized parameters for practical cases.

The goal of homogenization is to preserve certain integral properties[8,10,11,15] of each node. Koebke provides the following two postulates[8] that define a homogenized node to be equivalent to the same heterogeneous area.

> " Postulate A: The integral flux and integral reaction rates are conserved in the homogenized area.
>
> Postulate B: The integral net currents and integral fluxes are conserved at each interface of this area."

If the integral reaction rates and net currents are conserved, then the neutron balance equation from a nodal code is equivalent to the volume integrated neutron balance equations of a heterogeneous reference solution. This ensures that the multiplication factor of the nodal code will be identical to the reference multiplication factor. For the nodal neutron balance equation to be equivalent to a reference case, we only need to conserve reaction rates within the node and the sum of the leakages over all faces of the node. However, the second postulate states more than the sum of the leakages on all faces. The second postulate requires conservation of the net current along each surface. Koebke stated this postulate to ensure that the coupling of the neutron current between adjacent nodes is correct. The first postulate also contains a condition on the average flux in the volume. This condition provides a way to find equivalent homogenized cross sections

before obtaining a nodal solution. Conserving the surface integrated fluxes provides a method to account for deficiencies in the nodal code flux approximation.

We preserve reaction rates by requiring

$$\int_{V_i} \hat{\Sigma}_{\alpha,g} \hat{\phi}_g(\bar{r})\, dV = \int_{V_i} \tilde{\Sigma}_{\alpha,g}(\bar{r})\, \tilde{\phi}_g(\bar{r})\, dV \qquad \alpha = a, t, f, \ldots etc., \quad g = 1, 2, \ldots G \tag{1.1}$$

where α is a cross section type and g is the energy group. The symbols $\hat{}$ and $\tilde{}$ refer to homogeneous and heterogeneous values, respectively. By definition, the homogenized cross section is a constant parameter throughout the volume of the node. Therefore, we can remove it from the volume integral on the left side of equation (1.1). Koebke's first postulate states that the volume integral of the flux in the homogenized area must equal the volume integral of the flux in the heterogeneous area, or

$$\int_{V_i} \hat{\phi}_g(\bar{r})\, dV = \int_{V_i} \tilde{\phi}_g(\bar{r})\, dV \,. \tag{1.2}$$

Thus, the proper homogenized cross section is

$$\hat{\Sigma}_{\alpha,g} = \frac{\int_{V_i} \tilde{\Sigma}_{\alpha,g}(\bar{r})\, \tilde{\phi}_g(\bar{r})\, dV}{\int_{V_i} \tilde{\phi}_g(\bar{r})\, dV} \,. \tag{1.3}$$

Using Fick's law, we preserve the surface integrated currents on a particular surface, k, by requiring

$$-\int_{S_i^k} \hat{D}_g^k \nabla \hat{\phi}_g(\bar{r}) \cdot dS = \int_{S_i^k} \bar{J}_g(\bar{r}) \cdot dS \tag{1.4}$$

where the diffusion coefficient is constant along the surface of the node. The proper homogenized diffusion coefficient is

$$\hat{D}_g^k = -\frac{\int_{S_i^k} \bar{J}_g(\bar{r}) \cdot dS}{\int_{S_i^k} \nabla \hat{\phi}_g(\bar{r}) \cdot dS}. \tag{1.5}$$

Equation (1.5) is the only method to define rigorously correct diffusion coefficients simply because diffusion theory is based on Fick's law, equation (1.4). The numerator of equation (1.5) is a value from the reference solution and therefore creates no problem for defining a diffusion coefficient (assuming the reference solution is known). However, the denominator of equation (1.5) is dependent on the nodal code flux approximation. For most flux approximations, the derivative in the denominator of equation (1.5) is a known function of the volume integrated flux and the surface integrated edge fluxes. From Koebke's two postulates, these values are also known from the reference solution. Therefore, it is easy to find a diffusion coefficient for each surface of each node in the global reactor problem.

However, specifying a different diffusion coefficient for each node surface is not a common practice in reactor physics. The common practice is to use the divergence theorem[16] to transform the surface integrals of the neutron currents into volume integrals and specify one diffusion coefficient for each energy group that is valid on all surfaces of the node. Equation (1.6) demonstrates the divergence theorem applied to the leakage term in the diffusion equation. This action makes all terms in the neutron balance equation volume integrals rather than a mixture of volume integrals and surface integrals.

$$\int_{S_i^k} \bar{J}_g(\bar{r}) \cdot dS = \int_{S_i^k} -\hat{D}_g^k \nabla \hat{\phi}_g(\bar{r}) \cdot dS = \int_{V_i} -\hat{D}_{g,i} \nabla^2 \hat{\phi}_g(\bar{r})\, dV \qquad (1.6)$$

It is extremely unlikely that equation (1.5) will produce the same diffusion coefficient for all surfaces of a node. Therefore, after applying the divergence theorem and designating one diffusion coefficient, it is impossible to reproduce the reference solution in a rigorous sense unless a degree of freedom is added to the nodal diffusion equations. The surface integrated current is an important term in the neutron balance equation and the average flux is crucial in calculating reaction rates. Consequently, the degree of freedom cannot be added to these variables. However, the surface integrated edge flux serves only in the flux coupling equation between adjacent nodes. Since there is no need to directly conserve the surface integrated flux, a degree of freedom can be added to this variable in a way that allows for reproduction of the reference surface

integrated edge flux. Equivalence theory provided the first method to define and employ the degree of freedom to the neutron balance equations and the coupling equations.

Equivalence Theory[8,9]

Equivalence theory is the name given to the first procedure capable of reproducing all integral quantities of a known solution. Koebke[8,9] achieved this task by creating an additional homogenization parameter that he named the heterogeneity factor. This scheme assigns a heterogeneity factor to each surface of node i by

$$f_{g,i}^{k} \equiv \frac{\int_{S_i^k} \tilde{\phi}_{g,i}^{k}(\bar{r})\, dS}{\int_{S_i^k} \hat{\phi}_{g,i}^{k}(\bar{r})\, dS} . \tag{1.7}$$

Koebke's method multiplies the surface integrated fluxes in the nodal equation by the heterogeneity factor to arrive at the reference surface integrated fluxes. This satisfies his second postulate on the surface integrated edge flux.

Koebke limited the two heterogeneity factors that lie in a common direction to be identical. Thus, he relates the heterogeneity factors on the two opposite sides of a node (k and k') by

$$f_i^k = f_i^{k'} \tag{1.8}$$

where the energy group subscripts are dropped for convenience. Figure 1.1 shows the geometry orientation for two adjacent nodes.

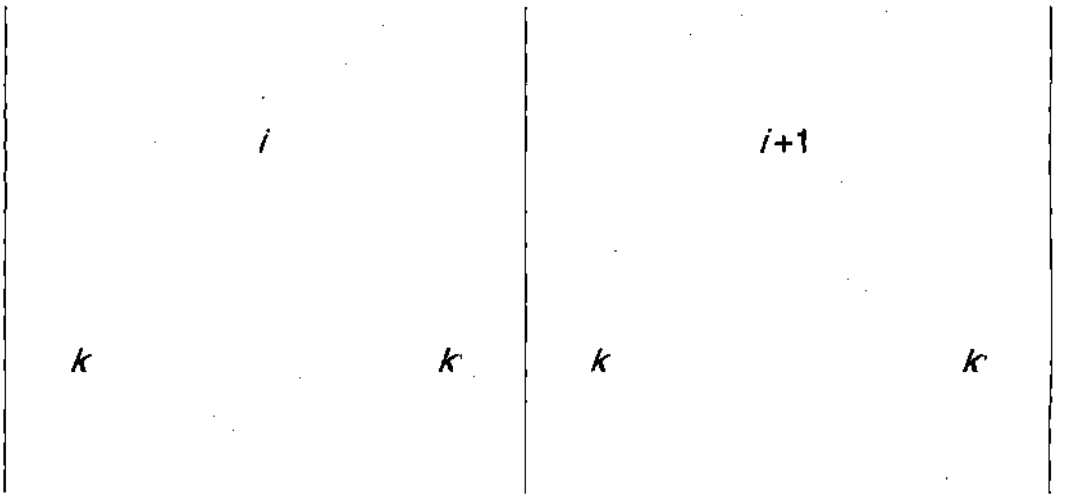

Figure 1.1. Nomenclature Associated with Two Adjacent Nodes.

Under Koebkes' condition, there exists one and only one diffusion coefficient in each coordinate direction that can preserve leakages while the heterogeneity factors are equivalent on the opposite surfaces of the node. This is because equations (1.7) and (1.8) add only one degree of freedom to the diffusion equations per direction. This method treats the diffusion coefficient as a purely artificial quantity.[11] The diffusion coefficient is not found from material properties within the node as it is with traditional flux weighted constants. The diffusion coefficient and heterogeneity factor are directionally dependent parameters in this method. This is due to the additional requirements for the net currents in the other directions. For example, in two-dimensional Cartesian geometries, there are four equations for the surface integrated fluxes (equation (1.7)), four equations for the diffusion coefficients (equation (1.5)), and one equation for the average flux (equation (1.2)). With the limit on the heterogeneity factor (equation (1.8)), the equations require directionally dependant diffusion coefficients. Nevertheless, the method can reproduce exact results.

The heterogeneity factor is dependent on the flux approximation used in the nodal code. Different flux approximations will result in different edge flux values. This, in turn, will result in a distinct heterogeneity factor for any given flux approximation. Therefore, the flux approximation used to find the heterogeneity factor must be consistent with the flux approximation used in the nodal code.

The use of heterogeneity factors requires us to modify the flux coupling equation between two adjacent nodes. In the actual reactor and in high order solutions, the flux is

everywhere continuous. The surface integrated reference flux of node i is equal to the surface integrated reference flux of node $i+1$ on the common surface. By employing equation (1.7), the flux coupling equation between nodes i and $i+1$ is

$$f_i^{k'} \int_{S_i^{k'}} \hat{\phi}_i^{k'}(\bar{r})\, dS = \int_{S_i^{k'}} \tilde{\phi}_i^{k'}(\bar{r})\, dS = \int_{S_{i+1}^{k}} \tilde{\phi}_{i+1}^{k}(\bar{r})\, dS = f_{i+1}^{k} \int_{S_{i+1}^{k}} \hat{\phi}_{i+1}^{k}(\bar{r})\, dS \tag{1.9}$$

where face k and k' are displayed in Figure 1.1.

Generalized Equivalence Theory[10,11,15]

Smith improved Koebke's equivalence theory to form generalized equivalence theory. In this method, each surface of the node has a separate discontinuity factor independent of all others. This results in a degree of freedom for each surface of the node and each energy group. By making this change, the diffusion coefficient can have any arbitrary non-zero value. This allows the diffusion coefficient to be found from material properties of the node or by any other preferred method. Regardless of the value of the diffusion coefficient (any non-zero value), the flux discontinuity factors have added enough degrees of freedom to the diffusion equations to allow Koebkes' two postulates to hold true.

Smith defines the flux discontinuity factor the same as Koebke defines the heterogeneity factor in equation (1.7). The coupling equation is similar to that of Koebke

with an important difference. The difference between the two coupling equations is that Smith's equation is face dependent while Koebkes equation is direction dependent. Because of this difference, equivalence theory has only one set of homogenized parameters that can satisfy Koebkes' two postulates while generalized equivalence theory has an infinite number of sets of homogenized parameters that satisfy the postulates.

Both equivalence theory and generalized equivalence theory can reproduce exact results. An interesting feature of these methods is that exact results are obtainable even when we solve the diffusion equation by approximate methods rather than analytic methods[9,11,17] assuming again that the exact solution is known. This means that, in principle, flux discontinuity factors or heterogeneity factors correct for heterogeneities within the node and errors in the diffusion theory approximation.

1.3 Approximations to Obtain Homogenized Parameters

For a homogenization scheme to be of practical use, it must be able to approximate homogenized parameters without knowledge of a reference solution. The formally exact method described in the preceding section assumed that the exact solution is available for use. If the exact solution were available, then there would be no need to solve the nodal diffusion equations. This section describes the traditional homogenization method and the approximate methods of Koebke and Smith.

All of the homogenization methods discussed in this section analyze two-dimensional slices of the node rather than a three-dimensional node. The axial direction of a node usually does not contain any heterogeneities. Therefore, a two-dimensional model is appropriate. In some cases such as control rod insertion or grid spacers, the axial direction does have strong heterogeneities. Smith and others[18] devised a method to account for these heterogeneities.

Traditional Homogenization

The traditional homogenization method models a fuel assembly as either one node or four nodes. The boundary conditions for the node are zero net current boundary conditions. If the currents were known, then we could use the currents as boundary conditions. However, at the time of homogenization, estimates for the current directions and magnitudes are unknown. Therefore, the best guess for the boundary conditions are zero net currents. Smith points out that homogenized parameters are primarily dependent on the heterogeneities within the node and of secondary importance on the location in the reactor.[11] This statement supports the use of zero net current boundary conditions.

After imposing these boundary conditions on a node, the neutron balance equation is solved to find a flux profile throughout the node. There are several different methods available to solve the neutron balance equations. These methods can range from continuous energy Monte Carlo methods to fine mesh finite difference methods. In traditional lattice homogenization, the flux profile is used to flux and volume weigh the heterogeneous cross sections by using equation (1.3). There are many different methods

to calculate diffusion coefficients from the assembly calculation.[11,19] Among these are flux and volume weighing either the diffusion coefficient or the transport cross section. However, we cannot employ equation (1.5) to define a diffusion coefficient because the currents (numerator of equation (1.5)) are equal to zero. Thus, the diffusion coefficient would also equal zero. After making these approximations, enough information is available to evaluate equation (1.3) for estimated values of the homogenized cross sections and diffusion coefficients. Traditional homogenization methods implicitly assumed flux discontinuity factors or heterogeneity factors to be equal to unity. Examining equation (1.9) with unity discontinuity factors shows that these equations are equivalent to the traditional continuity of flux condition.

Traditional homogenization still served as the basis for advanced homogenization methods after Koebke proved that an additional parameter was necessary. Both Koebke and Smith used the zero net current boundary condition to approximate homogenized parameters. Koebkes approximation is known as simplified equivalence theory.[8] In both methods, all cross sections are flux and volume weighted. However, there are differences in how the diffusion coefficients and the flux discontinuity factors or heterogeneity factors are found in each method.

Simplified Equivalence Theory[8,9]

Due to the manner that Koebke defines the heterogeneity factor and due to the geometric symmetry of PWR assemblies, Koebke could derive simplified equivalence theory. Simplified equivalence theory allows a code that does not use heterogeneity

factors (one that implies unity values) to improve global solutions to the reactor problem. Also, the method finds the diffusion coefficient from actual material properties rather than treating it as an artificial value.

Consider a two-dimensional slice of a fuel assembly that is perfectly symmetric about the center of the node. Equation (1.3) defines the homogenized cross sections of the node to be spatially constant. Therefore, if an assembly calculation uses zero net current boundary conditions, then the diffusion theory flux profile for the single assembly is constant throughout the node. By equation (1.2), the value of the flux is equal to the average value found from the heterogeneous assembly calculation. Therefore, the denominator of equation (1.7) is equal to the average flux from the heterogeneous assembly calculation. Since the heterogeneities in the region are symmetric, the surface integrated edge flux on all boundaries are equal to each other thus providing a value for the numerator of equation (1.7). Therefore, all surfaces have the same value for the heterogeneity factor. This satisfies Koebke's requirement for the heterogeneity factor (equation (1.8)) and no restrictions have been placed on the diffusion coefficient. This allowed Koebke to calculate the diffusion coefficient from actual material properties. Furthermore, the homogenized parameters have no directional dependencies and no limits are placed on the solution method for the diffusion equation. A single assembly calculation such as this corrects only for heterogeneities within the lattice. Since the currents are equal to zero on all surfaces, the method cannot correct for the flux approximation employed in the nodal code or an errant diffusion coefficient.

Koebke named this approximation *simplified* equivalence theory because he could deceive the nodal code and completely remove the heterogeneity factors from the diffusion equations. This allowed the nodal code to use the traditional flux coupling equation rather than the discontinuous flux coupling equation shown by equation (1.9). Nodal codes expand the second order derivative in the diffusion equation by approximating the derivative with an average flux and fluxes at the edges of the region. Koebke replaces the homogeneous edge fluxes in the diffusion equation with the heterogeneous edge flux by rearranging equation (1.7). This substitution incorporates the heterogeneity factor into the neutron balance equation (nodal diffusion equation) and the current coupling equations. The fluxes on the surface of the node are now the heterogeneous surface fluxes that are continuous at the node interfaces. Koebke separates the heterogeneity factor away from the surface fluxes by combining it with the diffusion coefficient. He defines a simplified diffusion coefficient by

$$\check{D}_i \equiv \frac{\hat{D}_i}{f_i}. \tag{1.10}$$

However, the diffusion equation multiplies the diffusion coefficient and average flux together. If the simplified diffusion coefficient replaces the actual diffusion coefficient, then, as a conservation principle, we must multiply the average flux by the heterogeneity

factor. In simpler terminology, we are multiplying and dividing this term by the heterogeneity factor. Thus, Koebke defines a simplified average flux as

$$\check{\phi}_j \equiv f_j \hat{\phi}_j. \tag{1.11}$$

Continuing, if the simplified flux replaces the actual flux, then, as before, we must divide the cross sections by the heterogeneity factor to preserve reaction rates. Accordingly, Koebke divides all cross sections by the heterogeneity factor to form the simplified cross sections,

$$\check{\Sigma}_{\alpha,j} \equiv \frac{\hat{\Sigma}_{\alpha,j}}{f_j}. \tag{1.12}$$

Before starting the diffusion theory calculation, all cross sections and the diffusion coefficient for each node and energy group are divided by the heterogeneity factor of that node and energy group. This completely removes the heterogeneity factor from the neutron balance equation and the current coupling equations and allows use of the traditional flux coupling equation. Once the diffusion calculation converges, the simplified average flux is divided by the heterogeneity factor to arrive at the actual average flux. The edge fluxes are the actual heterogeneous edge fluxes.

Generalized Equivalence Theory[10,11,15]

Koebke's simplified equivalence theory works ideally for fuel assemblies that are one-eighth symmetric; however, BWR assemblies are only one-half symmetric at best. Asymmetric nodes must employ Smith's homogenization scheme. The assembly calculation with zero net current boundary conditions computes a flux shape throughout the node. As before, if the nodal cross sections are to be spatially constant, then the flux shape from a diffusion calculation on the single node is also constant and equal to the average flux of the heterogeneous assembly calculation. The heterogeneous assembly calculation provides surface integrated fluxes for the numerator of equation (1.7) and the above argument provides a value for the denominator of equation (1.7). For asymmetric regions, the surface integrated fluxes from the lattice calculation are not equal on all surfaces and therefore each surface of the node will have a different flux discontinuity factor.

Since the flux discontinuity factors for the surfaces of a node are different, we cannot divide them into the cross sections and the diffusion coefficient for the node without creating several cross product terms. Therefore, we must incorporate the discontinuous flux coupling equation (equation (1.9)) into the nodal code.

Heterogeneity factors are not definable for asymmetric regions when the current boundary conditions are equal to zero. This is because the diffusion theory flux shape in a single node with zero net current boundary conditions is *always* flat despite the diffusion coefficient or the flux approximation employed in the nodal equations.

Therefore, it is impossible to define a heterogeneity factor when the heterogeneous assembly calculation computes different values of the surface integrated edge fluxes and when the diffusion theory flux profile is flat. As in Koebke's single assembly lattice homogenization technique, Smith's generalized equivalence theory corrects only for heterogeneities within the lattice and not for the nodal code flux approximation or discrepancies in the diffusion coefficient.

In this thesis, we will from now on use flux discontinuity factors rather than heterogeneity factors to avoid the restrictions on directional dependencies and complications due to using zero net current boundary conditions on asymmetric lattices.

1.4 Methods for More Accurate Homogenized Parameters

There are schemes that can obtain more accurate homogenized parameters than the methods discussed in Section 1.3 but at increased computer expenses. The only error in the methods discussed in Section 1.3 is the zero net current boundary condition. A more accurate method must therefore have a better approximation for the boundary conditions used in the assembly calculation. There are two ways to accomplish this task. One method is to extend the geometry around the assembly calculation. The other is an iterative technique between the lattice homogenization process and the global reactor calculation.

Extended Geometry Calculations

Extended geometry calculations model the region of interest and its closest neighbors. There are different ways to perform extended geometry calculations. The two

models discussed in this segment still employ zero net current boundary conditions. Other methods not discussed can use periodic boundary conditions if the geometry shows periodic tendencies. For example, some reactors may arrange a small group of assemblies periodically thus providing a strong argument to use periodic boundary conditions.

One extended geometry model surrounds the region of interest by all of its closest neighbors, as displayed in Figure 1.2.[10] The solid lines in the figure represent node boundaries and assembly boundaries. Small squares within each node portray heterogeneities. The five-node extended geometry still employs zero net current boundary conditions but the boundaries are not next to the region of interest but on the neighboring regions.

Since the material and geometric properties of the neighboring regions are most likely different from the region of interest, a current will be present at each interface. The current-to-flux ratio (using the average flux of the node) of the extended geometry calculation will be a good estimate of that found from a global calculation. However, the current is an estimated value because the zero net current boundary conditions on the neighboring regions are estimates. Nevertheless, this extended geometry method provides better estimates of the current directions and magnitudes on each surface of the node than zero net current boundary conditions. This leads to a more accurate intranodal flux shape needed to homogenize cross sections, specify the diffusion coefficient, and calculate the flux discontinuity factors.

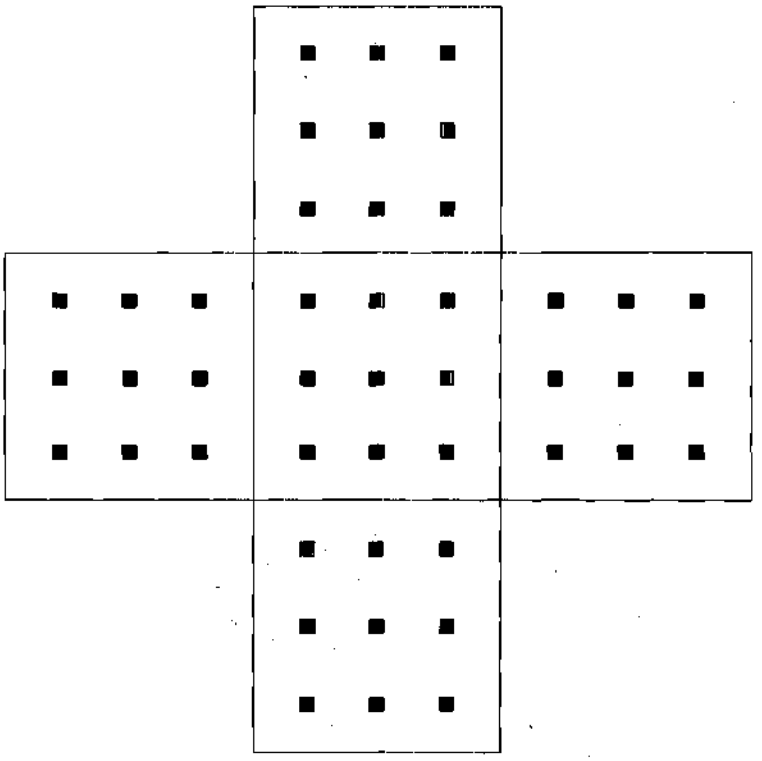

Figure 1.2. Five-Node Extended Geometry Representation.

Figure 1.3 displays another way to model an extended geometry calculation. This design is the color set or supercell design.[20] Assemblies of common geometric characteristics and burnup are assigned a similar color. The four assembly portions form a color set when located next to one another. This layout is useful for PWR assemblies because of their symmetry. The current at the center of a symmetric assembly will be closer to zero than at a boundary where material properties between adjacent nodes are different. As before, the solid lines distinguish the node boundaries. The dashed lines are assembly boundaries. Figure 1.3 shows four nodes per assembly. We can estimate that the currents along the midplane of each assembly are near but not exactly equal to zero. Therefore, this method also assumes zero net current boundary conditions. The interior solid lines of the figure are node boundaries where larger currents are expected.

Although the boxed area of Figure 1.3 is the same size as an assembly, this method does require more computer resources than the single assembly calculation. If each assembly is symmetric, the single assembly calculation discussed in Section 1.3 can use this knowledge to model only one-eighth of the assembly. Thus, the color set model would be eight times larger than the single assembly model. This design also increases computer resources because the color sets are location dependent. As an approximation, there is the same number of color sets in a reactor as there are assemblies. In the single assembly calculation, there are several assembly types that we can use at any location in the reactor. Although the number of color set calculations can be reduced, there are still many more combinations of color sets than there are assembly types.

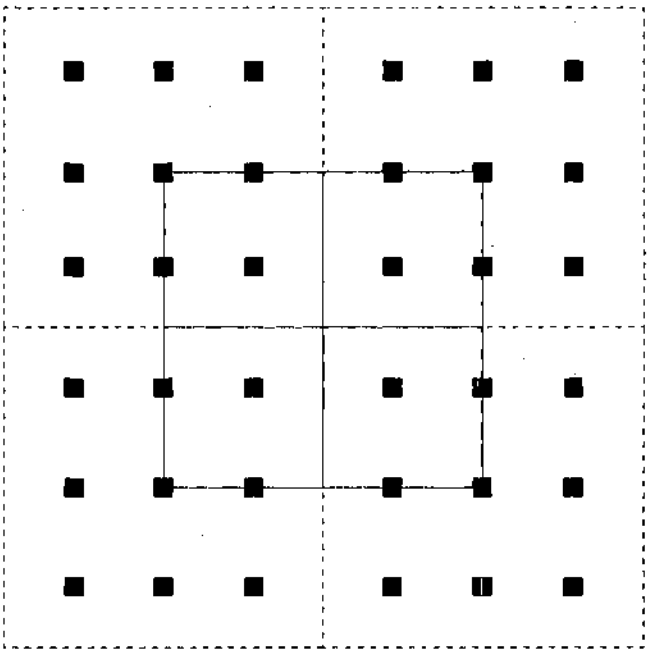

Figure 1.3. Color Set Extended Geometry Representation.

Iterative Techniques

At the end of the global calculation, approximate values for the currents are known compared to average fluxes in the node. These currents can be used to aid in finding more accurate homogenized parameters. Because zero net current boundary conditions were used to calculate the homogenized parameters for the global reactor calculation, the currents retrieved from the global reactor calculation are approximate values, but they are exceedingly good approximations. The information from the global reactor solution can be employed in one of three ways to improve the homogenized parameters. The currents can serve as boundary conditions to rehomogenize the node and then the improved homogenized parameters used in the global calculation to obtain more accurate global results. Another method uses response matrices and the global reactor information to update the homogenized parameters. A third method uses the global reactor information to adjust the homogenized parameters based on correlations.

The rehomogenization approach is an expensive process. Many nodes in a reactor are similar in material composition and geometric form, but all nodes will have different currents across their boundaries. This means that each node will need homogenization again using the currents from the global reactor solution. This leads to more accurate homogenized parameters, but the computer resources needed to rehomogenize each node makes this an unattractive process.

Smith showed that this method can successfully improve values for the homogenized parameters. Smith used fine mesh diffusion calculations to find

homogenized parameters.[10] After completing a global calculation using infinite lattice homogenized parameters, the currents and assembly powers serve as input conditions to rehomogenize each assembly. The resulting set of homogenized parameters were closer to reference values than the infinite lattice homogenized parameters. This, in turn, leads to a more accurate global reactor solution. The preceding steps form one iteration. In Smiths' examples, the method converged in very few iterations (two or three iterations).

Another iterative method studied by Cheng, Hoxie, and Henry[17] employed response matrices to update the homogenized parameters. This method computes response matrices based on a net current across segments of a node face rather than partial currents. In the conventional response matrix method,[7] the response matrices reflect how outgoing partial currents change due to an incoming partial current on only one surface. The conventional response matrix method does not directly produce a surface integrated edge flux needed to compute discontinuity factors. By basing the response matrices on net currents, the surface integrated flux is available and discontinuity factors are obtainable. This method also updates homogenized cross sections. However, the method finds net current response matrices from partial current response matrices. In several cases studied by Cheng, Hoxie, and Henry, the response matrice technique for improving homogenized parameters moderately improved the accuracy of the homogenized parameters and the global solution.

Koebke[8] and Rahnema[21,22] have introduced the concept of correlating the homogenized cross sections to global reactor information. They rendered general forms for correlations that the homogenized cross sections should follow. Both Koebke and

Rahnema propose the same characteristics. In the correlation equations, the homogenized parameters change as a function of the current-to-flux ratio. The correlations are linear and therefore contain no cross product terms. Their correlation is

$$\Sigma_{g,\alpha} = \Sigma^{\circ}_{g,\alpha}\left(1 + \sum_{g'=1}^{G}\sum_{k=1}^{K} a^{k}_{g',\alpha}\frac{J^{k}_{g'}}{\phi_{g'}}\right). \qquad (1.13)$$

In this correlation, the homogenized cross section, Σ, would change as the current-to-flux ratio deviates from the zero net current value used to calculate the initial homogenized cross section, Σ°.

To increase the accuracy of the global reactor calculation, the homogenized cross sections and flux discontinuity factors must be improved simultaneously. Smith showed that reference homogenized cross sections used with infinite lattice flux discontinuity factors actually leads to greater errors than using all infinite lattice homogenized parameters.[11] Similarly, he also showed that using infinite lattice cross sections with reference flux discontinuity factors also leads to greater errors than using all infinite lattice homogenized parameters. Therefore, equation (1.13) should apply not only to the homogenized cross sections but to the flux discontinuity factors as well (or a relationship involving the flux discontinuity factors). Smith states that these errors arise because the infinite lattice cross sections and flux discontinuity factors are a matched set of equivalence parameters.[11] This implies that any further improvements also should match

the infinite lattice calculation method. In particular, the same method used in lattice homogenization should decide any correlation parameters.

Equation (1.13) provides some promising characteristics. If it is possible to find the correlation coefficients $a_{g,\alpha}^{k}$ before starting the global reactor calculation, then the homogenized parameters can be adjusted during operation of the nodal code as needed. This allows us to improve the accuracy of the global reactor solution without iterating between the nodal calculation and the lattice homogenization calculation. Also, equation (1.13) implies that the homogenized parameters and correlation coefficients are independent of position in the reactor. If true, the correlation coefficients apply to all similar assemblies much like the infinite lattice homogenized parameters.

In an iterative technique such as this, the question arises if the solution converges toward or diverges away from a reference solution. Smith answered this question by first calculating a global reactor solution using a homogenization code (the homogenization code was a fine mesh finite difference calculation). Then he performed an iterative technique coupling the homogenization code and the nodal code. The homogenization in this case was on each node. Smith showed that the global solution of the iterative technique converged toward the global solution solved by the lattice homogenization code.[10] However, the solution will not converge exactly to this reference solution because the currents from the nodal code are surface integrated values. Thus, the current across a node face has no shape and the accuracy reduces.

1.5 Objectives

The objective of this thesis is to find a feasible method to use global reactor information to improve homogenized parameters used in nodal diffusion theory. The method should be applicable to multiple dimensions and multiple energy group analyses. The lattice homogenization code should be of any analysis type. Since lattice homogenization codes usually employ a transport theory method, work in this thesis also employs transport theory. Extended geometry and response matrix techniques for improving the accuracy of homogenized parameters are undesirable because of their increased computer resources. Also, iterative methods that completely rehomogenize each node are too expensive for the analysis also.

An iterative method that updates the homogenized parameters by correlations does appear attractive. For extremely simple geometries, correlations can be found by applying perturbation theory or variational analysis. However, these techniques are not used in this thesis because of the difficulty involved in lattice homogenization. Usually, lattice homogenization involves twenty energy groups[20] or more and trends in the nuclear industry are moving toward explicitly modelling all details of the fuel assembly, including explicit modelling of each fuel pin within the assembly.[23,24,25] These concerns eliminate using perturbation theory or variational analysis to find correlation coefficients. Thus, the method used to find correlation coefficients is a numerical approach. This approach is much more feasible than other methods due to its simplicity.

Two computer codes were written for this thesis. A description of these computer codes is provided in Chapter II as well as validation results for the codes. One code is a lattice homogenization code that uses discrete ordinates and the other is a nodal diffusion theory code. The remaining chapters develop the procedure to improved the homogenized parameters. In Chapter III, the method is developed in a one-dimensional geometry. This chapter discusses the dependency of the correlations to the energy groups and faces of the node. Also, a boundary condition necessary to obtain accurate correlations is introduced in Chapter III. The correctness of the linear correlation approximation is addressed. In Chapter IV, the method is extended to two dimensions and the effect of using different flux approximations in the nodal code and different values for the diffusion coefficients is examined. Dependencies of the correlation coefficients are also examined. Lastly, a review of the method is given in Chapter V along with ideas for future research.

CHAPTER II

ANALYSIS TOOLS

2.1 Analysis Tools Overview

Three different analysis tools are employed in this thesis to examine methods for improving homogenized parameters. One tool is a pin cell homogenization code. This code provides multigroup cross sections for each location in a fuel assembly. The second tool, a lattice homogenization code, collapses the pin cell cross sections to find homogenized parameters for each assembly. It is essential that the lattice homogenization code can perform reactor calculations on multiple assemblies so that reference solutions are available. The final tool, a nodal diffusion theory code, uses the homogenized parameters in a global reactor calculation in an attempt to reproduce reference results. The goal of this chapter is to validate the use of these tools.

The pin cell homogenization code used to calculate macroscopic cross sections is COMBINE/PC.[26] COMBINE/PC starts with ENDF/B-Version 5 cross sections and resonance parameters collapsed to 166 energy groups. It uses the Nordhiem numerical method for resolved resonances and the Wigner rational approximation for unresolved resonances. COMBINE/PC also uses the Dancoff-Ginsburg correction factor and the ABH method for spatial homogenization. The B_1 and B_3 approximations to the Boltzmann transport equation calculate the neutron spectrum needed to collapse the fine group cross

sections into broad energy groups. Its use in this thesis is to provide reasonable and consistent values for two-group pin cell, water gap, and control cross sections. This code provides the P_3 scattering cross sections used in Chapter III and the P_1 scattering cross sections used in Chapter IV. COMBINE/PC has been benchmarked to Monte Carlo techniques for cylindrical fuel rod cells, and several moderated and unmoderated critical assemblies.[27]

JTC is the lattice homogenization code written for use in this thesis. JTC has several options that are uncommon to many transport theory codes. For instance, the code has a unique boundary condition specification. Rather than reflective, periodic, or albedo boundary conditions, the user enters values for the odd moments of the angular flux along each boundary for each energy group. This option allows greater flexibility in the boundary condition specifications. The code can also spatially homogenize distinct regions within the geometry. With this option, reference homogenized parameters for each fuel assembly in a global reactor problem are readily available. Another feature of JTC is that flux discontinuity factors and edge-to-average flux ratios are direct output values. Section 2.2 describes the lattice homogenization code in greater detail.

Lastly, a nodal diffusion theory code, NDT, also written for this thesis, tests the homogenized parameters and any method to update them. NDT has the ability to update homogenized parameters during operation. Section 2.3 describes the nodal code in greater detail. Several different flux approximations are available in NDT.

2.2 JTC Description

The neutronics and lattice homogenization routines of JTC are described in this section. As a general overview, the code uses the diamond difference approximation to the discrete ordinates transport equation. However, it stores only the moments of the angular flux in each coordinate direction. The code contains two levels of iterations. Inner iterations update the moments of the angular flux in each coordinate direction and the outer iteration is the power method for finding the eigenvalue. The code employs a two-step acceleration[28] technique.

From Henry[7], the discrete ordinates transport equation including spherical harmonics is interpreted as

$$\mu_d \frac{\partial}{\partial x}\psi_{g,d} + \xi_d \frac{\partial}{\partial y}\psi_{g,d} + \sigma_g^t \psi_{g,d}$$

$$= \frac{1}{k_{eff}} \chi_g \sum_{g'=1}^{G} \nu\sigma_{g'}^f \sum_{d'=1}^{D} wt_{d'} \psi_{g',d'} \qquad (2.1)$$

$$+ \sum_{g'=1}^{G} \sum_{l=0}^{\infty} \sum_{m=-l}^{l} \sigma_{g'\to g,l}^s Y_{l,d}^m \left(\sum_{d'=1}^{D} wt_{d'} \overline{Y_{l,d'}^m} \psi_{g',d'} \right)$$

where Y and $\overline{Y}$ are the spherical harmonics function and its complex conjugate, respectively,

l and m are indexes to the spherical harmonics,

d and d' are discrete directions,

g and g' are energy groups,

$wt_{d'}$ is the weight associated with direction d',

k_{eff} is the effective multiplication factor,

ψ is the discretized angular flux,

and $\xi = \sqrt{1-\mu^2}\sin\Theta$ with $\mu = \cos\theta$.

The cross sections, σ, are macroscopic cross sections but are written using the lower case sigmas to avoid confusion with summation signs. The spherical harmonic function is

$$Y_{l,d}^{m} = \left(\frac{(2l+1)\ (l-m)!}{(l+m)!}\right)^{\frac{1}{2}} P_l^m(\mu)\ \exp(im\Theta) \qquad (2.2)$$

where $P_l^m(\mu)$ is the associated Legendre polynomial. A direction, d, has known values of μ, Θ and weights from the angular quadrature set.

Integrating equation (2.2) over all Θ reduces the source term in the transport equation to a one-dimensional form (m is an integer number). This is equivalent to setting m equal to zero. In this case, the spherical harmonics function and its complex conjugate reduce to

$$Y^0_{l,d} = \overline{Y^0_{l,d}} = \sqrt{2l+1}\; P^0_l(\mu_d) = \sqrt{2l+1}\; P_l(\mu_d) \tag{2.3}$$

causing the source term to become

$$\frac{1}{k_{eff}}\chi_g \sum_{g'=1}^{G} \nu\sigma^f_{g'}\phi^0_{g'} + \sum_{g'=1}^{G}\sum_{l=0}^{L}(2l+1)\,\sigma^s_{g'\to g,l}P_l(\mu_d)\,\phi^l_{g'} \tag{2.4}$$

where L is the truncation order of the scattering cross section and ϕ^l is the moment of the angular flux defined by

$$\phi^l = \sum_{d=1}^{D} wt_d P_l(\mu_d)\,\psi_d \quad . \tag{2.5}$$

In JTC, the indexes d and d' in the above three equations are only in the x direction. The source term in equation (2.4) depends on μ and the x direction moments (also a function of μ). Therefore, for $m = 0$, the source term has no y direction dependencies. The y direction contributions appear for $m \neq 0$ in the spherical harmonics function. By neglecting the y direction components in the scattering terms, a simple method emerges for solving the two-dimensional discrete ordinates equation.

JTC employs equations (2.3) through (2.5) when solving for the angular fluxes and their moments in the x direction. It finds the y direction angular fluxes and moments by

rotating the axis. In this case, we replace the direction cosine μ with ξ in equations (2.3) through (2.5). This provides identical equations necessary for finding the y direction angular fluxes and moments. Pivoting the directional sweeps is a common method employed in many multidimensional boundary value problems. This approach is named the ADI (alternating direction implicit[29,30]) method.

The purpose of JTC is a fuel assembly homogenization code. In such calculations, there is a large amount of fission throughout the geometry. Thus, anisotropic scattering is less important in these type problems than in deep penetration shielding calculations, for example. This means that neglecting the $m \neq 0$ terms in the spherical harmonics function is a reasonable assumption.

The outer iteration process converges to an eigenvalue, k_{eff}, using the power iteration method. This process is expressed mathematically by

$$\frac{1}{k_{eff}} \sum^{Vol} \sum_{g=1}^{G} \nu\sigma_g^f \phi_g^0 \Big|^{p+1} = \frac{1}{k_{eff}} \sum^{Vol} \sum_{g=1}^{G} \nu\sigma_g^f \phi_g^0 \Big|^{p} \qquad (2.6)$$

where the superscript p is the iteration index. At the beginning of an iteration, the method computes the total neutron source in the geometry from fission at iteration p and divides by the eigenvalue of that iteration. The upcoming inner iterations use the eigenvalue at iteration p. At the end of the inner iteration sweeps, the updated values for the scalar fluxes (index $p + 1$) cause the source term to change. Equation (2.6)

finds a new value for the effective multiplication factor to use during the next inner iteration sweeps. This method guarantees convergence to the largest eigenvalue.[29] As a comparative measure, at the end of all outer iterations, JTC computes the effective multiplication factor by dividing all neutron sources by the neutron losses.

The boundary condition specification in JTC is unique. The Boltzmann transport equation is a first order equation in each coordinate direction. If we solve the transport equation in two one-dimensional steps, then the transport equation is a first order equation in only one direction. Therefore, for each discretized angular flux, the transport equation requires one and only one boundary condition. The boundary condition is always a specification on the incoming angular flux. For example, a vacuum boundary condition states that all incoming angular fluxes are equal to zero. With this condition, the user has no control over the values of the outgoing angular fluxes. The geometry and cross sections of the problem influence the outgoing angular fluxes. A reflective boundary condition states that an incoming angular flux, index d, is equal to its complementary outgoing angular flux, index d', where symmetry requires that the complementary angle for μ_d is $-\mu_d$. Therefore, for a boundary, there are always $\frac{n}{2}$ boundary conditions where n is the S_n order of the transport equations. In JTC, the user specifies values for the odd moments ($\frac{n}{2}$ values for each boundary and energy group) and relationships between the incoming and outgoing angular fluxes at complementary angles are found. For a symmetric quadrature set, the odd moments of the angular flux are found by

$$\phi^{l} = \sum_{d=1}^{\frac{D}{2}} wt_d \, P_l(\mu_d) \, (\psi_d - \psi_{d'}) \tag{2.7}$$

for l equal to the odd integers. This equation results in $\frac{n}{2}$ equations for the moments with $\frac{n}{2}$ unknowns. When solved, the complementary angles are in the form

$$\psi_d - \psi_{d'} = C \tag{2.8}$$

where C is now a known constant. This boundary condition fixes values for the odd moments and yet allows freedom for the even moments. This is an important characteristic because the even moments of the problem are not input variables (particularly the scalar flux since it defines the flux discontinuity factor). With these boundary conditions, the user can control the shape of the angular flux profile while the geometry and cross sections control the magnitude of the angular fluxes.

The inner iteration solves the one-dimensional discrete ordinates transport equation with a constant leakage term. The process begins by computing a source term that remains constant throughout the inner iteration. The only part of the source term that changes is the within group scattering terms and the within group fission. The constant source term is

$$\frac{1}{k_{eff}}\chi_g \sum_{\substack{g'=1 \\ g' \neq g}}^{G} \nu\sigma_{g'}^{f}\phi_{g'}^{0} + \sum_{\substack{g'=1 \\ g' \neq g}}^{G}\sum_{l=0}^{L}(2l+1)\sigma_{g' \to g,l}^{s} P_l(\mu_d)\phi_{g'}^{l} - L_g^{y} \qquad (2.9)$$

where

$$\begin{aligned} L_g^{y} &= \int_{-1}^{1} \xi \frac{\partial}{\partial y}\psi_g(\xi)\, d\xi \\ &= \sum_{d'=1}^{D} wt_{d'}\,\xi_{d'}\frac{\Delta\psi_{g,d'}}{\Delta y} \end{aligned} \qquad (2.10)$$

The angular fluxes of group g will change at each inner iteration and change the moments of the angular flux. This results in changing the within group contribution to the source term. The within group source is

$$\frac{1}{k_{eff}}\chi_g\, \nu\sigma_g^{f}\phi_g^{0} + \sum_{l=0}^{L}(2l+1)\sigma_{g \to g,l}^{s} P_l(\mu_d)\phi_g^{l}\,. \qquad (2.11)$$

The complete source term is a function of the energy group and the angle, μ_d . Thus the transport equation becomes

$$\mu_d\frac{\partial}{\partial x}\psi_{g,d} + \sigma_g^{t}\psi_{g,d} = S_{g,d}\,. \qquad (2.12)$$

JTC uses the diamond difference approximation. This approximation relates the angular flux on the left boundary of the mesh, ψ^-, to the angular flux on the right boundary of the mesh, ψ^+, as

$$\left(\frac{\sigma_g^t}{2} + \frac{\mu_d}{\Delta x}\right)\psi_{g,d}^- + \left(\frac{\sigma_g^t}{2} - \frac{\mu_d}{\Delta x}\right)\psi_{g,d}^- = S_{g,d}\,. \tag{2.13}$$

The two complementary angles, d and d', are solved simultaneously for all mesh intervals in a directional sweep. There are two neutron balance equations written for each mesh interval, one for $\mu<0$ and the other for $\mu>0$. Adjacent meshes are coupled together by requiring that the angular flux across an interface is continuous,

$$\psi_{d,i}^+ = \psi_{d,i+1}^-\,. \tag{2.14}$$

The boundary conditions provide relationships between the incoming and exiting angular fluxes at the complementary angles. These equations provide a well-posed problem with a unique solution. After JTC solves for the angular fluxes for all discrete angles, it finds new moments of the angular flux and new within group source terms to continue the inner iteration.

JTC writes the boundary condition and neutron balance equations in a manner to aid in the solution of the angular fluxes. If written in its entire form, the problem matrix

is extremely sparse. The matrix will contain ones along the diagonal, non-zero values directly below the diagonal, and a non-zero value in the upper right corner. All other values are equal to zero. This matrix is similar to a band diagonal matrix.[30] We can easily write a reduced matrix that implies the zero values and the diagonal values of one. JTC also stores the term in the upper right corner of the problem matrix and implies its location. We can easily solve the resulting matrix for the angular fluxes non-iteratively.

At the end of each outer iteration, JTC checks the flux convergence. JTC stores moments of the angular flux in each coordinate direction. This includes the scalar flux (zeroth moment) meaning that there are two scalar fluxes for each mesh and energy group. If the problem has converged, then the scalar flux from the x direction iteration will equal the scalar flux from the y direction iteration. The maximum flux convergence value is the largest deviation between the x and y direction scalar fluxes from all meshes and energy groups or the largest change between two successive iterations. After the flux convergence is checked, JTC modifies the scalar fluxes so that they are equal in the two coordinate directions.

The homogenization process is a non-iterative operation to find the equivalent homogenized parameters. Section 1.2 discussed how to obtain the homogenized parameters. Equation (1.3) flux and volume weighs the heterogeneous cross sections and diffusion coefficients to find equivalent homogenized cross sections and diffusion coefficients. The flux discontinuity factors are found by employing equation (1.7). The surface integrated scalar fluxes from JTC are readily available. This provides a value for

the numerator of equation (1.7). The currents along node boundaries are also readily available. The current, diffusion coefficient, and nodal code flux approximation provide a value for the denominator of equation (1.7) when employed in Fick's law of diffusion.

A source situation to test the accuracy of JTC is provided in the Argonne Benchmark Book.[31,32,33] The geometry and material descriptions of the benchmark problem are described in Appendix A. The reference solution is an S_8 discrete ordinates solution from the DOT-III code using a 4×4 mesh spacing. A map of the two group scalar fluxes from JTC is also given in Table A.2. Comparison of JTC with the DOT-III solution shows that JTC overpredicts the fluxes in the regions that contain the poison pin (material 5) for both energy groups. This results in an eigenvalue that is lower than the reference solution (i.e., the thermal absorption cross section is much larger than the thermal production cross section for material 5). The remaining fluxes in the fuel pins are in good agreement with both DOT-III and TWOTRAN-II. Additionally, in the corners of the geometry, JTC underpredicts the fast energy group fluxes and overpredicts the fluxes in the thermal energy group. Comparison of the TWOTRAN-II solution to the DOT-III solution shows identical characteristics in the corners. Examining Table A.3 shows that JTC does not overpredict the fluxes by more than 1.2% or underpredict them by more than 2.3%. We conclude from the benchmark study that JTC is well suited for analyzing fuel assemblies.

2.3 NDT Description

NDT is a multigroup, three-dimensional, Cartesian geometry, nodal diffusion theory code designed to test methods to improve homogenized parameters. As an overview, the code has four flux approximations available, it uses no acceleration technique, and it adjusts homogenized parameters based on current-to-flux ratios.

The neutron diffusion equation is

$$-D_g\frac{\partial^2}{\partial x^2}\phi_g - D_g\frac{\partial^2}{\partial y^2}\phi_g - D_g\frac{\partial^2}{\partial z^2}\phi_g + \sigma_g^t\phi_g = \frac{1}{k_{eff}}\chi_g\sum_{g'=1}^{G}\nu\sigma_{g'}^f\phi_{g'} + \sum_{g'=1}^{G}\sigma_{g'\to g}^s\phi_{g'} \tag{2.15}$$

where

$$\sigma_g^t = \sigma_g^a + \sum_{g'=1}^{G}\sigma_{g\to g'}^s \tag{2.16}$$

The source term and total cross section in equations (2.15) and (2.16) include the within group scattering terms for stability reasons. Neglecting this term causes NDT to become unstable and diverge away from a solution.

NDT employs the transverse integration procedure.[5] This procedure breaks the three-dimensional diffusion equation into three one-dimensional equations with constant leakage terms. The leakage term in the x direction is

$$L_g^x = \frac{1}{\Delta x}\left(J_{g,x}^{+} - J_{g,x}^{-}\right) \tag{2.17}$$

where the superscripts - and + refer to the left and right sides of the node respectively. Currents moving to the right have positive values and currents moving to the left have negative values. The y and z directions have similar leakage terms. With the transverse integrated procedure, the diffusion equation becomes

$$-D_g \frac{\partial^2}{\partial x^2}\phi_g + \sigma_g^t \phi_g = \frac{1}{k_{eff}} \chi_g \sum_{g'=1}^{G} \nu\sigma_{g'}^f \phi_{g'} + \sum_{g'=1}^{G} \sigma_{g'\to g}^s \phi_{g'} - L_g^y - L_g^z \tag{2.18}$$

for the x direction with similar equations for the y and z directions.

The four flux approximations are the mesh centered finite difference, volume averaged finite difference, quadratic polynomial, and quartic polynomial approximations. In the mesh centered finite difference approximation, the flux in the center of the node is assumed to equal the average flux of the node. In this case, the second order derivative in the x direction is

$$\frac{1}{(\Delta x)^2}\left(2\phi_g^- - 4\phi_g^{ave} + 2\phi_g^+\right) \quad . \tag{2.19}$$

For the volume averaged finite difference approximation, the average flux in the node is a volume weighted quantity found from the values of the two edge fluxes and the center flux. The average flux for this assumption is

$$\phi_g^{ave} = \frac{1}{4}\phi_g^- + \frac{1}{2}\phi_g^c + \frac{1}{4}\phi_g^+ \tag{2.20}$$

where ϕ_g^c is the center flux value. It follows that the second order derivative is

$$\frac{1}{(\Delta x)^2}\left(4\phi_g^- - 8\phi_g^{ave} + 4\phi_g^+\right) \quad . \tag{2.21}$$

The polynomial used in the quadratic flux approximation is

$$\phi_g\left(\frac{x}{\Delta x}\right) = \phi_g^{ave} + \left(\phi_g^+ - \phi_g^-\right)\frac{x}{\Delta x} + \left(\phi_g^+ + \phi_g^- - 2\phi_g^{ave}\right)\left(3\left(\frac{x}{\Delta x}\right)^2 - \frac{1}{4}\right) \tag{2.22}$$

leading to a second order derivative of

$$\frac{1}{(\Delta x)^2}\left(6\phi_g^- - 12\phi_g^{ave} + 6\phi_g^+\right) \quad . \tag{2.23}$$

The polynomial used in the quartic flux approximation is

$$\begin{aligned}\phi_g\left(\frac{x}{\Delta x}\right) = \phi_g^{ave} + \left(\phi_g^+ - \phi_g^-\right)\frac{x}{\Delta x} + \left(\phi_g^+ + \phi_g^- - 2\phi_g^{ave}\right)\left(3\left(\frac{x}{\Delta x}\right)^2 - \frac{1}{4}\right) \\ + \phi_g^4\left(\left(\frac{x}{\Delta x}\right)^3 - \frac{1}{4}\left(\frac{x}{\Delta x}\right)\right) + \phi_g^5\left(\left(\frac{x}{\Delta x}\right)^4 - \frac{3}{10}\left(\frac{x}{\Delta x}\right)^2 + \frac{1}{80}\right)\end{aligned} \tag{2.24}$$

where the terms ϕ_g^4 and ϕ_g^5 are the fourth and fifth polynomial coefficients, respectively. This polynomial leads to the second order derivative

$$\frac{1}{(\Delta x)^2}\left(6\phi_g^- - 12\phi_g^{ave} + 6\phi_g^+ + \frac{2}{5}\phi_g^5\right) \quad . \tag{2.25}$$

The moments weighing technique[5] is a method to find the fourth and fifth polynomial coefficients. In the technique, the spatially dependent neutron balance equation is multiplied by the first moment, $\frac{x}{\Delta x}$, and integrated over the width of the node. Then, the spatially dependant neutron balance equation is multiplied by the second moment, $3\left(\frac{x}{\Delta x}\right)^2 - \frac{1}{4}$, and again integrated over the width of the node. The transverse direction leakage terms are expanded into quadratic polynomials for the integration. This technique

results in a representation of the flux profile across the node that is superior to the finite difference and quadratic polynomial approximations."

Adjacent nodes are coupled together by the continuity of flux condition and the continuity of current equation. The continuity of flux equation is that shown by equation (1.9) or

$$f^{+}_{g,i}\phi^{+}_{g,i} = f^{-}_{g,i+1}\phi^{-}_{g,i+1} \tag{2.26}$$

where i and $i+1$ are node indexes. The continuity of current equation is

$$J^{+}_{g,i} = J^{-}_{g,i+1} \quad . \tag{2.27}$$

Equation (2.27) is expanded using Fick's Law to rid the equations of net currents in favor of fluxes and, in the quartic polynomial case, the fourth and fifth polynomial coefficients. The continuity of current equation becomes

$$-\frac{D_i}{\Delta x_i}\left(2\phi_i^{+}-2\phi_i^{ave}\right)=-\frac{D_{i+1}}{\Delta x_{i+1}}\left(2\phi_{i+1}^{ave}-2\phi_{i+1}^{-}\right)$$

$$-\frac{D_i}{\Delta x_i}\left(3\phi_i^{+}+\phi_i^{-}-4\phi_i^{ave}\right)=-\frac{D_{i+1}}{\Delta x_{i+1}}\left(4\phi_{i+1}^{ave}-3\phi_{i+1}^{-}-\phi_{i+1}^{+}\right)$$

$$-\frac{D_i}{\Delta x_i}\left(4\phi_i^{+}+2\phi_i^{-}-6\phi_i^{ave}\right)=-\frac{D_{i+1}}{\Delta x_{i+1}}\left(6\phi_{i+1}^{ave}-4\phi_{i+1}^{-}-2\phi_{i+1}^{+}\right) \qquad (2.28)$$

$$-\frac{D_i}{\Delta x_i}\left(4\phi_i^{+}+2\phi_i^{-}-6\phi_i^{ave}+\frac{1}{2}\phi_i^{4}+\frac{1}{5}\phi_i^{5}\right)=$$

$$-\frac{D_{i+1}}{\Delta x_{i+1}}\left(6\phi_{i+1}^{ave}-4\phi_{i+1}^{-}-2\phi_{i+1}^{+}+\frac{1}{2}\phi_{i+1}^{4}-\frac{1}{5}\phi_{i+1}^{5}\right)$$

for the mesh centered finite difference, volume averaged finite difference, quadratic polynomial, and quartic polynomial approximations, respectively.

The boundary condition can be either zero scalar flux or zero net current. The boundary condition equations, coupling equations, and neutron balance equations form a well-posed problem with a unique solution for the scalar fluxes. The power method described in the previous section is also used in NDT to iterate to the largest eigenvalue, K_{eff}. For comparison, at the end of the outer iterations, NDT also computes the multiplication factor by dividing the production of neutrons by the absorption and leakage of neutrons. When the solution has converged, the multiplication factor from the two different methods should be equal.

At the end of a series of outer iterations (flux and eigenvalue iterations), NDT has very good estimates for the currents at the node boundaries and the average fluxes within the nodes. This information is used to adjust the homogenized parameters to more accurate values based on equation (1.13) with predetermined correlation coefficients. After making the adjustments, the flux and eigenvalue iteration process continues using the improved homogenized parameters.

Benchmark results for NDT are provided in Appendix B. The benchmark problem is the three-dimensional IAEA LWR model.[31] The reference solution to the benchmark problem is a fine mesh VENTURE solution (finite difference). Also given is the solution from QUANDRY.[1] This solution is an analytic solution to the nodal diffusion equations. For still another comparison, the IQSBOX solution[31] to the benchmark problem is provided in Appendix B. This solution is a fifth order polynomial flux approximation. Both QUANDRY and IQSBOX use the quadratic transverse leakage approximation. NDT results are provided in Table B.2 along with the VENTURE, QUANDRY, and IQSBOX solutions. Examining Table B.2 shows excellent agreement in the multiplication factor and the fuel assembly peaking factors for the quartic polynomial approximation in NDT. However, the finite difference solution and the quadratic solution from NDT both show larger errors in the multiplication factor and show an in/out flux tilt. These errors are due to a combination of the low order flux approximation and neglecting the transverse leakage shape. The quartic polynomial flux approximation in NDT using the quadratic transverse leakage shape does show results consistent with the other documented

solutions. The NDT quartic polynomial solution shows a slight in/out flux tilt but its cause is due to the boundary condition in NDT. All three NDT solutions use a zero scalar flux boundary condition for the external boundaries where the benchmark problem specifies no incoming current. Therefore, the scalar fluxes at the external boundaries are lower in NDT than the other solutions. This propagates through the geometry causing the power peaking factors in the outer fuel assemblies to be low and causing them to be high in the center of the reactor core.

2.4 Conclusions for the JTC and NDT Computer Codes

The neutronics of JTC and NDT have been presented in this chapter. Benchmark problems for the two codes demonstrate that both codes are sufficiently accurate for the analysis work performed in this thesis. JTC shows errors in strong absorber fuel pins for two-dimensional geometries. However, in one-dimensional situations, the streaming term and scattering terms in JTC do not contain any approximations to the discrete ordinates equations. The NDT results show that the finite difference and quadratic polynomial flux approximations are inaccurate, but the quartic polynomial flux approximation is accurate. These results are used in Chapter IV to illustrate the robustness of using correlated homogenized parameters.

An important feature of JTC is the flexible boundary conditions. The benchmark problem does not test to ensure that the boundary condition is correct, however, reference problems used in Chapter III do. The reference problems in Chapter III are

one-dimensional heterogeneous regions. At interfaces of adjacent heterogeneous regions, the odd moments are recorded and used as boundary conditions. Analysis of the geometries in Chapter III prove that the flexible boundary conditions do reproduce the reference results for one-dimensional cases.

Reference problems used in Chapter IV show consistency between JTC and NDT. The geometries of Chapter IV were used to ensure that homogenized parameters computed in JTC will reproduce reference results when used in NDT. This simply exhibits that NDT employs the homogenized parameters in a method compatible with how JTC computes them.

CHAPTER III

DEVELOPMENT OF A METHOD TO IMPROVE HOMOGENIZED PARAMETERS IN A ONE-DIMENSIONAL GEOMETRY

3.1 Chapter III Objectives

A method is developed in this chapter to obtain approximate correlations for homogenized parameters for one-dimensional geometries. To explore this method, two models are chosen which have certain characteristics common to BWRs and PWRs. The basis of the method relies on the general ability to correlate homogenized parameters rather than to derive a correlation through theoretical analysis. Therefore, the approach taken is to show that a general polynomial correlation will reduce to a simple form without a great loss of accuracy.

In the cases examined in this chapter, the lattice homogenization solution is an S_{16} discrete ordinates calculation using P_3 scattering cross sections and four meshes per centimeter. The flux approximation in the nodal code is the quadratic polynomial,

$$\phi(\xi) = \phi^{ave} + A\xi + B\left(3\xi^2 - \frac{1}{4}\right) \qquad \xi \equiv \frac{x}{h} \qquad -\frac{1}{2} \le \xi \le \frac{1}{2} \tag{3.1}$$

where h is the node width. Equation (3.1) defines the edge fluxes to be

$$\phi^{-} = \phi\left(\xi = -\frac{1}{2}\right)$$
$$\phi^{+} = \phi\left(\xi = \frac{1}{2}\right) . \tag{3.2}$$

These relations are necessary to find the quadratic coefficients A and B. The quadratic coefficients are shown explicitly in equation (2.22). The homogenization process requires knowledge of the nodal code flux approximation only to compute values of the flux discontinuity factors. As seen in the denominator of equation (1.7), the flux discontinuity factor is dependent on the nodal code flux approximation.

3.2 Test Geometries and Reference Solutions

The characteristic chosen to represent BWR and PWR fuel assemblies is the water gap width between the fuel assemblies. The BWR emulation contains a two centimeter water gap at the interface between adjacent fuel assemblies (one centimeter in each of the adjacent assemblies). The PWR emulation does not contain a water gap between adjacent assemblies. Both situations also contain heterogeneities (a neutron absorber and a moderator) designed to give a distinctive flux shape in the interior of the center fuel assembly and, therefore, result in unique flux and volume weighted homogenized cross sections.

The geometries for the two problem situations and the material cross sections used in the various regions within the geometry are given on the following pages. In both geometries, the two outer regions serve as buffer regions to provide realistic angular fluxes (and therefore moments of the angular flux) at the interface between assemblies and provide a global flux tilt. This supplies non-trivial interface conditions for the boundaries of the center assembly. Correlations are developed only for the center assembly.

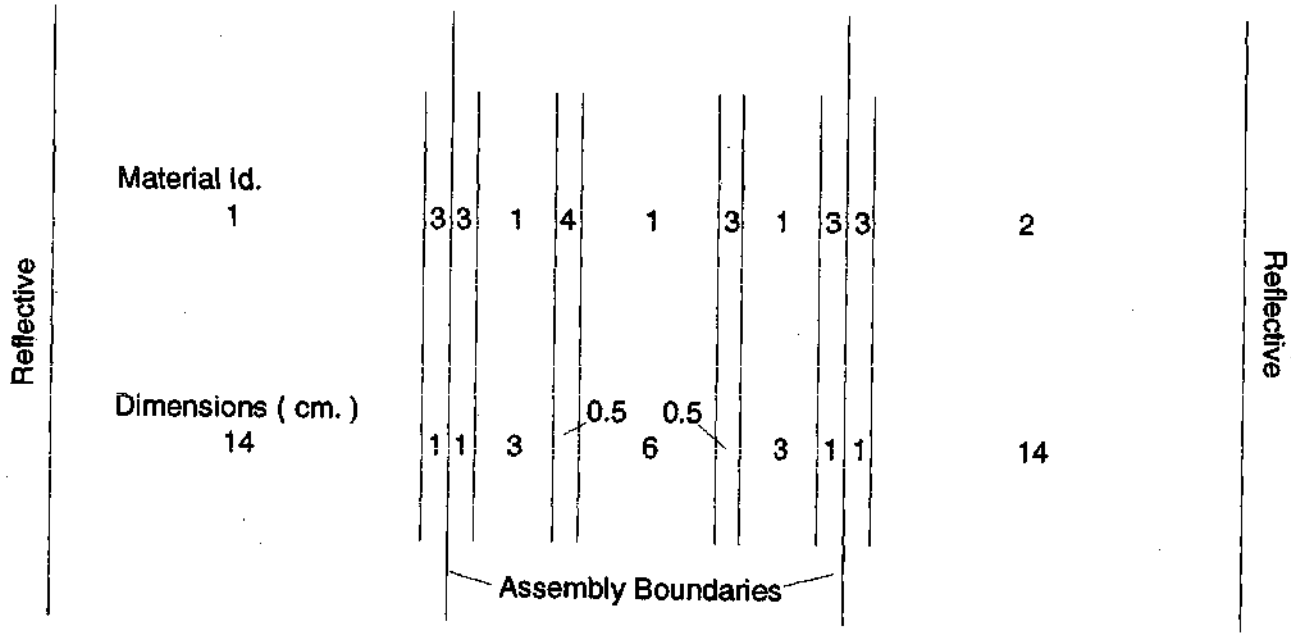

Figure 3.1. Reference 1-D BWR Geometry.

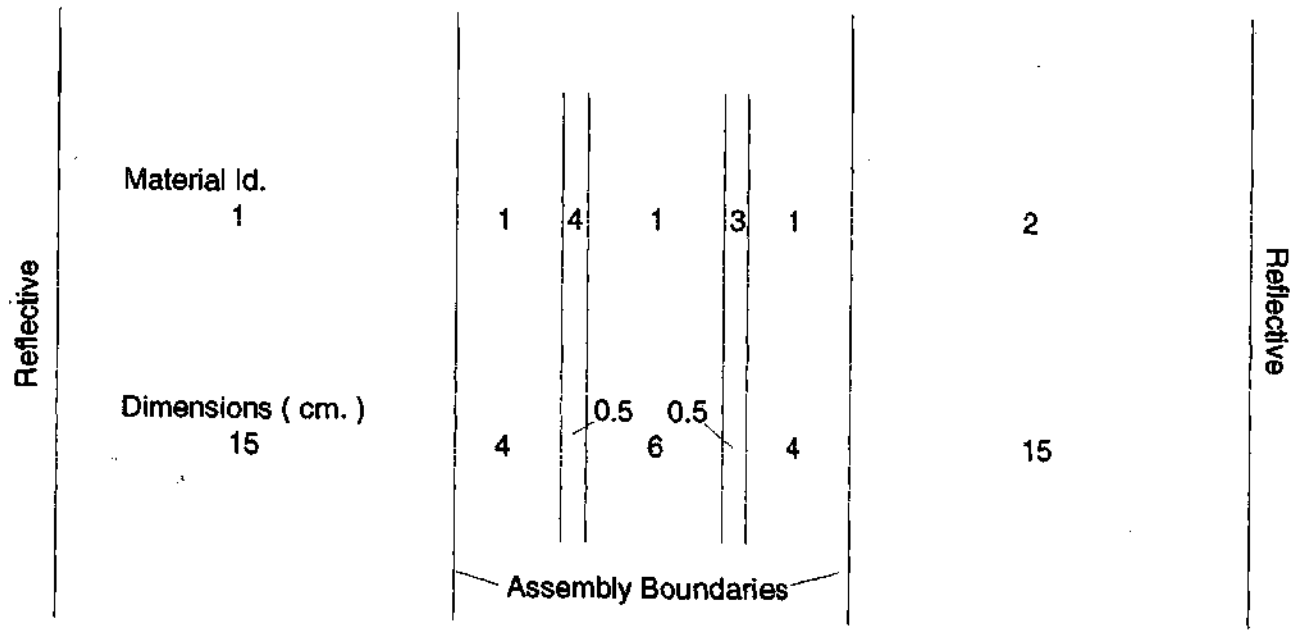

Figure 3.2. Reference 1-D PWR Geometry.

Table 3.1. Reference Transport Theory Cross Sections for the One-Dimensional Studies. cm^{-1} (No upscattering)

Material	Group	Σ_a	Σ_f	$\nu\Sigma_f$
1	1	1.016e-02	2.876e-03	7.346e-03
(Fuel)	2	1.003e-01	6.171e-02	1.504e-01
2	1	9.399e-03	2.274e-03	5.872e-03
(Fuel)	2	7.989e-02	4.346e-02	1.059e-01
3	1	9.461e-04	0	0
(Water)	2	3.639e-02	0	0
4	1	9.699e-03	0	0
(Absorber)	2	3.398e-01	0	0

	Scattering	Energy Group		
Material	Order	1 to 1	1 to 2	2 to 2
1	P_0	5.087e-01	1.557e-02	1.150e+00
(Fuel)	P_1	1.706e-01	3.981e-03	3.089e-01
	P_2	5.893e-02	0	0
	P_3	1.961e-02	0	0
2	P_0	5.099e-01	1.614e-02	1.173e+00
(Fuel)	P_1	1.712e-01	4.170e-03	3.087e-01
	P_2	5.909e-02	0	0
	P_3	1.960e-01	0	0
3	P_0	6.018e-01	3.570e-02	2.005e+00
(Water)	P_1	2.439e-01	7.074e-03	5.550e-01
	P_2	5.407e-02	0	0
	P_3	3.369e-03	0	0
4	P_0	4.325e-01	1.080e-02	8.745e-01
(Absorber)	P_1	1.399e-01	2.103e-03	2.662e-01
	P_2	4.523e-02	0	0
	P_3	9.274e-03	0	0

The reference scalar flux profiles shown in Figures 3.3 and 3.4 are necessary to compute the reference homogenized parameters. The heterogeneous cross sections and diffusion coefficients are flux and volume weighted to obtain homogenized parameters and equation (1.7) specifies how to compute the reference flux discontinuity factors. The reference homogenized parameters are provided in Table 3.2. Besides reference homogenized parameters, the ratios of the edge flux to the average flux for the center region is also furnished in Table 3.2. The usefulness of the edge-to-average flux ratios is discussed in the Section 3.4.

From the reference solution, the odd moments of the angular flux at the boundaries of the center region are given in Table 3.3. These odd moments can serve as boundary conditions to one region problems. For example, in one-dimensional cases only, we can use JTC to regenerate the reference homogenized parameters without the two outer buffer regions shown in Figure 3.1 or 3.2. This is achieved by using the odd moments shown in Table 3.3 as boundary conditions to the center assembly. This exercise serves as a test to ensure that the boundary condition for JTC discussed in Chapter II functions correctly. The average fluxes in the center regions is also given in Table 3.3. These values are necessary for normalization.

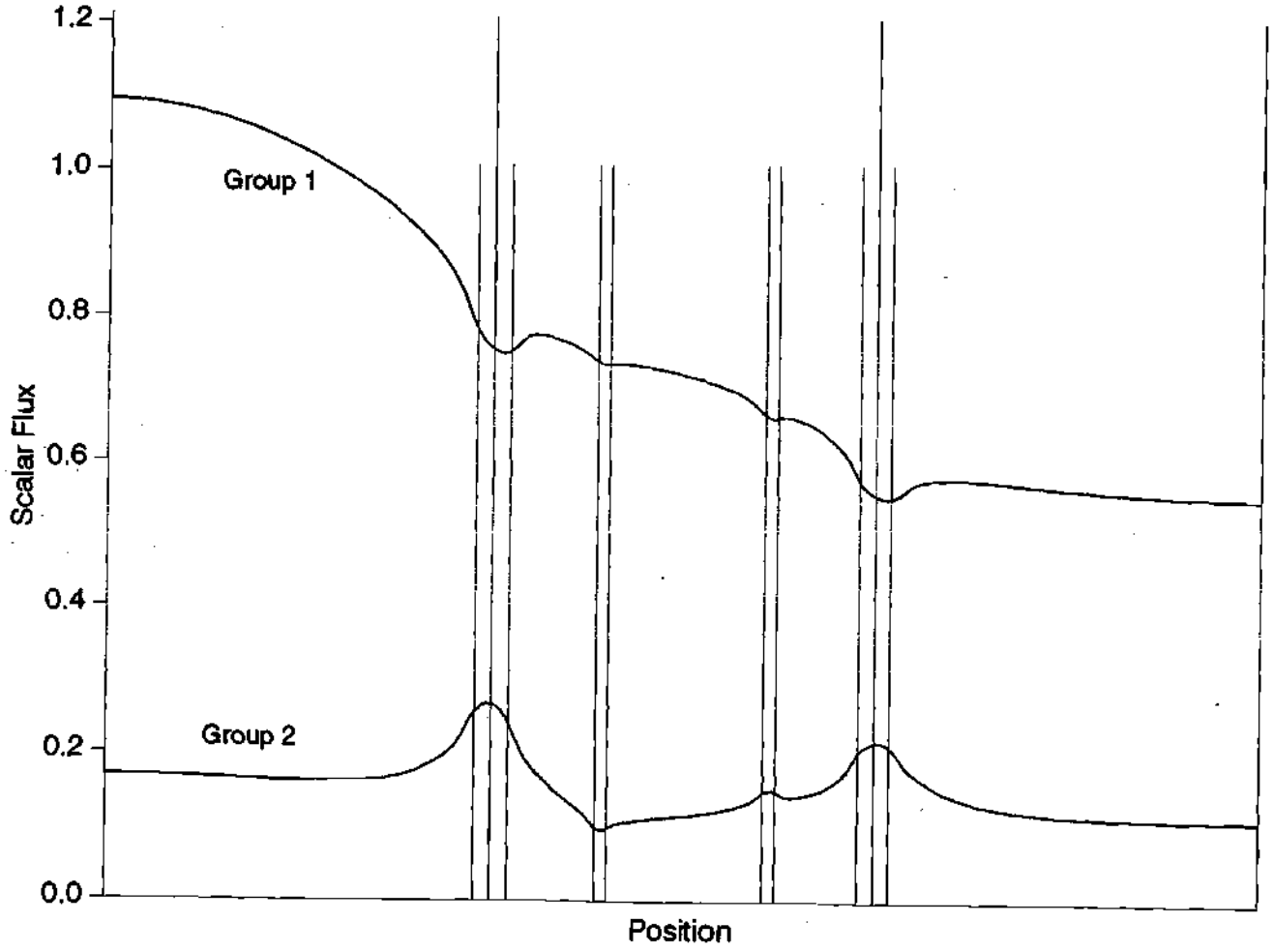

Figure 3.3. Reference Scalar Flux Profile for the BWR Geometry.

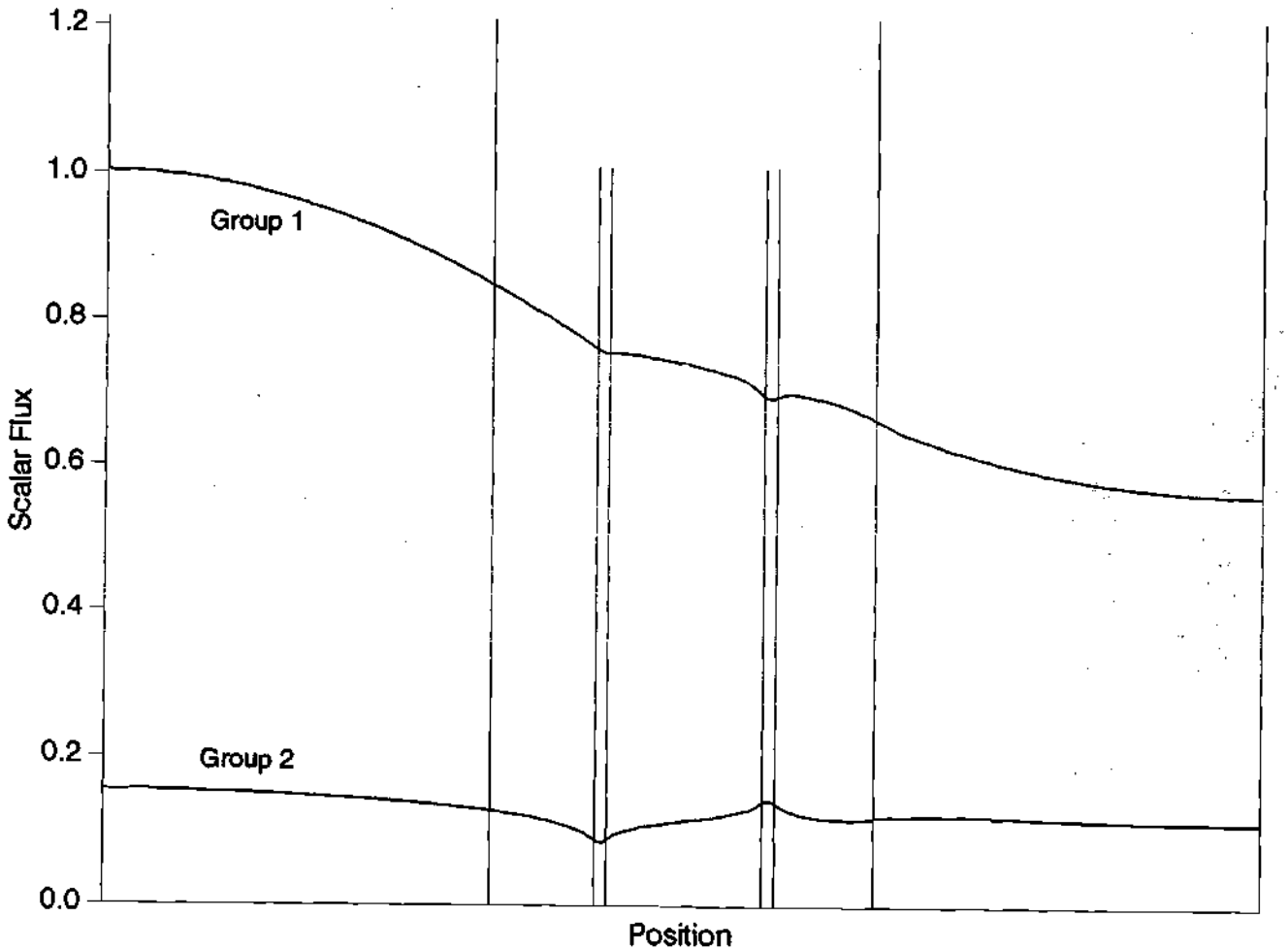

Figure 3.4. Reference Scalar Flux Profile for the PWR Geometry.

Table 3.2 Reference Homogenized Parameters for the Sample BWR and PWR Geometries.

BWR

Group	D (cm)	Σ_a (cm^{-1})	Σ_f (cm^{-1})	$\nu\Sigma_f$ (cm^{-1})	$\Sigma_{s\,1\text{-}2}$ (cm^{-1})
1	1.40533	8.69938e-03	2.32471e-03	5.93787e-03	1.85594e-02
2	0.39892	9.01053e-02	4.54538e-02	1.10780e-01	

	FDF		Edge-to-Average Flux Ratio	
Group	Left	Right	Left	Right
1	0.93597	0.89776	1.07491	0.78765
2	1.56928	1.58288	1.82868	1.48345

PWR

Group	D (cm)	Σ_a (cm^{-1})	Σ_f (cm^{-1})	$\nu\Sigma_f$ (cm^{-1})	$\Sigma_{s\,1\text{-}2}$ (cm^{-1})
1	1.35796	9.85700e-03	2.68851e-03	6.86710e-03	1.60355e-02
2	0.43343	1.03593e-01	5.76834e-02	1.40586e-01	

	FDF		Edge-to-Average Flux Ratio	
Group	Left	Right	Left	Right
1	1.01920	1.00857	1.14416	0.89275
2	0.99639	0.98442	1.09943	1.02672

Table 3.3. Reference Odd Moments of the Angular Flux at the Boundaries of the Center Region and Reference Average Fluxes.

		BWR		PWR	
Moment	Group	Left	Right	Left	Right
1	1	2.29946e-02	1.27787e-02	1.75466e-02	1.44103e-02
	2	2.09142e-03	-3.09804e-04	1.68857e-03	-1.27995e-03
3	1	-1.03634e-04	-3.58409e-04	-2.29030e-04	-1.23542e-03
	2	-1.80008e-05	-1.03898e-05	1.56353e-05	2.70164e-04
5	1	-7.98326e-05	-1.28025e-05	-1.35203e-05	5.03508e-04
	2	3.73161e-06	6.54685e-06	-5.06405e-07	-1.04958e-04
7	1	4.01471e-05	4.52050e-05	7.41994e-06	-2.98796e-04
	2	-1.00898e-07	-2.61790e-07	-2.90088e-07	6.47520e-05
9	1	-2.08952e-05	-3.99888e-05	-1.39822e-06	2.22913e-04
	2	-4.67127e-07	-8.57474e-07	2.37903e-08	-4.95458e-05
11	1	1.65230e-05	3.44251e-05	5.21561e-07	-1.95939e-04
	2	3.94900e-07	7.63833e-07	-2.53980e-09	4.36529e-05
13	1	-2.13205e-05	-3.02109e-05	-2.42737e-06	2.00342e-04
	2	-4.40541e-08	-1.07379e-07	5.63131e-08	-4.39385e-05
15	1	2.60125e-05	1.06828e-05	-1.79550e-06	-2.49298e-04
	2	-1.19097e-06	-1.52759e-06	4.91183e-07	5.35428e-05
		Average Flux			
	1	7.04241e-01		7.43327e-01	
	2	1.46832e-01		1.16972e-01	

3.3 Analysis Procedure

The analysis procedure is to attempt to reconstruct reference homogenized parameters by using initial homogenized parameters and correction components. Zero net current (or reflective) boundary conditions are placed on the boundaries of the center region shown in Figures 3.1 and 3.2. This will generate, in JTC, the initial homogenized parameters for the center node for each of the two geometries. These values are provided in Table 3.4.

The correction component for a homogenized parameter is defined as a change from the initial homogenized parameter caused by placing odd moments of the angular flux on the node boundaries. By defining the correction component in this manner, the correction component can include contributions:

- from polynomial terms in a general correlation,
- from using higher ordered odd moments for the boundary condition, and
- from cross product terms involving different energy groups and different node faces.

The correction component is a sum of different combinations of the contributions listed above. By defining the correction component this way, we do not have any information as to how the various effects interact with each other or how much each effect contributes to the correction component. However, it does provide a means to figure out how much neglecting a certain effect has on the reconstructed homogenized parameter.

The reconstructed homogenized parameter is the initial homogenized parameter plus the correction component (or components) required to re-establish the reference currents on all node surfaces and energy groups. If a certain effect is neglected, then summing the initial homogenized parameter to the proper correction components will result in a reconstructed homogenized parameter that is not equal to the reference homogenized parameter. The difference between the reconstructed homogenized parameter and the reference homogenized parameter is related to the error. Thus, the error in a homogenized parameter is given by

$$Error = \frac{Reference - Reconstructed}{Reference} \quad . \tag{3.3}$$

If the error is small, then the effect being tested is weak and the general polynomial correlation will reduce to a simpler form.

Table 3.4 Initial (Infinite Lattice) Homogenized Parameters for the Sample BWR and PWR Geometries.

BWR

Group	D (cm)	Σ_a (cm^{-1})	Σ_f (cm^{-1})	$\nu\Sigma_f$ (cm^{-1})	$\Sigma_{s\,1\text{-}2}$ (cm^{-1})
1	1.40533	8.69485e-03	2.33061e-03	5.95295e-03	1.85848e-02
2	0.39892	8.98508e-02	4.57609e-02	1.11529e-01	

	FDF		Edge-to-Average Flux Ratio	
Group	Left	Right	Left	Right
1	0.86899	0.95108	0.86899	0.95108
2	1.45919	1.71854	1.45919	1.71854

PWR

Group	D (cm)	Σ_a (cm^{-1})	Σ_f (cm^{-1})	$\nu\Sigma_f$ (cm^{-1})	$\Sigma_{s\,1\text{-}2}$ (cm^{-1})
1	1.35796	9.83579e-03	2.68823e-03	6.86640e-03	1.60953e-02
2	0.43343	1.03016e-01	5.75925e-02	1.40365e-01	

	FDF		Edge-to-Average Flux Ratio	
Group	Left	Right	Left	Right
1	0.96489	1.05794	0.96489	1.05794
2	0.90820	1.09680	0.90820	1.09680

Examining the root mean square (RMS) error for distinct categories of homogenized parameters gives a general indication for the strength or weakness of a particular correlation event. There are three distinct categories of homogenized parameters; cross sections, flux discontinuity factors, and edge-to-average flux ratios from the lattice homogenization solution. The RMS errors for each category of homogenized parameters for both test geometries are presented in the text of this chapter and individual errors of the homogenized parameters are listed in tables in Appendix C. The RMS errors in the initial homogenized parameters are shown in Table 3.5. RMS errors in the cross section category include errors in the absorption, production, and downscatter cross sections only. The error in the fission cross section is identical to the error in the production cross section, therefore, including both would be redundant. Errors in the diffusion coefficients are excluded from the RMS errors. Using the ideas presented in Section 1.2 for formally exact homogenization, we can explicitly alter the diffusion coefficient to the reference diffusion coefficient and allow the flux discontinuity factors to adjust accordingly. As addressed in Section 1.2 for generalized equivalence theory, there exist an infinite set of diffusion coefficients and flux discontinuity factors that can all produce identical results. However, it is incorrect to compare the different sets of diffusion coefficients and flux discontinuity factors and form errors if all sets produce the same result in a nodal analysis. Accordingly, to generate errors for the flux discontinuity factors, the analysis procedure requires the diffusion coefficients to equal the reference diffusion coefficients. The diffusion coefficients in Table 3.4 were manually changed to

the reference values. Changing the diffusion coefficients cannot affect the initial flux discontinuity factors because, with reflective boundary conditions, the nodal flux shape is always flat. This causes the initial flux discontinuity factor to equal the initial edge-to-average flux ratio.

Table 3.5. RMS Errors in the Initial (Infinite Lattice) Homogenized Parameters.

BWR	
Cross Sections	0.3529%
Flux Discontinuity Factors	7.2311%
Edge-to-Average Flux Ratios	19.0849%
PWR	
Cross Sections	0.3226%
Flux Discontinuity Factors	8.0780%
Edge-to-Average Flux Ratios	15.3052%

The coupling characteristics (energy group and node face), boundary condition specification, and polynomial fitting are examined in this chapter. We can avoid assumptions in the analysis procedure by finding errors from these effects in the order mentioned. By using all the odd moments as boundary conditions for the coupling characteristics, there are no approximations in the boundary conditions or any polynomial fit associated with the correlation. Thus the correction components have lumped these effects into one term. Similarly, by using the reference currents only, we can analyze approximations for boundary conditions without any information of an accurate polynomial fit for the homogenized parameters.

Referring to equation (1.13) shows that the current is normalized to the average flux. This choice of normalization allows the correlation to perform at all power levels. However, there are other choices to consider. For instance, the scalar flux on the boundary of the node could normalize the current and other odd moments rather than the average flux of the node. However, this choice of normalization is unsuitable because, without an exact reference boundary condition (i.e., a current and higher odd moments), the edge flux is likely to have significant errors that can easily propagate in the correlations. A simpler view of this is that the edge fluxes are much more sensitive to a boundary condition than the average flux. Another choice is to normalize the current and odd moments to a reaction rate. However, normalizing the current in a region such as the reflector would create problems with this choice. The reflector has no power output from fission and the absorption reaction rate is very small. Therefore, this choice of

normalization is not the best choice either. Thus, the choice of normalization shown in equation (1.13) is the best decision.

3.4 Coupling Characteristics

Energy Group Coupling

The coupling relationship between the fast and thermal energy groups of the two group problems is examined in this segment. We can find the correction components associated with the fast energy group by using the reference boundary conditions for the fast energy group on both surfaces and reflective boundary conditions for the thermal energy group on both surfaces. A similar procedure finds the correction components associated with thermal energy group currents. The correction components include coupling between the two node faces so that any node face coupling errors are not present.

Errors in the reconstructed homogenized parameters for both geometries are displayed in Table C.1. Trends in Table C.1 are also seen in Table 3.6 below. Examining Table 3.6 shows that the RMS errors of the reconstructed homogenized parameters are less than errors in the initial homogenized parameters seen in Table 3.5 for all three categories of homogenized parameters. In comparing Tables 3.5 and 3.6, the errors in the homogenized cross sections and in the edge-to-average flux ratios dramatically decreased by a factor of 50 and higher. However, the flux discontinuity factors moderately improved

by a factor of 10 or less. This small improvement in the flux discontinuity factor suggests that the fast and thermal energy groups do contain significant cross product terms.

Table 3.6. RMS Errors in the Energy Group Reconstructed Homogenized Parameters.

BWR	
Cross Sections	0.0053%
Flux Discontinuity Factors	1.4065%
Edge-to-Average Flux Ratios	0.2163%
PWR	
Cross Sections	0.0065%
Flux Discontinuity Factors	0.8497%
Edge-to-Average Flux Ratios	0.2081%

Expanding equation (1.7) illustrates a major cause of the energy group coupling for the flux discontinuity factors. Since equivalence theory states that the average flux in the nodal code must equal the average flux of the reference solution, we can divide the numerator and denominator of equation (1.7) by the average flux for energy group g as seen in equation (3.4). The numerator of equation (3.4) is the edge-to-average flux ratio from the lattice homogenization code. This value depends on the current-to-flux ratios from all energy groups and node faces. The denominator of equation (3.4) is derived directly by applying Fick's law to each surface of the node. Thus, the denominator of

equation (3.4) is also a function of the current-to-flux ratios. Dividing the numerator by the denominator produces cross product terms between the different current-to-flux ratios.

$$f_g^k = \frac{\left(\frac{\bar{\phi}_g^k}{\phi_g^{ave}} \right)_{cor}}{\left(\frac{\hat{\phi}_g^k}{\phi_g^{ave}} \right)_{nodal}} \tag{3.4}$$

Fick's law provides the relationship between the current on a node boundary and the flux values for a given nodal flux approximation. For the quadratic polynomial of equation (3.1), the denominator of equation (3.4) for the left or right boundary of the node is

$$\begin{aligned} \frac{\hat{\phi}_g^-}{\phi_g^{ave}} &= 1 + \frac{h}{6 D_g}\left(2\frac{\hat{J}_g^-}{\phi_g^{ave}} + \frac{\hat{J}_g^+}{\phi_g^{ave}} \right) \\ \frac{\hat{\phi}_g^+}{\phi_g^{ave}} &= 1 - \frac{h}{6 D_g}\left(\frac{\hat{J}_g^-}{\phi_g^{ave}} + 2\frac{\hat{J}_g^+}{\phi_g^{ave}} \right) \end{aligned} \tag{3.5}$$

where h is the width of the node, $-$ represents the left boundary, and $+$ represents the right boundary.

Correlating edge-to-average flux ratios from the lattice homogenization procedure and using them to find the flux discontinuity factors allows us to easily account for the dominating cross product terms in the flux discontinuity factors. The procedure to

improve the flux discontinuity factors is demonstrated in Table 3.7 and the resulting errors that remain in the flux discontinuity factors are given. The first column of Table 3.7 is the edge-to-average flux ratios for a nodal code using the quadratic flux polynomial (equation (3.5)) for the two reference geometries. Values for the currents and average fluxes are provided by Table 3.3 and the diffusion coefficients are from Table 3.2. These values and the reconstructed edge-to-average flux ratio from the lattice homogenization are employed in equation (3.4) to produce the second column; the alternative method for reconstructing flux discontinuity factors. Errors in the flux discontinuity factors from this alternative approach are shown in the third column. The error column clearly shows that flux discontinuity factors found by employing equation (3.4) are much lower than those found by reconstructing the flux discontinuity factors directly. Using this procedure has reduced the RMS error of the flux discontinuity factors to 0.2163% and 0.2081% for the BWR and PWR geometries, respectively. Since the denominator is a known function derived from Fick's law, the error in the flux discontinuity factor is equal to the error in the reconstructed edge-to-average flux ratio.

Table 3.7. Flux Discontinuity Factors and Errors Computed by the Alternative Method for the Energy Group Coupling.

Face (Group)	Edge-to-Average Flux Ratio (Nodal)	FDF	% Error
	BWR		
Left (1)	1.14845	0.93674	-0.0828%
Right (1)	0.87736	0.89686	0.0997%
Left (2)	1.16530	1.57380	-0.2884%
Right (2)	0.93718	1.57820	0.2957%
	PWR		
Left (1)	1.12261	1.02024	-0.1018%
Right (1)	0.88516	1.00741	0.1147%
Left (2)	1.10341	0.99918	-0.2800%
Right (2)	1.04297	0.98179	0.2669%

Other than improving the accuracy of the flux discontinuity factors, correlating the edge-to-average flux ratios from the lattice homogenization code shows other benefits over directly correlating the flux discontinuity factors. The flux discontinuity factors are dependent on the flux approximation used in the nodal code. However, the edge-to-average flux ratio correlations from the lattice homogenization are not dependent on the nodal code flux approximation. This means that any nodal code flux approximation can use the correlation. The nodal code can readily figure out the denominator of equation (3.4) for any nodal code flux approximation and in turn, compute the appropriate flux discontinuity factor. Therefore, correlating the edge-to-average flux ratios allows for correction of the nodal code flux approximation.

Another advantage of this approach is that the flux discontinuity factor can correct for any uncertainty in the diffusion coefficient. The edge-to-average flux ratio correlation found from the lattice homogenization is also independent of the diffusion coefficient. However, the edge-to-average flux ratio from the nodal code is dependent on the diffusion coefficient. Again by equation (3.5), changing the diffusion coefficient will change the value of the flux discontinuity factor.

Node Face Coupling

This segment is similar to the preceding segment except the coupling is between the two opposite faces of the node rather than the energy groups. To avoid energy group coupling errors, the energy groups remain coupled together in this segment. Correction components are found for the left and right node faces by using appropriate combinations of reference and reflective boundary conditions. Errors in the reconstructed homogenized parameters are displayed in Table C.2 and the RMS errors of the three different categories of homogenized parameters for both geometries are displayed in Table 3.8.

Comparing Table 3.8 to Table 3.5 shows that errors in the homogenized cross sections and edge-to-average flux ratios significantly reduce for both geometries while the flux discontinuity factors again only moderately reduce. As in the energy group coupling, this suggests that the node face dependency in the cross sections and edge-to-average flux ratios is weak. However, there are significant cross product terms in reconstructing the flux discontinuity factors directly.

Table 3.8. RMS Errors in the Node Face Reconstructed Homogenized Parameters.

BWR	
Cross Sections	0.0053%
Flux Discontinuity Factors	0.5743%
Edge-to-Average Flux Ratios	0.0684%
PWR	
Cross Sections	0.0023%
Flux Discontinuity Factors	0.9703%
Edge-to-Average Flux Ratios	0.0941%

Correlating the edge-to-average flux ratios over the flux discontinuity factors is also supported by the trends seen in Table 3.8. As before, using correlated edge-to-average flux ratios in equation (3.4) results in an easy method to include cross product terms in the flux discontinuity factors. As seen in Table 3.9, the RMS errors in the flux discontinuity factors will easily reduce to 0.0684% and 0.0941% by this approach for the BWR and PWR geometries, respectively. As before, this approach to find the flux discontinuity factor includes effects of the nodal code flux approximation and diffusion coefficient.

Table 3.9. Flux Discontinuity Factors and Errors Computed by the Alternative Method for the Node Face Coupling.

Face (Group)	Edge-to-Average Flux Ratio (Nodal)	FDF	% Error
	BWR		
Left (1)	1.14845	0.93517	0.0858%
Right (1)	0.87736	0.89822	-0.0516%
Left (2)	1.16530	1.56783	0.0924%
Right (2)	0.93718	1.58309	-0.0134%
	PWR		
Left (1)	1.12261	1.01785	0.1331%
Right (1)	0.88516	1.00967	-0.1091%
Left (2)	1.10341	0.99573	0.0655%
Right (2)	1.04297	0.98480	-0.0386%

In conclusion, correlations cannot accurately model the effects that current-to-flux ratios have on the flux discontinuity factors directly. However, an accurate approach to find the flux discontinuity factors is to correlate the edge-to-average flux ratio from the lattice homogenization calculation. This approach is very successful because it is not only accurate, but it accounts for the flux approximation in the nodal code and the diffusion coefficient used for the node. The edge-to-average flux ratio from the nodal code is readily available for use in equation (3.4).

3.5 Boundary Condition Approximations

In the preceding section, all odd moments of the angular flux from the reference calculations provided the boundary conditions for the center region of the two sample geometries. However, if the reference solution is not known, neither are the higher ordered odd moments of the angular flux, particularly the third moment. The third moment plays a more important role in the angular flux shape than the remaining higher odd moments. The boundary condition that best duplicates the third moment of the angular flux (and higher odd moments) and consequently the scalar flux for the sample BWR and PWR geometries is explored in this section.

Common boundary conditions in transport theory codes are reflective, periodic, vacuum, albedo, and white boundary conditions.[34,35,36] Only one of the above boundary conditions can create a current on one surface of a node. Reflective boundary conditions specify that the angular flux that exits a boundary returns into the boundary at its complementary angle. This means that the angular flux is symmetric and, because of the symmetry, this condition cannot create any odd moments of the angular flux. Periodic boundary conditions cannot create a current on only one face of the node. As such, we cannot decouple the node face dependencies of the current and other odd moments to form a correlation. We can view a vacuum boundary condition as an albedo condition that is equal to zero and, therefore, it will not be used. Furthermore, a vacuum boundary condition is unrealistic for fuel lattices. A white boundary condition finds an incoming angular flux (constant for all incoming μ) that does not result in a current. Therefore,

it is also of no use for this analysis. Only the albedo boundary condition can create a current on only one face of the node.

The boundary conditions can be written in a functional form, $\psi(\mu)$, and integrated to find values for the moments of the angular flux. The integral that defines the moments of the angular flux is

$$\phi_n = \frac{1}{2}\int_{-1}^{1} \psi(\mu)\, P_n(\mu)\, d\mu \tag{3.6}$$

where ϕ_n is the n^{th} moment of the angular flux and P_n is the n^{th} Legendre polynomial.[37] The shapes of the angular flux can be described using common geometry functions in *x-y* coordinates and then transformed to polar coordinates to arrive at an expression for $\psi(\mu)$. The relations in equation (3.7) are used to convert from *x-y* to polar coordinates.

$$\begin{aligned} x &= \psi(\mu)\cos\theta = \psi(\mu)\mu \\ y &= \psi(\mu)\sin\theta = \psi(\mu)\sqrt{1-\mu^2} \end{aligned} \tag{3.7}$$

In this section, characteristics of the albedo boundary condition are examined followed by a comparison of the albedo condition to the reference angular flux shapes on the node boundaries. The albedo is shown to be insufficient for creating a current and accurately modelling the node edge scalar flux. Lastly, a boundary condition is proposed

in this section that creates a current and provides good approximations to the node edge scalar flux. Accurately predicting the scalar flux on a node boundary for a given current is a crucial task because the node edge scalar flux defines the flux discontinuity factor.

Albedo Boundary Condition

The albedo boundary condition specifies that a known portion of the current that exits a boundary reflects back into the medium. Mathematically, this is

$$\epsilon = \frac{\psi(\mu)}{\psi(-\mu)} \quad . \tag{3.8}$$

Three possible shapes for the albedo condition are shown in Figure 3.5. The dotted lines represent a constant value and the solid lines represent albedo shapes that are elliptic.

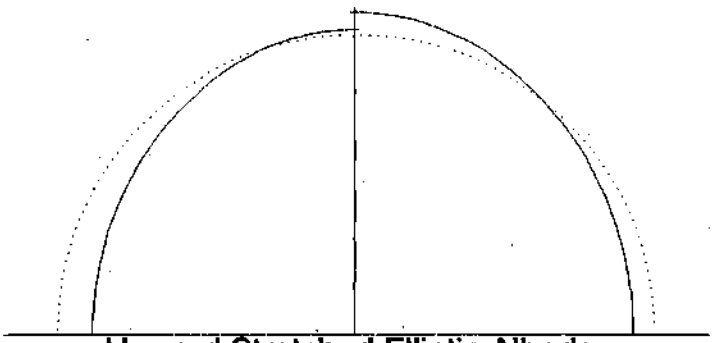

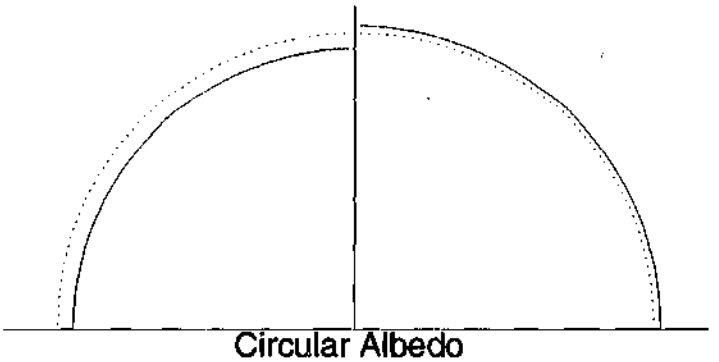

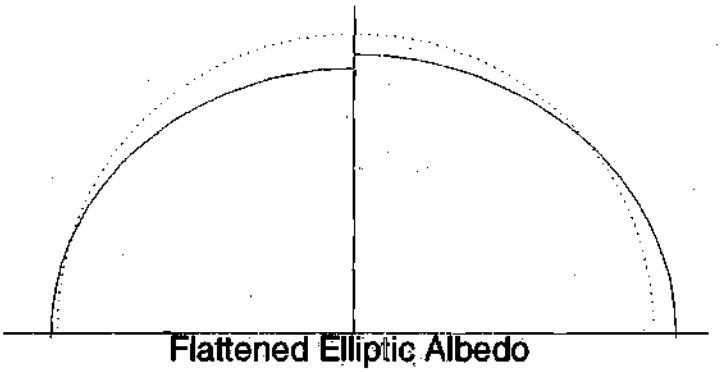

Figure 3.5. Polar Plot of Possible Angular Flux Shapes for an Albedo Boundary Condition.

We can define each shape in Figure 3.5 by the ellipse

$$\left(\frac{x}{a}\right)^2 + \left(\frac{y}{b}\right)^2 = 1 \tag{3.9}$$

and use the transformations in equation (3.7) to write the angular flux shape as

$$\psi(\mu) = \left(\frac{1}{b^2} + \left(\frac{1}{a^2} - \frac{1}{b^2}\right)\mu^2\right)^{-\frac{1}{2}} . \tag{3.10}$$

The constants a and b are different for $\mu > 0$ and $\mu < 0$, but the albedo condition (equation (3.8)) forms a relation between the values. Also, for an upward stretched elliptic albedo, $a < b$; a circular albedo, $a = b$; and a flattened elliptic albedo, $a > b$.

All three shapes show a current arbitrarily moving to the right. Integrating the angular flux shape given in equation (3.10) in equation (3.6) shows that the second moment is negative for an upward stretched ellipse, zero for the circular ellipse, and positive for the flattened ellipse. However, the important feature of the shapes is the value of the third moment relative to the first moment. Regardless of the value of the albedo, the ratio of the third moment to the first moment is constant for any given a and b constants. The ratio of the third moment to the first moment ranges from -0.1 for a

flattened ellipse to -0.4 for an upward stretched ellipse. The ratio is -0.25 for the circular albedo shape. These values cover a wide range of normalized current values.

Reference Angular Flux Shapes on the Node Boundaries

The solutions in this chapter used an S_{16} angular quadrature set which provides several angular fluxes to form a polar plot. Then, it is easy to examine the polar plot and learn characteristics of the angular flux shape in the sample BWR and PWR geometries. This information will reveal if we expect an albedo to reliably serve as a boundary condition.

Figures 3.6 and 3.7 show polar plots of the reference angular fluxes for the BWR and PWR geometries, respectively. The dotted line in each drawing is a constant value equal to the scalar flux for the node face and energy group. The angular fluxes are shown for both energy groups and on both node faces. In each drawing, the first angular flux points to the far right and the sixteenth angular flux points to the far left. The eighth and ninth angular fluxes point upwards.

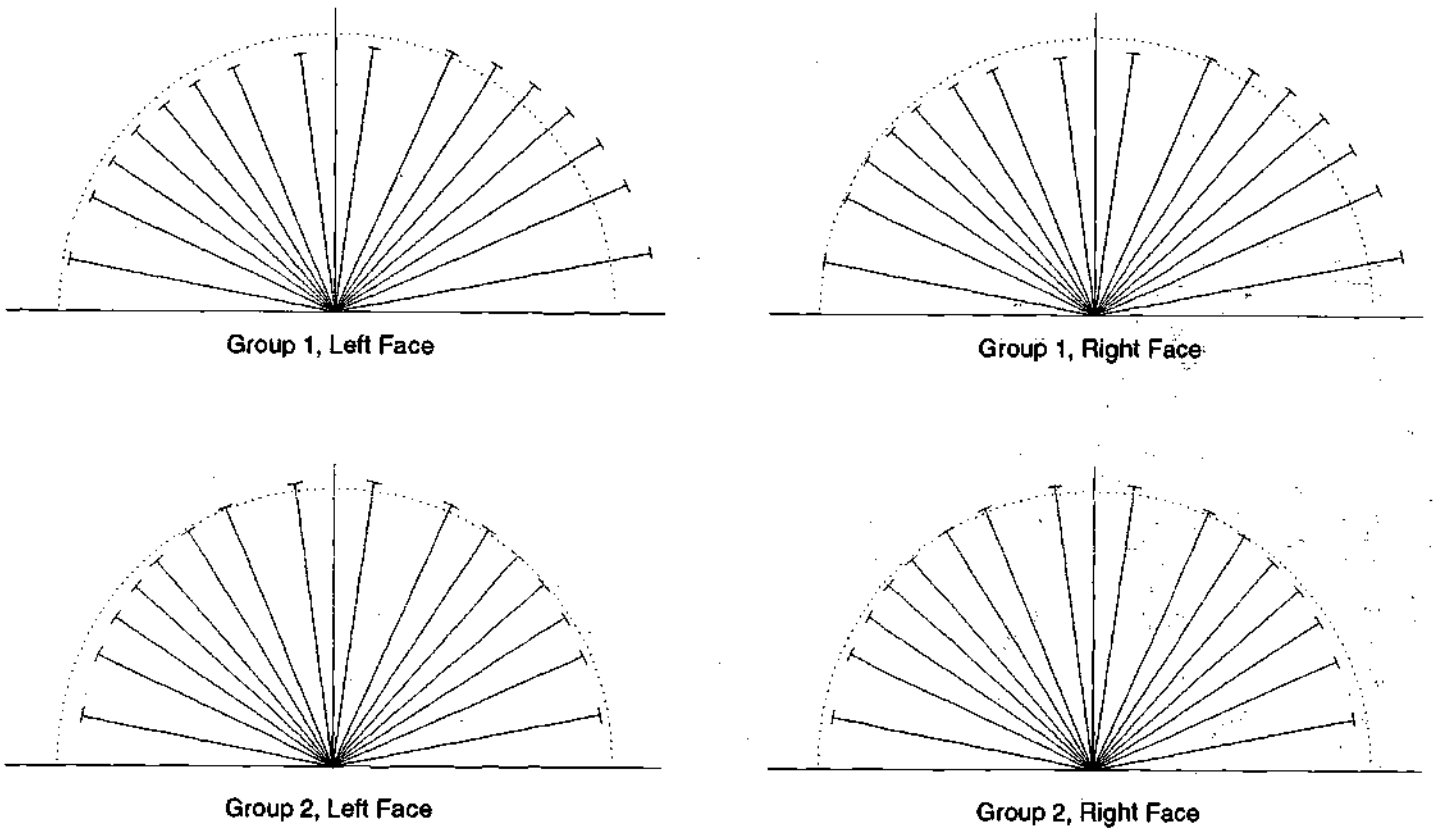

Figure 3.6. Polar Plots of the Reference Angular Fluxes
on the Node Surfaces of the BWR Geometry.

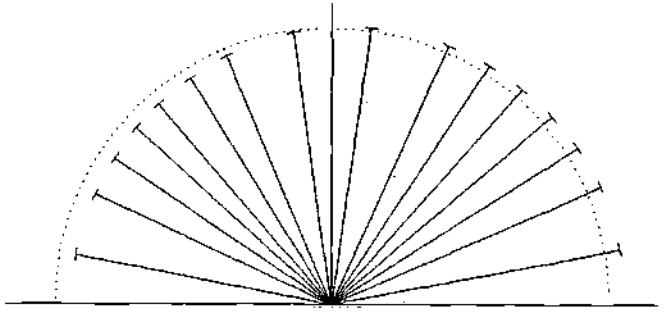

Group 1, Left Face

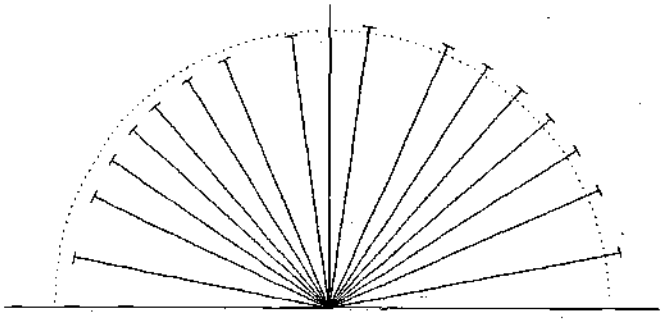

Group 1, Right Face

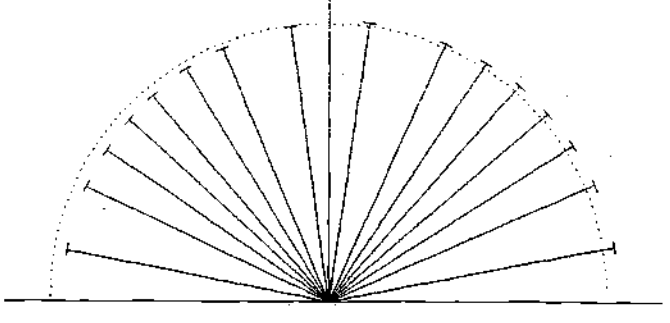

Group 2, Left Face

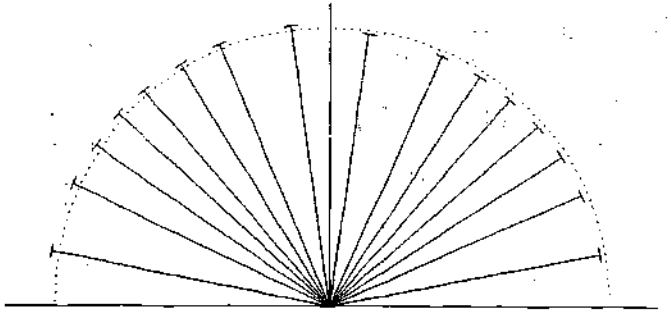

Group 2, Right Face

Figure 3.7. Polar Plots of the Reference Angular Fluxes
on the Node Surfaces of the PWR Geometry.

In the albedo condition shown by equation (3.8), the ratio of the first to sixteenth angular flux will equal the ratio of the eighth to ninth angular flux. In the BWR geometry, the only angular flux shape in Figure 3.6 that shows this characteristic is the thermal energy group on the right surface. However, this shape is nearly symmetric meaning that all odd moments are approximately equal to zero as seen in Table 3.3. In the other three angular flux shapes of the BWR geometry, the ratio of the eighth and ninth angular fluxes is approximately equal to one while the ratio of the first and sixteenth angular fluxes are not. This is not a characteristic of the albedo boundary condition and, therefore, the albedo boundary condition is not expected to create a current and adequately predict the scalar flux and other odd moments of the angular flux.

Examining the angular flux shape on the surfaces of the PWR geometry shows that the left face does not exhibit characteristics of an albedo boundary condition, however, the right face does. The angular flux shape on the right face of the fast energy group shows some resemblance to the upward stretched ellipse seen in Figure 3.5. The angular flux shape for the thermal energy group on the right face is similar to the circular albedo shape. Therefore, the albedo boundary condition might be sufficient to model the right face of the PWR, but it will not provide a good boundary condition for the left boundary.

Nevertheless, the individual errors of the homogenized parameters found by using albedo boundary conditions to reproduce the reference currents are listed in Table C.3. The flux discontinuity factors are excluded from Table C.3 because the edge-to-average flux ratios are used to arrive at the them. To avoid energy group and node face coupling

errors, this analysis created the currents in both energy groups and on both surfaces simultaneously. Examining the RMS errors in Table 3.10 shows that the errors in the cross sections are small, but the errors in the edge-to-average flux ratios are larger than those from the energy group or node face decoupling. Since cross sections are volume weighted quantities, they are expected to be less sensitive to the boundary condition than the edge-to-average flux ratio. However, the edge-to-average flux ratio is extremely sensitive to the boundary condition.

Table 3.10. RMS Errors using Albedo Boundary Conditions to Reconstruct the Homogenized Parameters.

BWR	
Cross Sections	0.0320%
Edge-to-Average Flux Ratios	1.5806%
PWR	
Cross Sections	0.0031%
Edge-to-Average Flux Ratios	1.3306%

Scalar flux profiles near the boundaries of the center node for the two energy groups are shown in Figures 3.8 and 3.9 for the two geometries. The node boundary and the 2.5 cm toward the interior of the node are displayed in the figures. The dotted line is the reference S_{16} scalar flux profile and the solid line is the S_{16} scalar flux profile using the albedo boundary condition to create the reference currents. In each figure, the albedo boundary condition accurately predicts the scalar flux profile toward the interior of the node. However, at the node boundary, the albedo boundary condition has created small tails that are clearly visible in the fast energy group. These tails lead to inaccurate correlations for the edge-to-average flux ratios from the lattice homogenization code and, it follows, lead to inaccurate flux discontinuity factors.

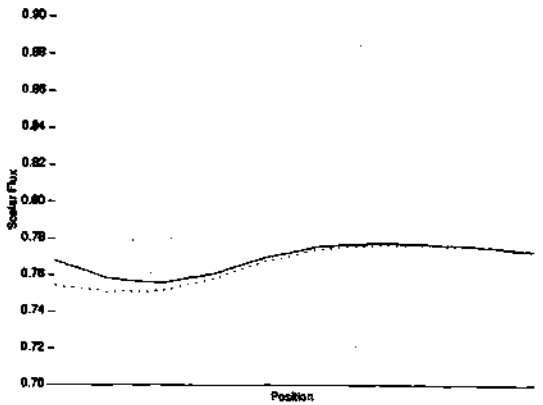

Left Surface, Group 1

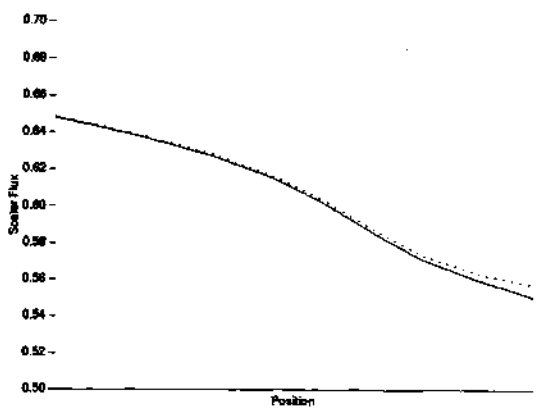

Right Surface, Group 1

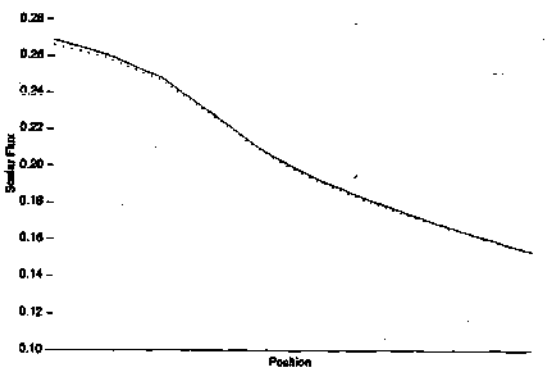

Left Surface, Group 2

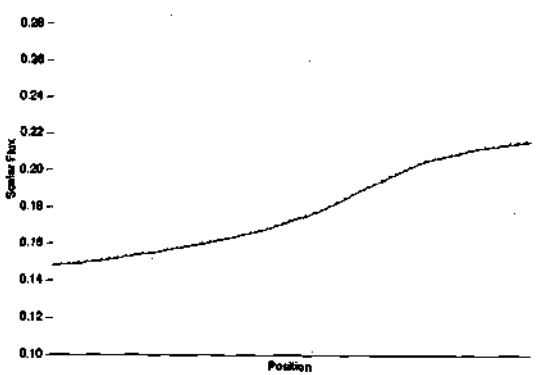

Right Surface, Group 2

Figure 3.8. Scalar Flux Profiles near the Boundaries of the BWR Geometry created by the Albedo Boundary Condition.

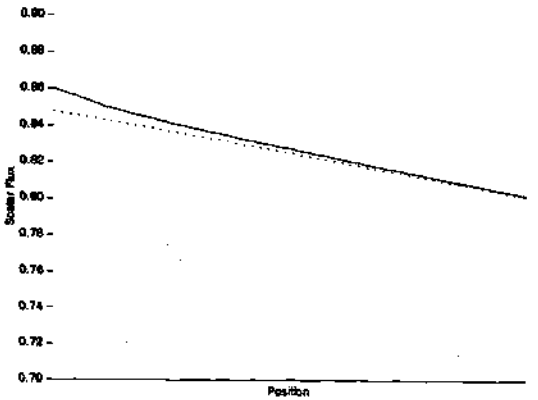

Left Surface, Group 1

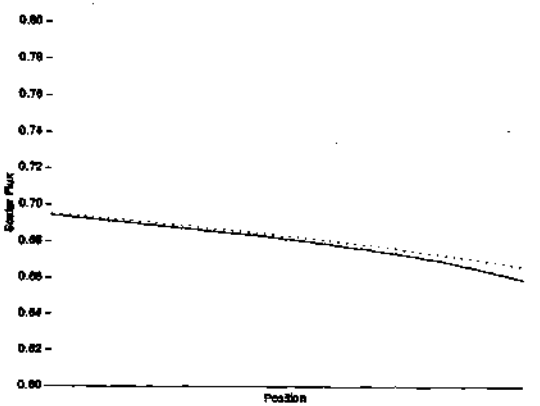

Right Surface, Group 1

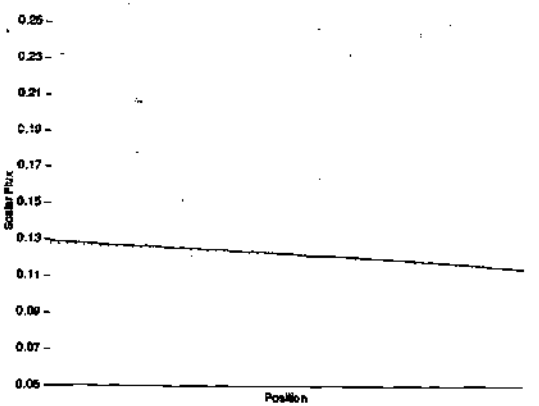

Left Surface, Group 2

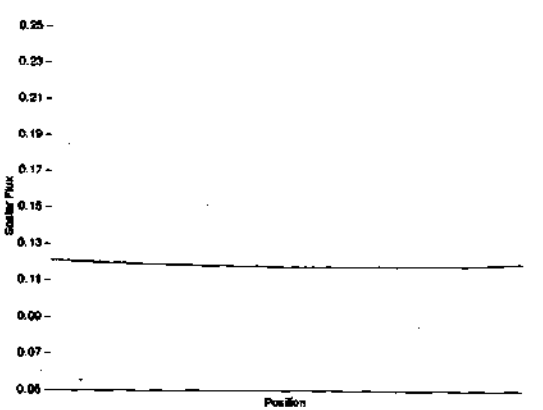

Right Surface, Group 2

Figure 3.9. Scalar Flux Profiles near the Boundaries of the PWR Geometry created by the Albedo Boundary Condition.

Shifted Circle Boundary Condition

In the previous segments, it was shown that the albedo boundary condition does not sufficiently model the scalar flux profile near node boundaries. Examining the values of the reference odd moments given in Table 3.3 shows that the higher odd moments are small compared with the current. Also, many of the angular flux profiles in Figures 3.6 and 3.7 imply that the angular flux is continuous near $\psi(\mu=0)$ unlike an albedo condition. A boundary condition that can create a current and yet cause the higher odd moments to equal zero may provide a good boundary condition to correlate the homogenized parameters.

An angular flux profile that can create a current without creating higher odd moments is a shifted circle shape. In this profile, the angular flux is circular around a point to the left or right of the origin. A sample polar plot of this condition is displayed in Figure 3.10. An equation for the angular flux shape is obtained by writing in *x*-*y* coordinates the equation for a circle with radius a and shift b,

$$(x-b)^2 + y^2 = a^2 . \tag{3.11}$$

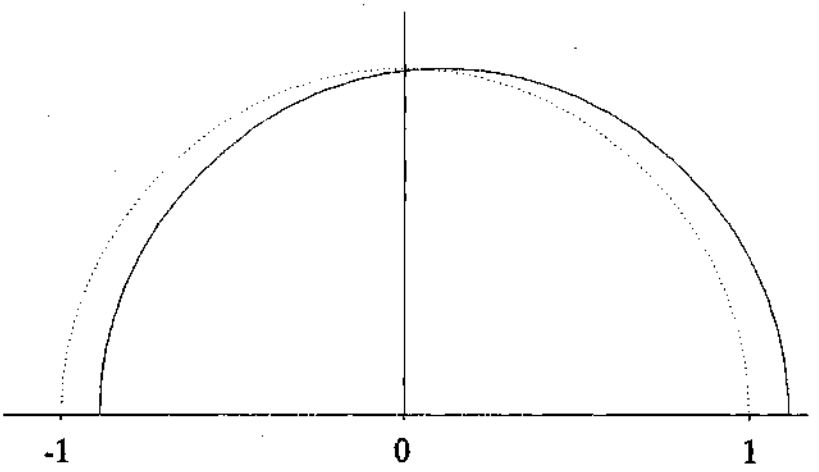

Figure 3.10. Polar Plot of a Shifted Circle Angular Flux Profile.

Equation (3.11) is transformed to polar coordinates by using equation (3.7). These equations result in a form for the angular flux as a function of μ,

$$\frac{\psi(\mu)}{a} = \frac{b}{a}\mu + \sqrt{1 - (1-\mu^2)\frac{b^2}{a^2}} \quad . \tag{3.12}$$

In examining this equation, the first term is a constant times the first Legendre polynomial and the second term is an even function. When evaluating equation (3.6) for the odd moments, the first term only contributes to the current (ϕ_1) because of the orthogonal relationship of the Legendre polynomials. Because the second term is an even function, it never contributes to the odd moments. Therefore, equation (3.12) creates a current but all other odd moments are exactly equal to zero.

For the two sample geometries, this boundary condition creates the reference currents on both node surfaces and both energy groups simultaneously in an attempt to reproduce the reference homogenized parameters. The boundary condition was used on all surfaces simultaneously to avoid the coupling errors discussed in Section 3.4. The errors for each homogenized cross section and the edge-to-average flux ratios are listed in Table C.4 and summarized in Table 3.11.

Table 3.11. RMS Errors using the Shifted Circle Boundary Conditions to Reconstruct the Homogenized Parameters.

BWR	
Cross Sections	0.0022%
Edge-to-Average Flux Ratios	0.0615%
PWR	
Cross Sections	0.0010%
Edge-to-Average Flux Ratios	0.3351%

Comparing Tables 3.10 and 3.11 show that the shifted circle boundary condition is far superior to the albedo boundary condition for creating the global flux tilt through the sample nodes. However, Table 3.11 does create some concerns. The RMS errors in the edge-to-average flux ratios for the PWR geometry are much higher than those for the BWR geometry. Examining Table C.4 shows that the larger errors of the PWR geometry occur on the right surface. This surface is a material boundary as well as a node boundary. In the reference angular flux profiles for this boundary shown in Figure 3.7, the angular flux does slightly resemble an albedo shape. Nevertheless, for the geometry at hand, the shifted circle boundary condition is better than the albedo boundary condition even on the material boundary. For some interfaces that are vastly different such as the fuel and baffle/reflector interface, the albedo boundary condition may be necessary.

However, it is common to analyze the baffle/reflector regions using one-dimensional extended geometry calculations.[11]

Figures 3.11 and 3.12 are similar to Figures 3.8 and 3.9. In these figures, the scalar flux profiles near the node boundaries are shown for the BWR and PWR geometries when the reference currents were created using the shifted circle boundary condition. The dotted line in both figures is the reference scalar flux shape and the solid lines are the scalar flux shapes created by using the shifted circle boundary condition. Unlike the albedo boundary condition, employing the shifted circle boundary condition has not created the tails on the node surfaces. Concluding, for fuel/fuel interfaces, the shifted circle boundary condition more accurately predicts the scalar flux on the edge of the node than the albedo boundary condition.

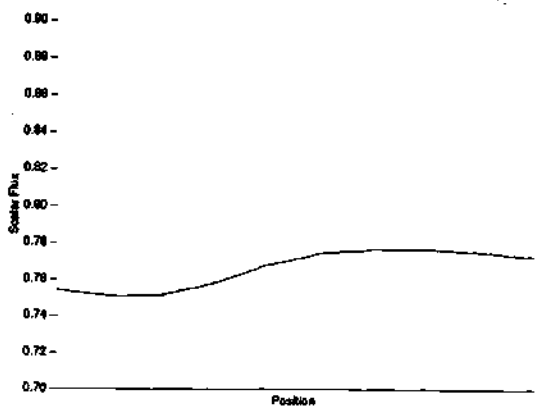

Left Surface, Group 1

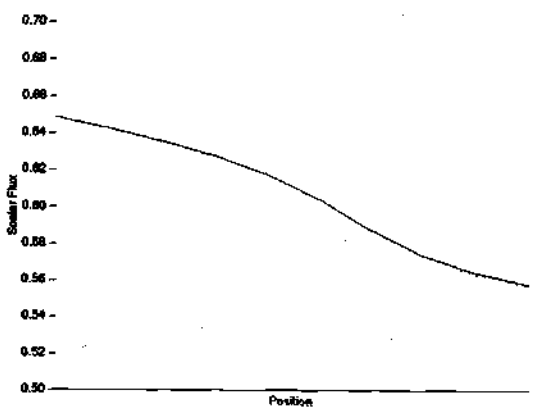

Right Surface, Group 1

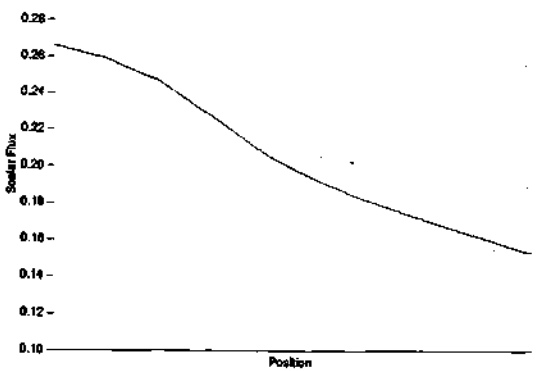

Left Surface, Group 2

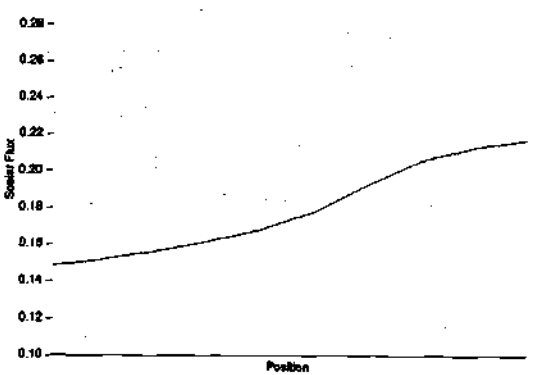

Right Surface, Group 2

Figure 3.11. Scalar Flux Profiles near the Boundaries of the BWR Geometry created by the Shifted Circle Boundary Condition.

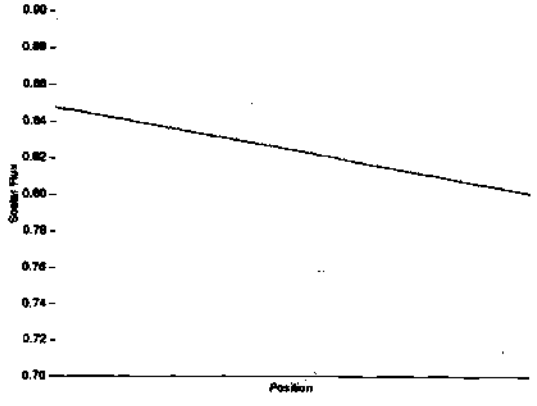

Left Surface, Group 1

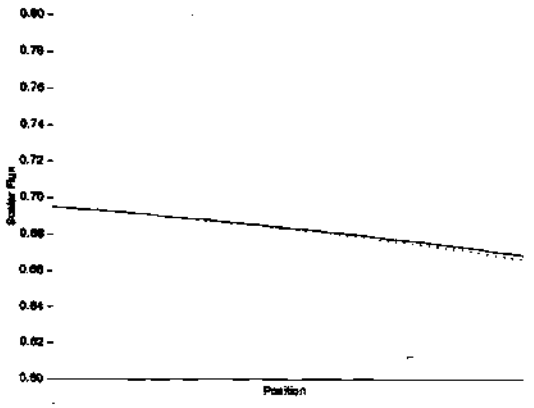

Right Surface, Group 1

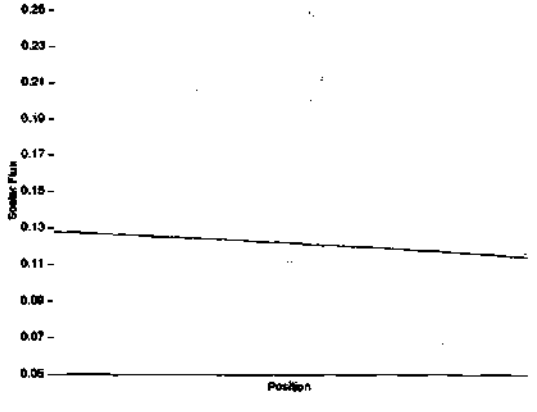

Left Surface, Group 2

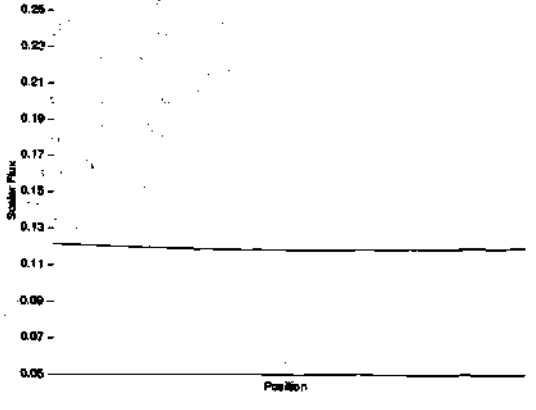

Right Surface, Group 2

Figure 3.12. Scalar Flux Profiles near the Boundaries of the PWR Geometry created by the Shifted Circle Boundary Condition.

3.6 Polynomial Fitting

In this section, we examine if the correlations for the homogenized cross sections and the edge-to-average flux ratios are linear as shown in equation (1.13). It was shown in Section 3.4 that terms multiplying the current-to-flux ratio from different energy groups or from different node surfaces together are small. However, terms that raised the current-to-flux ratio to a power were not discussed in that section.

For each surface and each energy group of the two sample geometries, the shifted circle boundary condition is used to create different currents (and therefore current-to-flux ratios) on the surface of the node. This is necessary to fit the correlation coefficients to a power series. The currents created on the surface result in current-to-flux ratios of -0.10, -0.05, 0.0, 0.05, and 0.10. The five different current-to-flux ratios will truncate the power series to a fourth order polynomial.

$$1 + \sum_{n=1}^{4} a_n \left(\frac{J}{\phi} \right)^n \tag{3.13}$$

The energy group and node face subscripts have been omitted for convenience. Multiplying the power series and the infinite lattice homogenized parameter together result in the reconstructed homogenized parameter.

Typically, the current-to-flux ratios are within a range from -0.10 to 0.10. If the current-to-flux ratio were as high as ±0.10, then the coefficient for the second order power term would need to be ten times as large as the linear coefficient term to produce equivalent change in the homogenized parameter. Similarly, to produce the same change, the third order power coefficient needs to be one hundred times larger than the linear coefficient, and the fourth order power coefficient needs to be one thousand times larger than the linear coefficient. For smaller current-to-flux ratios, the higher ordered polynomial terms become less important. Therefore, a linear correlation should be sufficient to approximate the correlations provided the second, third, and fourth ordered polynomial coefficients are less than 10, 100, and 1000 times the linear coefficient, respectively. In Tables C.5 through C.12, the correlation coefficients are provided for the two sample geometries corresponding to currents on both node surfaces and energy groups. Examining these tables will show that the second, third, and fourth polynomial coefficients should not result in significant changes to the homogenized parameters for current-to-flux ratios as high as ±10%.

Errors in the reconstructed homogenized parameters found by using all polynomial coefficients with the reference current-to-flux ratios are listed in Table C.13. Likewise, errors in the reconstructed homogenized parameters using only the first two polynomial coefficients with the reference current-to-flux ratios are listed in Table C.14 and errors using only the linear coefficient are listed in Table C.15. These errors are summarized in Tables 3.12 through 3.14.

Table 3.12. RMS Errors using a Fourth Ordered Polynomial to Reconstruct the Homogenized Parameters.

BWR	
Cross Sections	0.0041%
Edge-to-Average Flux Ratios	0.1051%
PWR	
Cross Sections	0.0036%
Edge-to-Average Flux Ratios	0.3817%

Table 3.13. RMS Errors using a Quadratic Polynomial to Reconstruct the Homogenized Parameters.

BWR	
Cross Sections	0.0037%
Edge-to-Average Flux Ratios	0.0954%
PWR	
Cross Sections	0.0033%
Edge-to-Average Flux Ratios	0.3811%

Table 3.14. RMS Errors using a Linear Fit to Reconstruct the Homogenized Parameters.

BWR	
Cross Sections	0.0085%
Edge-to-Average Flux Ratios	0.3219%
PWR	
Cross Sections	0.0048%
Edge-to-Average Flux Ratios	0.3709%

In addition to the polynomial fit, the errors in Tables C.13 through C.15 and Tables 3.12 through 3.14 include errors caused by energy group decoupling, node face decoupling, and the shifted circle boundary condition. Many of the RMS errors in Tables 3.12 through 3.14 are less than the energy group decoupling errors and the node face decoupling errors. Thus, the combination of these errors can cancel each other out. In this event, the fourth order polynomial fit cannot claim superior accuracy to the quadratic polynomial or even the linear fit. Tables 3.12 through 3.14 simply support that the errors in a linear fit for the homogenized parameters are insignificant compared to the remaining errors in the energy group coupling and the node face coupling.

The linear correlation coefficient can be approximated by performing only one additional lattice homogenization for each energy group and each node face. The additional calculation imposes a current on one face of the node and in one energy group. This is repeated for each face and energy group combination.

3.7 Conclusions for Finding Correlations to Homogenized Parameters

A method to approximate a correlation for improving homogenized parameters using one-dimensional geometries is revealed in this chapter. At the beginning of the chapter, it was assumed that we can find a correlation that couples all energy groups and node faces together. However, to find this correlation for a polynomial of the second order would require many lattice homogenization calculations even for a one-dimensional problem. Performing many lattice homogenization calculations is obviously undesirable. It was shown in Section 3.4 that we can decouple the energy groups and node faces to reduce the number of calculations without a great loss of accuracy. A linear correlation can reduce the number of additional lattice homogenization calculations to one for each energy group and node face combination. In a common two-dimensional two-group problem, this would require eight additional calculations assuming no geometric symmetry of the assembly.

A key to calculating accurate flux discontinuity factors is to correlate the edge-to-average flux ratio and then use equation (3.4) with the nodal code flux approximation and diffusion coefficient to figure out the flux discontinuity factors. This method greatly improves the accuracy of the flux discontinuity factor over directly correlating the flux discontinuity factor. This approach has several advantages over a direct correlation of the flux discontinuity factor. The method corrects for uncertainties in the diffusion coefficient. For any given diffusion coefficient (non-zero value), the

denominator of equation (3.4) allows us to account for the diffusion coefficient and find a proper flux discontinuity factor. Thus, we do not need to correlate the diffusion coefficient or even calculate the diffusion coefficient. Additionally, the correlated edge-to-average flux ratios are independent of the nodal code flux approximation unlike the flux discontinuity factors. This means that we can change the flux approximation in the nodal code without requiring additional calculations for the flux discontinuity factor correlation coefficients.

If the method to find correlation coefficients for the homogenized parameters is a transport theory procedure, then there will exist a boundary condition dilemma. The nodal code can produce values for the scalar flux and current at the node boundaries, but it cannot provide values for the other higher moments of the angular flux. It was demonstrated in Section 3.5 that the albedo boundary condition does not accurately model the remaining higher moments of the angular flux for the two sample geometries examined in this chapter. An angular flux shape that resembles a shifted circle does model the angular flux shape of the two sample geometries rather well. The higher odd moments of the shifted circle boundary condition are equal to zero. Conversely, the albedo boundary condition has higher ordered odd moments of the angular flux that are relatively large. Accuracy of the albedo boundary condition improves if the node boundary is also a material boundary. However, even for this condition, the shifted circle boundary condition still outperformed the albedo boundary condition.

Section 3.6 showed that a linear correlation sufficiently models the homogenized cross sections and edge-to-average flux ratios as a function of the current-to-flux ratio. If the correlation is linear, then we need only one additional lattice homogenization calculation to find the correlation coefficient associated with a particular node face and energy group. Therefore, equation (1.13) is valid for correlating the cross sections and edge-to-average flux ratios provided that the shifted circle boundary condition creates the currents on a node boundary to form the correlations.

CHAPTER IV

APPLICATIONS OF CORRELATED HOMOGENIZED PARAMETERS IN A TWO-DIMENSIONAL GEOMETRY

4.1 Chapter IV Objectives

It was confirmed in Chapter III that for sample one-dimensional BWR and PWR geometries, a linear correlation can accurately model changes in homogenized cross sections and edge-to-average flux ratios from a lattice homogenization analysis when a flux tilt is present across a node. However, for a procedure to be applicable, there are several more issues that need to be addressed that were not discussed Chapter III. Among these issues are:

- how are the correlations employed in a reactor analysis,
- do the adjusted homogenized parameters actually lead to improved global reactor results and, if so, how much of an improvement is gained,
- do the correlations lead to identical answers using different flux approximations and diffusion coefficients as suggested by equation (3.4),
- how do these correlations interact with changes in the heterogeneous cross sections, and
- which homogenized parameters show strong and weak dependencies on the current-to-flux ratios.

Responses to these queries will emphasize the necessity of applying global reactor information to the homogenized parameters.

4.2 Iteration Method for Homogenized Parameters

The method to update homogenized parameters based on current-to-flux ratios is similar to adjusting homogenized parameters based on thermal feedback effects. Essentially, the current-to-flux ratios are feedback effects, only they are not thermal effects as are temperatures and densities. Homogenized parameters are adjusted when the global reactor solution obtains good estimates for the independent parameters. In this case, the independent parameters are the current-to-flux ratios. In this chapter, adjustments to the homogenized parameters occur within the nodal code after the flux and eigenvalue reach their convergence criteria, 1.0e-06.

The procedure used to solve the global reactor solution begins by using infinite lattice homogenized parameters in the global reactor problem to converge on the fluxes and eigenvalue. This converged solution should be sufficiently accurate (relative to a reference solution) to provide current-to-flux ratios used to adjust the homogenized parameters. Then, the flux and eigenvalue iterations resume using the adjusted homogenized parameters to arrive at yet another global reactor solution. The second solution should be more accurate than its predecessor because the homogenized parameters now consider the global reactor effects. Since the current-to-flux ratios of the second solution will be different from the first, the correlations are used to adjust the

homogenized parameters again and a third global reactor solution is found. Each improvement in the homogenized parameters should result in a more accurate global reactor solution. Thus, adjusting the homogenized parameters is an iterative technique that is contained within the nodal code. When the homogenized parameters between two successive iterations are equal to within a convergence criteria, then the global reactor solution has completely converged on the eigenvalue, fluxes, and homogenized parameters used to find the eigenvalue and fluxes. The iterative method is shown in Figure 4.1.

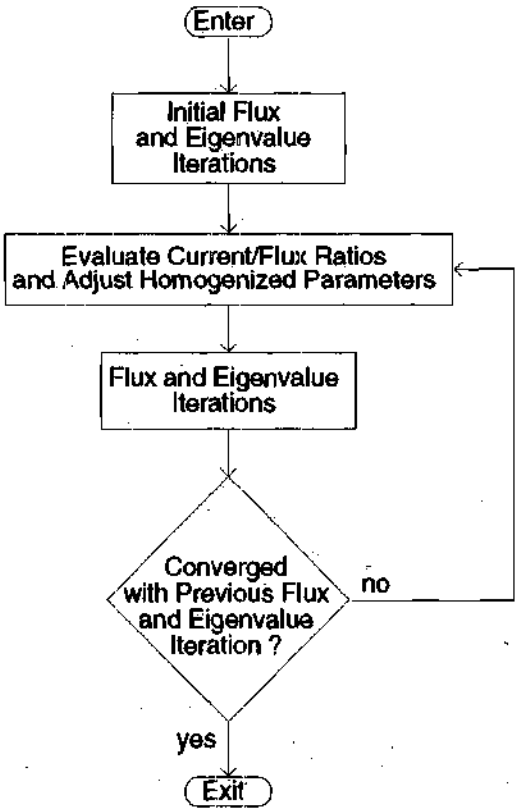

Figure 4.1. Iteration Procedure to Adjust Homogenized Parameters.

4.3 Global Reactor Descriptions

In this section, the two-dimensional sample geometries that resemble BWR and PWR fuel patterns are described. Each global reactor problem is composed of nine fuel assemblies arranged in a 3×3 pattern. Problems larger than this would create difficulties in finding a reference solution using JTC. The geometries in this chapter model many heterogeneities in the BWR and PWR fuel assemblies.

Geometry Descriptions

The geometry dimensions and location of materials for all fuel assemblies in the BWR problem are identical, only the cross sections of the fuel materials are different. Each BWR assembly is analyzed with and without a cruciform control blade inserted. All BWR fuel assemblies are one-half symmetric. For the PWR fuel assemblies, again the geometry dimensions and location of materials are identical for each fuel assembly. The difference between the assemblies is the fuel reactivity. The PWR fuel assemblies are one-eighth symmetric. The most reactive PWR fuel assembly is also analyzed with a control rod cluster inserted. Dimensions for the two geometries are provided in Table 4.1.

Table 4.1. Fuel Assembly Dimensions for the Two-Dimensional Problems.

BWR	
Pitch	1.63 cm
Can Thickness	0.4 cm
Wide Water Gap	1.0 cm
Narrow Water Gap	0.5 cm
Control Blade Thickness*	0.8 cm
PWR**	
Pitch	1.43 cm

* The control blade thickness is the full width of the control blade, only half of which is in a fuel assembly.

** The thin water gap between PWR assemblies is neglected.

BWR Fuel Assemblies. The geometries of the BWR fuel assemblies are shown in Figures 4.2 through 4.4. The BWR fuel can and the control blade are shown in these figures. Each assembly is analyzed with and without the control blade inserted. The fuel pin loading is homogeneous with the exception of the fuel in the most reactive assembly shown by Figure 4.2. This assembly contains three fuel pins in the upper right corner that have a lower reactivity than the remaining fuel.

The global reactor problem is displayed in Figure 4.5 along with the location of the control blade. The outer boundaries of the global reactor problem are reflective. Also shown in Figure 4.5 is the rotation of each fuel assembly. The rotation places the wide water gap and the control blade position in the proper location. Fuel assemblies with an asterisk have the control blade inserted. As seen in Figure 4.5, the global reactor problem is composed of six distinct fuel assemblies. These six assemblies are the three different fuel reactivities with and without the inserted cruciform control blade. Assembly A is more reactive than assembly B and assembly B is more reactive than assemble C.

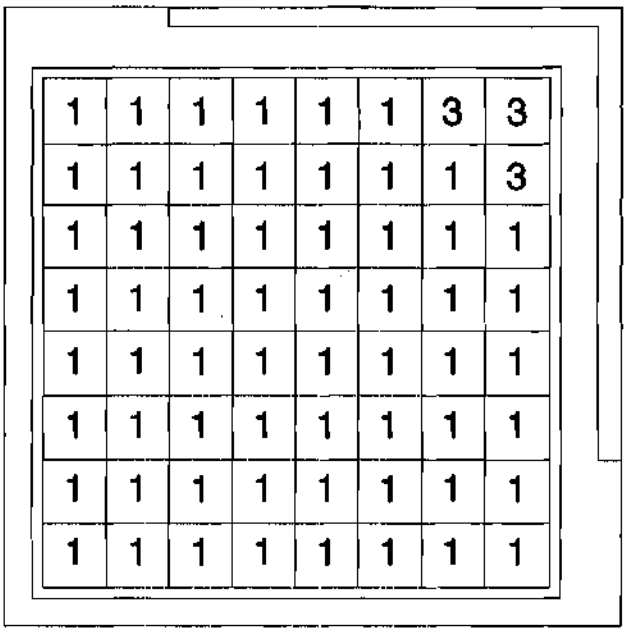

Figure 4.2. Geometry of BWR Fuel Assembly A.
(Most reactive BWR assembly.)

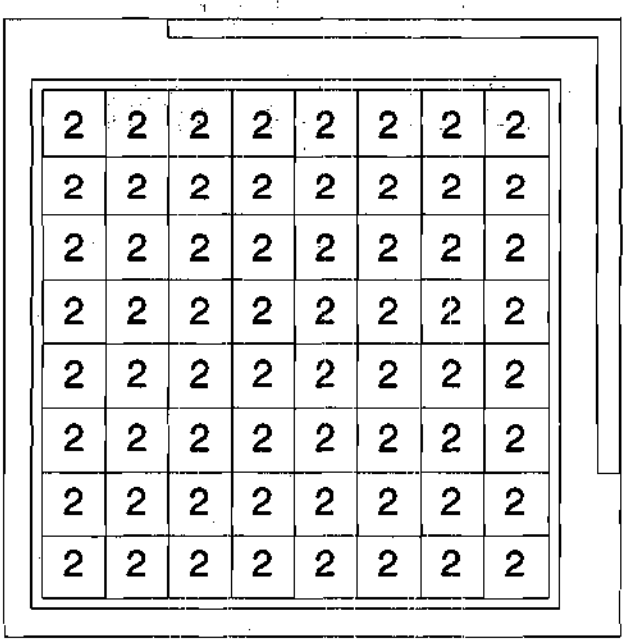

Figure 4.3. Geometry of BWR Fuel Assembly B.

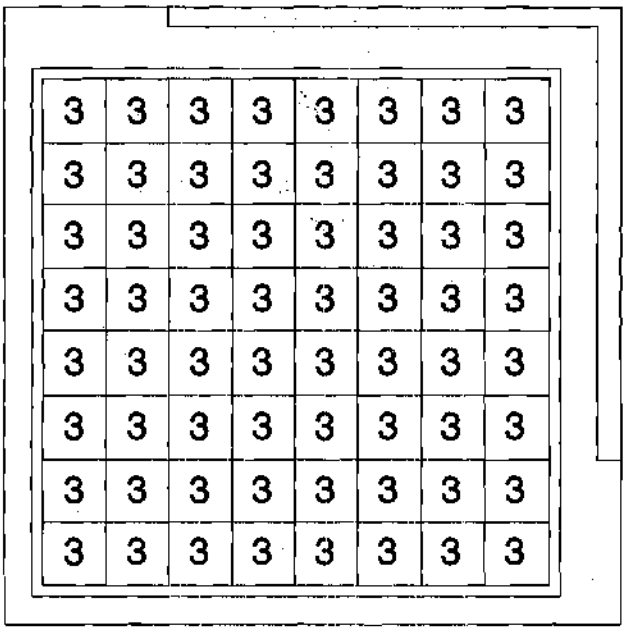

Figure 4.4. Geometry of BWR Fuel Assembly C.
(Least reactive BWR assembly.)

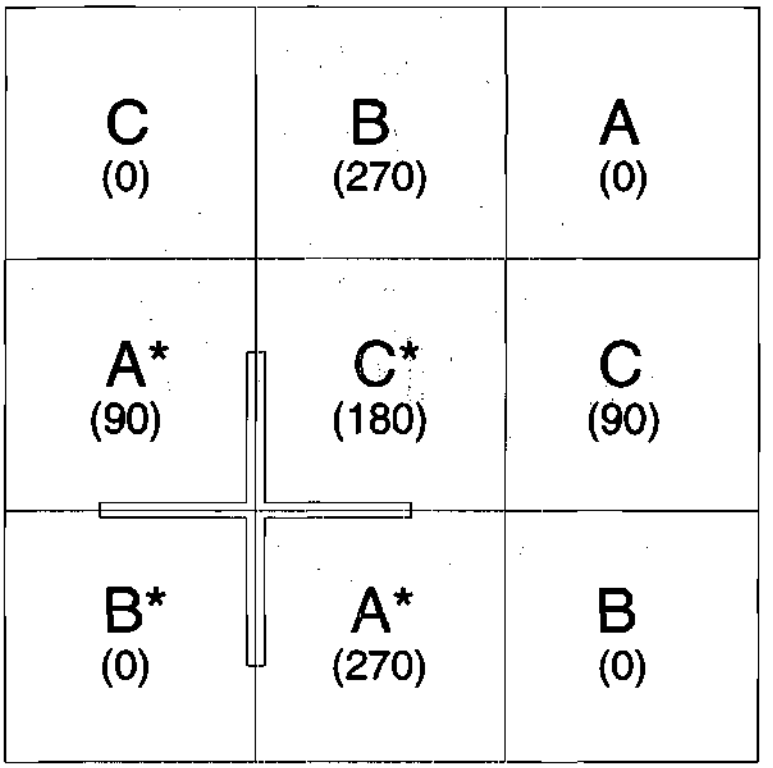

Figure 4.5. Global Reactor Geometry for the BWR Problem.

PWR Fuel Assemblies. The PWR fuel assemblies have a 15×15 pin design with 21 water holes. The water holes represent the only heterogeneity in the assemblies except for a control rod cluster inserted in the most reactive assembly. The control rod cluster contains eight control pins. Asterisks in Figure 4.6 show the location of the eight pins. The PWR fuel assembly geometries are displayed in Figures 4.6 through 4.8.

The global reactor problem for the PWR geometry, seen in Figure 4.9, shows that two of the most reactive fuel assemblies have a control rod cluster inserted. Since the PWR fuel assemblies are one-eighth symmetric, no rotation of the fuel assemblies is necessary. The outer boundaries of the global reactor problem are reflective. As seen in Figure 4.9, the global reactor geometry is composed of four distinct fuel assemblies. Assembly D is more reactive than assembly E and assembly E is more reactive than assembly F.

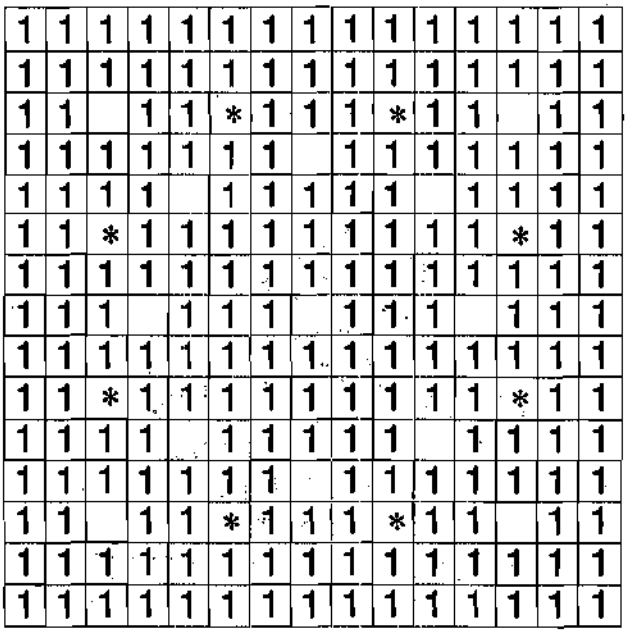

Figure 4.6. Geometry of PWR Fuel Assembly D.
(Most reactive PWR assembly.)

2	2	2	2	2	2	2	2	2	2	2	2	2	2	2
2	2	2	2	2	2	2	2	2	2	2	2	2	2	2
2	2		2	2		2	2	2		2	2		2	2
2	2	2	2	2	2	2		2	2	2	2	2	2	2
2	2	2	2		2	2	2	2	2		2	2	2	2
2	2		2	2	2	2	2	2	2	2	2		2	2
2	2	2	2	2	2	2	2	2	2	2	2	2	2	2
2	2	2		2	2	2		2	2	2		2	2	2
2	2	2	2	2	2	2	2	2	2	2	2	2	2	2
2	2		2	2	2	2	2	2	2	2	2		2	2
2	2	2	2		2	2	2	2	2		2	2	2	2
2	2	2	2	2	2	2		2	2	2	2	2	2	2
2	2		2	2		2	2	2		2	2		2	2
2	2	2	2	2	2	2	2	2	2	2	2	2	2	2
2	2	2	2	2	2	2	2	2	2	2	2	2	2	2

Figure 4.7. Geometry of PWR Fuel Assembly E.

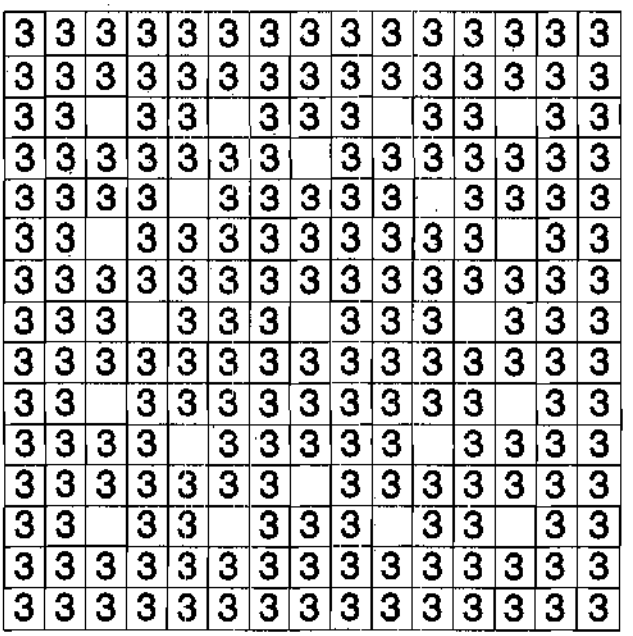

Figure 4.8. Geometry of PWR Fuel Assembly F.
(Least reactive PWR assembly.)

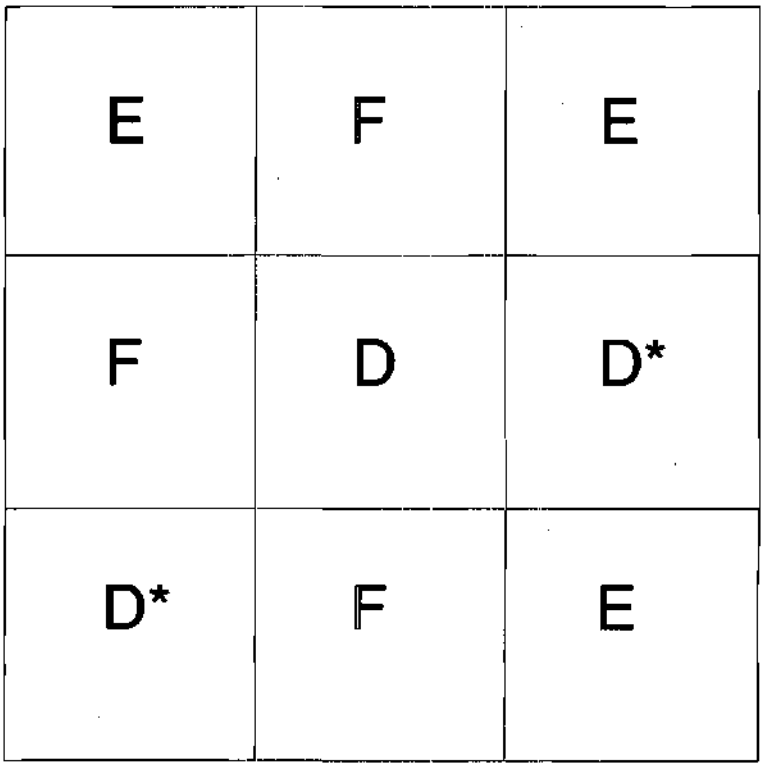

Figure 4.9. Global Reactor Geometry of the PWR Problem.

Heterogeneous Cross Sections

The heterogeneous cross sections for the BWR and PWR assemblies are listed in Table 4.2. The BWR assemblies use the water gap material (material 4) and the PWR assemblies use the water hole material (material 5). The absorber material is used for the cruciform control blade in the BWR assemblies and the control rod cluster of the PWR assemblies.

Heterogeneous diffusion coefficients are not listed in Table 4.2. The COMBINE cross section generation code has as output P_1 or P_3 scattering cross sections and diffusion coefficients. Scattering cross sections are given in Table 4.2 because they are essential for the transport calculations but the diffusion coefficients are not. From a transport calculation, there are several methods to compute a homogenized diffusion coefficient. Therefore, because of the arbitrary nature of the homogeneous diffusion coefficient, Table 4.2 excludes the heterogeneous diffusion coefficients.

In the heterogeneous cross section set, Fuel 1 is UO_2 with an enrichment of 3.1%, Fuel 2 is UO_2 with an enrichment of 2.6%, and Fuel 3 is UO_2 with an enrichment of 2.1%. These different enrichments provide the different reactivities for the fuel assemblies.

Table 4.2. Reference Transport Theory Cross Sections for the Two-Dimensional Studies. cm^{-1} (No upscattering)

Material	Group	Σ_a	Σ_f	$\nu\Sigma_f$
1	1	1.016e-02	2.876e-03	7.346e-03
(Fuel)	2	1.003e-01	6.171e-02	1.504e-01
2	1	9.789e-03	2.580e-03	6.622e-03
(Fuel)	2	9.027e-02	5.274e-02	1.285e-01
3	1	9.399e-03	2.274e-03	5.872e-03
(Fuel)	2	7.989e-02	4.346e-02	1.059e-01
4	1	9.461e-04	0	0
(W. Gap)	2	3.639e-02	0	0
5	1	1.025e-03	0	0
(W. Hole)	2	3.309e-02	0	0
6	1	9.699e-03	0	0
(Absorber)	2	3.398e-01	0	0
7	1	1.043e-03	0	0
(Can)	2	4.394e-03	0	0

	Scattering	Energy Group		
Material	Order	1 to 1	1 to 2	2 to 2
1	P_0	5.087e-01	1.557e-02	1.150e+00
(Fuel)	P_1	1.706e-01	3.981e-03	3.089e-01
2	P_0	5.093e-01	1.585e-02	1.161e+00
(Fuel)	P_1	1.709e-01	4.073e-03	3.088e-01
3	P_0	5.099e-01	1.614e-02	1.173e+00
(Fuel)	P_1	1.712e-01	4.170e-03	3.087e-01
4	P_0	6.018e-01	3.570e-02	2.005e+00
(W. Gap)	P_1	2.439e-01	7.074e-03	5.550e-01
5	P_0	5.767e-01	3.240e-02	1.813e+00
(W. Hole)	P_1	2.300e-01	6.959e-03	4.965e-01
6	P_0	4.325e-01	1.080e-02	8.745e-01
(Absorber)	P_1	1.399e-01	2.103e-03	2.662e-01
7	P_0	2.071e-01	9.095e-03	4.704e-01
(Can)	P_1	0.000e+00	0.000e+00	0.000e+00

4.4 Reference Solutions and Solutions using Infinite Lattice Homogenized Parameters

In this section, reference solutions are established for the two global reactor problems. An S_8 angular quadrature set is used to analyze the global reactor geometries to obtain the reference solutions. In the BWR geometry, the mesh spacing for the fuel pins is 3 meshes per pin. The BWR can, narrow water gap, and control blade are divided into 2 meshes and the wide water gap is divided into 4 meshes. Thus, the global BWR problem size is 102×102 meshes. For the PWR geometry, each fuel pin is divided into 3 meshes and so the global problem size is 135×135 meshes. The convergence criterion for the multiplication factor is 1.0e-06 and the convergence criterion for the scalar flux is 5.0e-06. All single assembly calculations use the same quadrature set, mesh spacing and convergence criteria as the reference global solution.

Infinite lattice homogenized parameters are found for each distinct fuel assembly using reflective boundary conditions. The homogenized parameters are listed in Tables D.1 through D.3 for the BWR fuel assemblies and Tables D.4 through D.6 for the PWR fuel assemblies. For infinite lattice homogenized parameters, the flux discontinuity factor is equal to the edge-to-average flux ratio.

Using NDT, global reactor solutions are found using the infinite lattice homogenized parameters along with different flux approximations. Normalized powers from the reference solutions are provided in Tables 4.3 and 4.4 for the BWR and PWR geometries, respectively, and errors in the normalized powers from the various nodal

solutions are also given in these tables. The multiplication factor found by each solution is also listed in Tables 4.3 and 4.4.

The nodal solutions used in Tables 4.3 and 4.4 are the mesh centered finite difference (F.D.), quadratic polynomial, and quartic polynomial flux approximations. Examining these two tables does not clearly show that one flux approximation is any better than the next, but rather that different flux approximations simply produce different results as expected. Nevertheless, in the BWR geometry, the quartic polynomial flux approximation produces the most favorable results for the power profiles. With this solution, the maximum error and RMS error of the assembly powers are 2.30% and 1.21%, respectively. The mesh centered finite difference flux approximation provides the most favorable results for the PWR geometry. This solution results in a maximum assembly power error of 3.83% and a RMS assembly power error of 2.11%. These tables provide comparison results for any method to improve homogenized parameters.

Table 4.3. Reference Normalized Powers and Errors using Different Flux Approximations with the Infinite Lattice Homogenized Parameters for the BWR Geometry.

	Eigenvalue			
		0.8608	1.1375	1.4317
		-3.94%	0.33%	2.35%
		-5.39%	1.92%	7.36%
		-1.68%	0.10%	2.30%
Reference	1.02600	0.8977	0.7940	1.0066
F.D.	1.02544	-1.81%	2.83%	1.82%
Quadratic	1.02385	-3.69%	-2.44%	-0.06%
Quartic	1.02402	-1.65%	-0.40%	-0.22%
		0.7856	0.9691	1.1169
		-3.93%	0.82%	-0.45%
		-6.50%	0.38%	1.76%
		-1.22%	0.66%	0.35%

Table 4.4. Reference Normalized Powers and Errors using Different Flux Approximations with the Infinite Lattice Homogenized Parameters for the PWR Geometry.

	Eigenvalue			
		1.0070	0.9128	1.1448
		-1.57%	1.89%	1.16%
		-1.23%	-1.33%	2.80%
		-1.26%	-0.66%	2.97%
Reference	1.10516	0.8119	1.1887	1.1179
F.D.	1.10531	-1.99%	-3.34%	3.83%
Quadratic	1.10416	-4.91%	2.25%	4.27%
Quartic	1.10437	-3.99%	1.72%	3.25%
		0.8494	0.8520	1.1155
		-1.47%	0.11%	0.88%
		-3.98%	-3.40%	1.84%
		-5.48%	-2.31%	2.39%

4.5 Global Reactor Solutions using Homogenized Parameter Correlations

In this section, the two global reactor problems are analyzed using correlations to adjust homogenized parameters based on information from the global reactor solutions. First, correlations for the BWR and PWR fuel assemblies are found. Then, the number of times to adjust the homogenized parameters to arrive at a final solution is discussed. In Chapter III, it was stated that correlations can account for differences in flux approximations and diffusion coefficients. Thus, a portion of this section is devoted to analyzing the global solutions with different flux approximations and diffusion coefficients.

Finding Correlation Coefficients

A procedure to find correlation coefficients for the homogenized parameters is described in this segment. Since equation (1.13) shows how to use the correlation coefficients after they are found, it should also show how to find the correlation coefficients. Comparing different sets of homogenized parameters, each with different current-to-flux ratios on the boundary, leads to values for the correlation coefficients by employing equation (1.13). Rearranging equation (1.13) defines the correlation coefficient associated with a node face and energy group for each homogenized parameter. One calculation needed to find the correlation coefficient is the infinite lattice calculation that is readily available for nodal analyses. The other has a current imposed on one boundary of the node to simulate a global flux tilt through the node volume. As discussed in

Chapter III, the shifted circle boundary condition accurately models the global flux tilt and so it is implemented throughout this chapter. Once the current created by the boundary condition and the average flux in the node are known, then it is a simple procedure to use equation (1.13) to compute the correlation coefficients associated with the current.

The value of the current used to create a global flux tilt through the node should be large enough to reveal changes in the node conditions (i.e., much larger than truncation and round-off errors) and yet within a practical current-to-flux ratio range. Therefore, a current-to-flux ratio of approximately ±5% should be sufficient for BWR and PWR analyses. Each of the ten distinct fuel assemblies (six BWR assemblies and four PWR assemblies) of Section 4.3 are analyzed using this current-to-flux ratio.

Using symmetry conditions reduces the number of single assembly calculations needed to find a complete set of correlation coefficients. The complete set of correlation coefficients describes changes due to current-to-flux ratios from all node surfaces and energy groups. With symmetry conditions, the BWR assembly requires four single assembly calculations in addition to the infinite lattice calculation to form a complete set of correlation coefficients and the PWR assembly requires two additional single assembly calculations. The symmetry conditions do not describe the model for the fuel assembly, as is usually the case, but the manner that a current-to-flux ratio affects the homogenized parameters. For instance, symmetry for the BWR assembly in Figure 4.2 does not refer that only half the assembly is modelled but that a current-to-flux ratio on the left

boundary affects the homogenized parameters identically to a current-to-flux ratio on the bottom boundary. If we used symmetry to model only half of the BWR assembly in Figure 4.2 with a current on the left boundary, then this is identical to modelling the full assembly with a current on the left and bottom boundaries. In this case, the effect that each current places on the cross sections can be decoupled because each current affects the cross sections equally (cross sections are volume integrated). However, it is impossible to separate the effect that each current has on an edge-to-average flux ratio without additional calculations (edge fluxes are surface integrated). Obviously, the current on the left boundary affects the left edge-to-average flux ratio differently than the current on the bottom boundary. Assuming that both currents affect the edge-to-average flux ratios equally will create extremely large errors in the correlation coefficients.

The correlation coefficients for the six BWR fuel assemblies are provided in Tables D.7 through D.12 and the coefficients for the four PWR fuel assemblies are provided in Tables D.13 through D.16. The correlation coefficients are based on a current entering the node having a positive value as opposed to currents moving the right or upward being positive.

Convergence Characteristics using Different Flux Approximations

It is demonstrated in this segment that computing the flux discontinuity factors by equation (3.4) results in identical solutions when the nodal code uses different flux approximations. The homogenized parameters are adjusted twenty times for each analysis to arrive at a solution that is well within practical convergence limits. The flux approximations used in the nodal code are the mesh centered finite difference, quadratic polynomial, and quartic polynomial approximations. The eigenvalue and errors in the assembly powers for the two sample geometries are presented in Tables 4.5 an 4.6. Also examined in this segment are the convergence rates of the three flux approximations.

Table 4.5. Eigenvalues and Errors in the Power Profiles using Different Flux Approximations found after updating the Homogenized Parameters Twenty Times for the BWR Geometry.

Flux Approx.	Eigenvalue			
		0.11%	-0.30%	0.77%
		0.11%	-0.29%	0.77%
		0.11%	-0.30%	0.77%
F.D.	1.02608	-1.20%	0.34%	0.10%
Quadratic	1.02608	-1.20%	0.34%	0.10%
Quartic	1.02608	-1.21%	0.34%	0.11%
		0.31%	-0.51%	0.09%
		0.31%	-0.51%	0.09%
		0.30%	-0.51%	0.10%

Table 4.6. Eigenvalues and Errors in the Power Profiles using Different Flux Approximations found after updating the Homogenized Parameters Twenty Times for the PWR Geometry.

Flux Approx.	Eigenvalue			
		-1.06%	0.37%	0.61%
		-1.06%	0.39%	0.62%
		-1.08%	0.38%	0.64%
F.D.	1.10531	-0.35%	-0.91%	1.64%
Quadratic	1.10532	-0.34%	-0.92%	1.63%
Quartic	1.10532	-0.35%	-0.92%	1.64%
		-0.41%	-0.09%	-0.01%
		-0.44%	-0.07%	-0.01%
		-0.46%	-0.07%	-0.01%

As seen in Tables 4.5 and 4.6, all three flux approximations result in identical solutions (neglecting round-off and truncation errors). For the BWR problem, the maximum assembly power error reduced from 2.30% to 1.21% and the RMS error of the assembly powers reduced from 1.21% to 0.54%. The difference in the eigenvalue from reference reduced from 0.00198 to -0.00008. Similarly for the PWR problem, the maximum assembly power error reduced from 3.83% to 1.64% and the RMS assembly power error reduced from 2.11% to 0.78%. The difference in the eigenvalue from reference reduced from 0.00079 to -0.00016. These results show that the employing the correlations in the nodal analyses causes errors in the assembly powers to reduce by approximately a factor of two. As a conservative measure, the results in Tables 4.5 and 4.6 were compared to the best infinite lattice solution from Tables 4.3 and 4.4. These results demonstrate that the final solution is independent of the flux approximation used in the nodal code.

The final solution being independent of the flux approximation is an extremely important result because it proves that the correlations allow a simple flux approximation such as the finite difference model to produce solutions identical to complex flux approximations such as the quartic polynomial that uses a moments weighing technique and a quadratic transverse leakage shape. Because of the moments weighing technique and quadratic transverse leakage shape, the complex flux approximation is more expensive to code and more expensive to solve a problem than the simpler finite difference approximation. This obviously benefits using simpler flux approximations.

However, further examination of the number of times to adjust the homogenized parameters to reach practical convergence clearly favors the more complex flux approximation. The eigenvalue reached at the end of each flux and eigenvalue convergence loop associated with each adjustment in the homogenized parameters is listed in Tables 4.7 and 4.8 for the BWR and PWR geometries, respectively. It is seen in both tables that the quartic polynomial flux approximation requires fewer adjustments to reach practical convergence on the problem than the mesh centered finite difference approximation. This consequence is directly associated to the accuracy of the flux approximation. Because the quartic polynomial is generally a more accurate approximation than the quadratic and finite difference approximations, it produces better global reactor results (i.e., better current-to-flux ratios) than the other approximations and, in turn, these improved results lead to faster convergence with the correlations.

A good measure of the convergence rate is to compare the eigenvalue after the first homogenized parameter adjustment to the eigenvalue found after twenty adjustments. The eigenvalue after the twentieth adjustment is used because this is the solution that the nodal code ultimately reaches rather than the reference solution. For the BWR problem using the finite difference approximation, the difference in the eigenvalues is 0.00023. This shows good improvement compared to the 0.00064 difference found without adjusting the homogenized parameters. The quadratic polynomial also shows good improvement for the BWR geometry by having a difference in eigenvalues of 0.00016. However, after only one adjustment, the quartic polynomial approximation shows

excellent agreement with the eigenvalue for the BWR geometry. Similar results are seen in the PWR geometry. In these cases, the quartic polynomial needs only one adjustment on the homogenized parameters to result in excellent agreement with the converged eigenvalue.

Table 4.7. Eigenvalue at the End of Each Flux and Eigenvalue Convergence Loop for the BWR Geometry using Different Flux Approximations.

Adjustment #	F.D.	Quadratic	Quartic
Initial	1.02544	1.02385	1.02402
1	1.02585	1.02592	1.02608
2	1.02585	1.02599	1.02606
3	1.02592	1.02603	1.02607
4	1.02597	1.02605	1.02607
5	1.02600	1.02606	1.02607
6	1.02602	1.02607	1.02607
7	1.02604	1.02607	1.02607
8	1.02605	1.02607	1.02607
9	1.02606	1.02607	1.02607
10	1.02606	1.02608	1.02607
11	1.02607	1.02608	1.02608
12	1.02607	1.02608	1.02608
13	1.02607	1.02608	1.02608
14	1.02607	1.02608	1.02608
15	1.02607	1.02608	1.02608
16	1.02607	1.02608	1.02608
17	1.02608	1.02608	1.02608
18	1.02608	1.02608	1.02608
19	1.02608	1.02608	1.02608
20	1.02608	1.02608	1.02608

Table 4.8. Eigenvalue at the End of Each Flux and Eigenvalue Convergence Loop for the PWR Geometry using Different Flux Approximations.

Adjustment #	F.D.	Quadratic	Quartic
Initial	1.10531	1.10416	1.10437
1	1.10490	1.10507	1.10531
2	1.10499	1.10517	1.10532
3	1.10507	1.10523	1.10532
4	1.10512	1.10526	1.10532
5	1.10516	1.10528	1.10532
6	1.10520	1.10530	1.10532
7	1.10522	1.10530	1.10532
8	1.10524	1.10531	1.10532
9	1.10526	1.10531	1.10532
10	1.10527	1.10531	1.10532
11	1.10528	1.10531	1.10532
12	1.10529	1.10531	1.10532
13	1.10529	1.10532	1.10532
14	1.10530	1.10532	1.10532
15	1.10530	1.10532	1.10532
16	1.10530	1.10532	1.10532
17	1.10531	1.10532	1.10532
18	1.10531	1.10532	1.10532
19	1.10531	1.10532	1.10532
20	1.10531	1.10532	1.10532

Convergence Characteristics using Different Diffusion Coefficients

The two global reactor geometries are analyzed in this segment using abnormal diffusion coefficients. The goal of performing these analyses is to determine if the diffusion coefficient is an arbitrary parameter as discussed in Section 3.4. Since it was found that the quartic polynomial flux approximation provides superior convergence results than the finite difference or quadratic polynomial flux approximations, analyses in this segment use the quartic flux approximation. For all assemblies in both geometries, typical values for the diffusion coefficients are approximately 1.4 cm and 0.7 cm for the fast and thermal energy groups, respectively. This segment replaces the diffusion coefficients given in Tables D.1 through D.6 with the following combinations; (i) 1.0 cm and 0.5 cm, (ii) 0.7 cm and 0.2 cm, and (iii) 2.8 cm and 0.8 cm for the fast and thermal energy groups, respectively. These values will not affect the continuity of current equations (equations (2.28)) because the diffusion coefficients in adjacent nodes are equal and will cancel out. However, they will alter the leakage in the neutron balance equation and, thus, alter the currents and the average fluxes in each node.

Table 4.9. Eigenvalues and Errors in the Power Profiles using Various Diffusion Coefficients with the Quartic Flux Approximation after updating the Homogenized Parameters Twenty Times for the BWR Geometry.

Diffusion Coefficients	Eigenvalue			
		0.10% 0.11% -	-0.30% -0.29% -	0.77% 0.77% -
1.0 / 0.5	1.02607	-1.22% -1.21% -	0.34% 0.34% -	0.12% 0.11% -
0.7 / 0.2	1.02608			
2.8 / 0.8	diverged			
		0.28% 0.30% -	-0.51% -0.52% -	0.11% 0.09% -

Table 4.10. Eigenvalues and Errors in the Power Profiles using Various Diffusion Coefficients using the Quartic Flux Approximation after updating the Homogenized Parameters Twenty Times for the PWR Geometry.

Diffusion Coefficients	Eigenvalue			
		-1.08% -1.06% -	0.39% 0.39% -	0.64% 0.62% -
1.0 / 0.5	1.10532	-0.35% -0.34% -	-0.92% -0.92% -	1.64% 1.63% -
0.7 / 0.2	1.10532			
2.8 / 0.8	diverged			
		-0.46% -0.45% -	-0.07% -0.07% -	-0.01% 0.00% -

As seen in Tables 4.9 and 4.10, two of the three diffusion coefficient sets converged to identical solutions as presented in Tables 4.5 and 4.6. Therefore, using diffusion coefficient sets of 1.0/0.5 and 0.7/0.2 also reduced assembly power errors by a factor of two compared to the best solution using infinite lattice homogenized parameters without correlations. Also, these two sets of diffusion coefficients reduced the error in the eigenvalue compared to the best nodal solution using infinite lattice homogenized parameters. Results from these tables prove that evaluating the flux discontinuity factor by correlating the transport theory edge-to-average flux ratio does account for uncertainties in the diffusion coefficient provided that values of the diffusion coefficients are within reason. A reasonable diffusion coefficient can be found by any of the common techniques presently used to find diffusion coefficients. This can include flux and volume weighing the heterogeneous diffusion coefficients, flux and volume weighing the heterogeneous transport cross sections then multiplying by three and inverting, or any other well-known method. These methods should all result in diffusion coefficients that are within a general expected range. For example, a range of 1.0 to 1.8 for the fast energy group of a light water reactor.

In the analyses where the solution diverged, the large diffusion coefficients overpredicted the currents on the node boundaries. This, in turn, caused the current-to-flux ratios of the nodal solution to be larger than the reference current-to-flux ratios and, therefore, the adjusted homogenized cross sections were overpredicted. More importantly, the correlated values of the edge-to-average flux ratios were also overpredicted. These

adjustments lead to an oscillating effect of overpredicting and underpredicting the homogenized parameters and, thus, the iterative procedure diverged. Negative values of the diffusion coefficient were not examined because of convergence characteristics of the neutron balance equation associated with the negative diffusion coefficients.

As in the previous segment, an important feature to examine is how often the homogenized parameters are adjusted to reach practical convergence for the various sets of diffusion coefficients. As before, examining the eigenvalue at the end of a series of outer iterations (when the flux and eigenvalue have converged for the given set of homogenized parameters) provides some insight to the dilemma. The eigenvalue found after each adjustment to the homogenized parameters is listed in Tables 4.11 and 4.12 for the BWR and PWR geometries, respectively. Comparing the third column of Table 4.7 to Table 4.11 shows that the reasonable values for the diffusion coefficients (~1.4/0.4 from Table 4.7) require fewer adjustments to the homogenized parameters to reach practical convergence than the arbitrary diffusion coefficients used to generate Table 4.11. However, results in the first column of Table 4.11 suggests that great accuracy (accuracy greater than one-tenth) for the diffusion coefficient may be unnecessary. Comparing Tables 4.8 and 4.12 show the same conclusions for the PWR geometry.

These results can aid in simplifying the diffusion equations. For example, if the diffusion coefficients for an energy group are equal for all assemblies, then the diffusion coefficient will cancel out in the continuity of current equation (equation (2.28)). This leads to a simpler equation to program in a nodal code.

Table 4.11. Eigenvalue at the End of Each Flux and Eigenvalue Convergence Loop for the BWR Geometry using Various Diffusion Coefficients.

Adjustment #	1.0 / 0.5	0.7 / 0.2	2.8 / 0.8
Initial	1.02527	1.02773	1.02259
1	1.02611	1.02599	1.02596
2	1.02607	1.02605	1.02607
3	1.02607	1.02607	1.02609
4	1.02607	1.02607	1.02605
5	1.02607	1.02608	1.02612
6	1.02607	1.02608	1.02599
7	1.02607	1.02608	1.02616
8	1.02607	1.02608	1.02587
9	1.02607	1.02608	1.02638
10	1.02607	1.02608	diverged
11	1.02607	1.02608	
12	1.02607	1.02608	
13	1.02607	1.02608	
14	1.02607	1.02608	
15	1.02607	1.02608	
16	1.02607	1.02608	
17	1.02607	1.02608	
18	1.02607	1.02608	
19	1.02607	1.02608	
20	1.02607	1.02608	

Table 4.12. Eigenvalue at the End of Each Flux and Eigenvalue Convergence Loop for the PWR Geometry using Various Diffusion Coefficients.

Adjustment #	1.0 / 0.5	0.7 / 0.2	2.8 / 0.8
Initial	1.10497	1.10570	1.10376
1	1.10531	1.10523	1.10521
2	1.10532	1.10528	1.10537
3	1.10532	1.10530	1.10529
4	1.10532	1.10531	1.10533
5	1.10532	1.10531	1.10531
6	1.10532	1.10532	1.10532
7	1.10532	1.10532	1.10532
8	1.10532	1.10532	1.10532
9	1.10532	1.10532	1.10532
10	1.10532	1.10532	1.10533
11	1.10532	1.10532	1.10536
12	1.10532	1.10532	1.10543
13	1.10532	1.10532	1.10556
14	1.10532	1.10532	1.10615
15	1.10532	1.10532	1.10649
16	1.10532	1.10532	diverged
17	1.10532	1.10532	
18	1.10532	1.10532	
19	1.10532	1.10532	
20	1.10532	1.10532	

Conclusions for Applying Correlations to Homogenized Parameters

It was numerically proven in this section that applying global reactor information (current-to-flux ratios) to the homogenized parameters increases the accuracy of the global reactor solution by approximately a factor of two compared to solutions that do not use global reactor information to adjust the homogenized parameters. Additionally, it was shown that concerns for the accuracy of the nodal code flux approximation and diffusion coefficients are eased by applying correlations to the homogenized parameters. Except for large values for the diffusion coefficients, it was demonstrated that different flux approximations and diffusion coefficients all result in identical solutions for the two sample geometries. This is because the infinite lattice homogenized parameters and correlations to adjust them are independent of the flux approximation in the nodal code and the homogenized diffusion coefficient.

However, it was also pointed out that better flux approximations and diffusion coefficients require fewer adjustments to the homogenized parameters to reach a practically converged solution. A fully converged solution results in identical flux profiles before and after making adjustments to the homogenized parameters. It was shown that, with a superior flux approximation and reasonable values for diffusion coefficients, only a couple of adjustments to the homogenized parameters are necessary to reduce the assembly power errors by a factor of two.

For the diffusion coefficients, only reasonable values are necessary for the flux and eigenvalue iterations. This means that computer codes can eliminate storage requirements

for the diffusion coefficient in favor of one approximate diffusion coefficient for each energy group for all fuel assemblies. For example, in common BWR or PWR fuel assemblies, the diffusion coefficient can simply be set at 1.4 cm and 0.4 cm for two group problems. The reflector may need a separate diffusion coefficient for each energy group.

4.6 Approximations to Correlation Coefficients

In this section, the correlation coefficients for the different fuel assemblies are compared to each other. As seen in Appendix D for the BWR assemblies, each set of homogenized parameters requires storage of 52 correlation coefficients assuming one-half symmetry and two energy groups (5 cross sections plus 8 edge-to-average flux ratios times 4 current-to-flux ratios). This increase in the storage requirements is a disadvantage to applying global reactor information to the homogenized parameters. The purpose of this section is to examine methods to reduce the storage requirements for the correlation coefficients by finding and eliminating the weak dependencies.

In a quick comparison of values for the correlation coefficients in Appendix D, the magnitudes of the cross section coefficients are different from the magnitudes of the edge-to-average flux ratio coefficients. The edge-to-average flux ratio coefficients are much larger than the coefficients for the cross sections. Therefore, no comparison is made between these two categories of homogenized parameters.

Effect of Thermal Group Currents on Fast Group Homogenized Parameters

For the two group problems in this thesis, examining the correlation coefficients shows that thermal energy group current-to-flux ratios do not show strong effects on the fast energy group homogenized parameters. These coefficients are approximately a factor of ten smaller than the other coefficients. This suggests that these effects are weak and opens the possibility of neglecting the them. However, for the BWR geometry, neglecting these effects results in a maximum assembly power error of 1.97% and the RMS assembly power error is 0.90%. Similarly for the PWR geometry, the maximum error is 3.70% and the RMS error is 1.69%. These errors do not show much improvement over the best solution using infinite lattice homogenized parameters without correlations. Thus, the thermal group current-to-flux ratio correlation coefficients affecting the fast group homogenized parameters are smaller than other coefficients, but they are necessary to obtain accurate global reactor solutions.

Effect of a Current on the Edge-to-Average Flux Ratios of Orthogonal Surfaces

Another observance in most sets of correlation coefficients is that a current crossing one surface (the left surface for instance) minutely affects the edge-to-average flux ratio correlation coefficients on an orthogonal surface (the top or bottom edge-to-average flux ratios). In the PWR fuel assemblies, this consequence is not surprising because of the symmetry of the fuel assemblies. Looking along the face of any of the PWR assemblies, the top face of Figure 4.6 for example, the materials are all fuel pins with identical cross sections. Thus, the flux shape across the top boundary will not

have a local maxima or minima. In this figure, if a current is present on the left surface coming into the assembly, then we expect the edge-to-average flux ratio on the top boundary near the left side to be high and the edge-to-average flux ratio near the right boundary to be low. Since equivalence theory is concerned with integral results, integrating the edge flux shape across the top boundary when a current is present on the left surface has little effect on the top edge flux value. For the PWR global reactor problem, neglecting these effects results in a maximum assembly power error of 1.65% and a RMS error of 0.80%. These errors are minutely increased from errors that include the orthogonal effects.

However, in the BWR fuel assemblies, the effect that a current has on an edge-to-average flux ratio on a surface with a control blade inserted is large. In Figure 4.2 for example, a current on the left boundary has a significant effect on the edge-to-average flux ratio on the top surface but not the bottom surface. This is because the material along the bottom surface is uniform (water) and the materials along the top surface are part water and part absorber. When the edge flux is integrated along the top surface, a current on the left boundary causes a large change in the top edge flux value.

Surprisingly, neglecting the effect that currents have on the edge-to-average flux ratio on orthogonal surfaces actually leads to improved results for the BWR geometry. The maximum assembly power error is 0.66%, almost half that of the maximum error when accounting for these effects. Leaving out these orthogonal effects also reduces the RMS assembly power error from 0.54% to 0.36%. However, these results for the BWR

geometry should not imply that ignoring the effects that a current has on an edge-to-average flux ratio on an orthogonal surface always improves the global reactor solution. In the geometry at hand, the outer boundaries are reflective (i.e., no current) and they do not contain the control blade. As such, there are few surfaces that actually contribute to these effects. In a full model of a BWR reactor, the global solution will contain many currents that affect the edge-to-average flux ratio on the orthogonal surfaces. Thus, it may be acceptable to overlook the effect that a current has on the edge-to-average flux ratio on an orthogonal surface provided that the material near the orthogonal surface is uniform.

Effects of Currents in Assemblies with Similar Material Arrangements

It can be seen in the tables in Appendix D that the correlation coefficients are largely dependent on the material arrangement in the assembly. In the BWR fuel assemblies analyzed, the geometries (dimensions) are identical. However, the correlation coefficients for an assembly with the control blade inserted are vastly different from an assembly without the control blade. This difference represents a different material arrangement. Each assembly is also analyzed with different fuel cross sections. This is not a different material arrangement because fuel is not replaced by a different material type such as water or absorber. Examining the three BWR fuel assemblies without the control blade shows that the correlation coefficients are nearly identical. The same holds true for the BWR fuel assemblies with the control blade and the PWR fuel assemblies without the control rod cluster inserted. This implies that the coefficients show little dependence on

details of the fuel cross sections provided that the fuel cross sections are equal in all fuel pins.

Analyzing the global reactor problems with identical correlation coefficients for similar assemblies does not create significant errors in the global reactor solutions. The BWR geometry using the correlation coefficients of Table D.7 for the five assemblies without control and the correlation coefficients of Table D.8 for the four assemblies with the control blade results in a maximum assembly power error of 1.22% and a RMS error of 0.66%. Similarly for the PWR geometry, using the coefficients of Table D.13 for all fuel assemblies without a control rod cluster inserted results in a maximum assembly power error of 1.49% and a RMS error of 0.87%. These errors are commensurate to errors using the correct correlation coefficients for all assemblies.

In the previous discussion, the only differences in the various assemblies are values of the heterogeneous fuel cross sections. Another consideration to explore is the change in the correlation coefficients when the fuel temperature changes or when voiding of water occurs in a BWR assembly. The heterogeneous fuel pin cross sections used in previous sections correspond to hot zero power conditions (565 °K). When the fuel temperature is increased from 565 °K to 1000 °K, the resulting change in the correlation coefficients, listed in Table D.17, are small. Thus, correlation coefficients have a very weak dependency on fuel temperature changes, again, provided that the fuel temperatures uniformly change in all fuel pins in an assembly. Listed in Table D.18 are the correlation coefficients for the BWR assembly B with a control blade inserted when the water is 40%

voided. Comparing these correlation coefficients to Table D.10 (0% void) shows noticeable changes in the coefficients for both cross sections and edge-to-average flux ratios. However, these changes are not much different than the changes between assemblies with different fuel enrichments.

Still another consideration is related to burnup effects. Often, computer codes use quadratic polynomials to keep track of intra-assembly burnup characteristics. If the burnup is not flat throughout the fuel pins, then the correlations coefficients can show a notable change. To test this, the heterogeneous fuel cross sections are adjusted linearly for the BWR fuel assembly B that has the control blade inserted. Each cross section in the fuel material is adjusted according to

$$\Sigma' = \Sigma\,(1.125 - 0.025\,i) \tag{4.1}$$

where i is an index for the fuel pin cell. For the far left fuel pin cells, $i = 1$ and for the far right pin cells, $i = 8$. Thus the fuel cross sections range from a ten percent increase to a seven and a half percent decrease in all cross sections. The fuel cross sections are constant across a top to bottom traverse.

The correlation coefficients for this assembly are given in Table D.19. Comparing to Table D.10, a current on the left face of the assembly does show a significant change in the correlation coefficients for the cross sections but not a large difference for the

edge-to-average flux ratio coefficients. Thus, the linear gradient in the heterogeneous fuel cross sections is reflected in the flux and volume weighted homogenized cross sections. However, the linear gradient in the heterogeneous fuel cross sections does not significantly alter the manner that a current on the left boundary affects the edge-to-average flux ratios. Comparison of Tables D.10 and D.19 also shows that a current on the top face of the assembly produces little change in the cross section coefficients and edge-to-average flux ratio coefficients. This is expected since the fuel cross sections are constant in the top to bottom traverse. Because the assembly is asymmetric, a current on the right face of the node will also create a significant change in the cross section coefficients. These results are important because they show that gradual changes in the heterogeneous fuel cross sections do not strongly affect the edge-to-average flux ratio correlation coefficients.

Weak Global Reactor Correlation Coefficient Dependencies

It has been pointed out in this section that computer storage requirements for correlation coefficients can be larger than desired. This is because the correlations are dependent on the node surface, energy group, and homogenized parameter. Finding and removing the weak dependencies from the set of correlation coefficients can amply reduce the storage requirements for the coefficients. This section shows that the thermal group current-to-flux ratios do not affect the fast group homogenized parameters as much as other effects, but this dependency is definitely not a weak dependency and the correlation set must include it to obtain accurate global reactor results. One dependency that is often

weak is the effect that a current-to-flux ratio has on a surface orthogonal to the current. However, as discussed, this effect is necessary when the material along a node surface is not uniform. Such a case is always present in BWR fuel assemblies when a cruciform control blade in inserted in between the BWR fuel elements.

It was also shown that the correlation coefficients are dominated by the geometry and material arrangements in the fuel assembly. The material arrangement refers to types of materials (fuel, water, absorber, etc.) as opposed to specific cross sections of similar types of materials. This awareness provides a successful method to vastly reduce computer storage requirements for the coefficients and, perhaps more importantly, reduce the number of lattice homogenization solutions necessary to find a complete set of correlation coefficients. Using identical correlation coefficients for all fuel assemblies of similar geometries and material arrangements does not noticeably diminish the accuracy of the global reactor solution. However, if the reactivity of each fuel pin changes within the assembly as in burnup analyses, then the correlation coefficients for the homogenized cross sections do appreciatively change.

4.7 Conclusions from the Two-Dimensional Analyses

Global reactor information has been applied in this chapter to correlations to adjust homogenized parameters for sample two-dimensional BWR and PWR geometries. Reference transport theory solutions were found and presented for the two geometries for comparison results. Also, solutions that use widely practiced nodal analysis methods

(infinite lattice homogenized parameters only) were found and comparisons were made between the nodal solutions and the reference transport solutions.

It was explained in Section 4.5 how to find the correlation coefficients for the fuel assemblies and how the coefficients are used in conjunction with the infinite lattice homogenized parameters. Once the coefficients were available, they were applied to the global reactor problems to prove, numerically, that the method introduced in Chapter III to compute flux discontinuity factors does account for the nodal code flux approximation and uncertainties in the diffusion coefficients. Thus, correlating the edge-to-average flux ratios from the lattice homogenization solution allows different flux approximations and diffusion coefficients to produce equivalent nodal solutions (with exception of large values for the diffusion coefficients). The results from these solutions showed that applying the correlations reduces the maximum assembly power error and the RMS errors by approximately a factor of two compared to not applying correlations.

Because adjusting the homogenized parameters is an iterative procedure, convergence characteristics of the method were also examined in Section 4.5. The convergence characteristics examined in this chapter are assumed to be independent of the flux and eigenvalue convergence loops. The solutions have converged when the global reactor information does not result in any further change to the homogenized parameters and, thus, the upcoming global reactor solution will not change either. Because different flux approximations in the nodal analysis and different diffusion coefficients produce identical results (with exception of large values for the diffusion coefficients), it may

at first seem advantageous to employ the simplest flux approximation and use haphazard diffusion coefficients, diffusion coefficients equal to one for instance. However, a different conclusion was found in Section 4.5. As shown in that section, employing a more accurate flux approximation in the nodal code will require fewer adjustments to the homogenized parameters to reach convergence than employing a simpler flux approximation. Likewise, the nodal analysis will reach convergence with fewer adjustments to the homogenized parameters when it uses reasonable values for the diffusion coefficients rather than haphazard values. However, quick convergence does not require the diffusion coefficients to be accurate. Values to only one decimal place are sufficient.

The computer storage requirements for the correlation coefficients are criticized in Section 4.6. Thus, the dominating influences on the correlation coefficients were found. It was shown that the material arrangements in the assembly dominate the correlation coefficients. If one material type replaces another, then the correlation coefficients will drastically change. An example of this is when an absorber material replaces a location previously occupied by water. Negligible change in the correlation coefficients will occur when a material replaces another material of a similar type uniformly throughout the assembly. For instance, when fuel of one enrichment replaces fuel of a different enrichment. However, when the heterogeneous fuel cross sections have a gradient across the assembly, the correlation coefficients for the homogenized cross sections will show stronger dependency to the gradient. These cases occur when the nodal code models the

intra-assembly burnups, for example. Nevertheless, the gradient in the fuel cross sections do not appreciably alter the edge-to-average flux ratios, but, as discussed in the first chapter, both homogenized cross sections and flux discontinuity factors have to be adjusted simultaneously to improve global reactor results.

In conclusion, correlating the homogenized parameters to account for global reactor effects can reduce the maximum assembly power error and the RMS errors of all assemblies by approximately a factor of two. Also, using an accurate flux approximation in the nodal code and reasonable diffusion coefficients lessens to number of times to adjust the homogenized parameters to about two adjustments. Relationships between similar assemblies can be used to reduce the computer storage requirements for the correlation coefficients and reduce the number of lattice homogenization calculations required to find a complete set of correlation coefficients. It is imperative to employ the shifted circle boundary condition to find the correlation coefficients.

CHAPTER V

SUMMARY AND CONCLUSIONS

5.1 Overview of the Investigation

The goal of this thesis is to develop a feasible method for improving the accuracy of homogenized parameters used in nodal diffusion theory by applying global reactor information. The global reactor information used to improve homogenized parameters are the currents along node boundaries relative to the average flux of the same energy group within the node. An iterative method that uses correlations to adjust infinite lattice homogenized parameters can fulfill this objective. This approach can contain the adjustments to the homogenized parameters within the nodal code. Thus, nodal diffusion theory codes can incorporate global effects into a final solution in a similar manner as thermal feedback effects.

Common nodal diffusion theory analyses use infinite lattice homogenized parameters without any adjustments for the global reactor information. These analyses have been shown to provide good solutions to global reactor problems. However, some analyses do account for global reactor information by using extended geometry calculations to find homogenized parameters and others use a strategy that iterates between the lattice homogenization analyses for each node and a nodal solution for the global reactor problem. These analyses are superior to analyses using infinite lattice

homogenized parameters only, but they are also more costly and therefore less feasible than the approach taken in this thesis. It was demonstrated numerically that correlations for the homogenized parameters are accurate and the increased cost to generate and apply the correlations makes the method feasible.

Two computer codes were written to investigate methods to improve homogenized parameters for nodal diffusion theory codes. One code is a lattice homogenization code (JTC) and the other is a nodal diffusion theory code (NDT). For this thesis, it is important that the lattice homogenization code is not based on diffusion theory. This is because lattice homogenization codes used for production analyses are based on transport theory and because appropriate boundary conditions for transport theory lattice homogenization are crucial to accurately correlate homogenized parameters. NDT is a nodal diffusion theory code that has several different flux approximations available. Both codes have been benchmarked and show favorable results compared to more popular reactor analysis codes. In the case of NDT, the simpler flux approximations show expected results. The simpler flux approximations converge to a solution, but the power profiles are not as accurate as the more complex flux approximations.

It was demonstrated numerically that linear correlations for the homogenized parameters are sufficiently accurate. Correlations can easily be found that include higher ordered polynomials of the current-to-flux ratio and cross product terms between current-to-flux ratios from different energy groups or surfaces of the node. However, including these terms will obviously make the method to improve homogenized

parameters more expensive because of the large number of lattice homogenization calculations required to form such a set of correlations.

In Chapter III, it was emphasized that flux discontinuity factors should not be correlated as homogenized parameters, but that edge-to-average flux ratios from the homogenization analysis should be correlated. In the case of infinite lattice homogenized parameters, the two are equal and there is no need to distinguish between them. However, when adjusting the homogenized parameters to reflect effects of the global reactor solution, there are several reasons for this distinction. First, flux discontinuity factors cannot be accurately modeled by a linear correlation but the edge-to-average flux ratios from the lattice homogenization can. If the edge-to-average flux ratio from the lattice homogenization is known by a correlation or any other method, then the flux discontinuity factor can be easily found. Also, when a current is present on any surface of the node, the flux discontinuity factor is dependent on the flux approximation in the nodal code and the diffusion coefficient. The edge-to-average flux ratio from the lattice homogenization is completely independent of the nodal code flux approximation and the diffusion coefficient. Thus, correlating the edge-to-average flux ratio can allow the nodal code to account for the flux approximation and diffusion coefficients that it is using. Koebkes' postulates state that equivalence theory should preserve the lattice homogenization edge fluxes and average flux. They do not state that equivalence theory should preserve the flux discontinuity factor.

A new assembly boundary condition named the shifted circle boundary condition was introduced in this thesis. In an *x-y* coordinate system, this boundary condition causes the angular flux shape to be circular about a point to the left or right of the origin. Linear correlations for the edge-to-average flux ratio are accurate provided that the lattice homogenization code uses this boundary condition to create a current along a node boundary necessary to find the correlation coefficients. A numerical analysis demonstrated that the albedo boundary condition in transport theory codes is capable of creating a current but it does not accurately model the scalar flux profile near the node boundary. This causes the edge flux to be faulty and, thus, the edge-to-average flux is also faulty. These inaccurate values lead to errant correlation coefficients for the edge-to-average flux ratios. It was also demonstrated numerically that the shifted circle boundary condition does model the scalar flux profile near the node boundaries accurately. This results in finding accurate correlation coefficients for the edge-to-average flux ratios.

In two-dimensional problems that represent small portions of a BWR and PWR reactor, the linear correlations for the homogenized parameters were shown to reduce the maximum and root mean square errors in assembly powers by a factor of two. It was demonstrated numerically that with the correlations, different flux approximations in the nodal code and different diffusion coefficients all result in identical final solutions to the global reactor problem. However, it was pointed out that a final solution rapidly converges when a more accurate flux approximation is used in the nodal code along with

reasonably accurate diffusion coefficients. With these conditions, practical convergence is reached in only two adjustments to the homogenized parameters.

Sensitivity of the correlations to the material arrangement in the fuel assemblies and the heterogeneous cross sections was examined. This investigation showed that correlations are strongly dependent on the fuel assembly geometry and the material arrangement in the fuel assembly. The material arrangement refers to materials of a similar type being in identical locations in the fuel assembly. A numerical analysis showed that inserting a control blade in a BWR assembly, for instance, will greatly alter the correlation coefficients. The analysis also showed that altering the cross sections uniformly throughout the assembly does not significantly alter the correlation coefficients. This dependency is important because it allows correlations to be found for one assembly and used for all assemblies of similar geometries and material arrangements. This significantly reduces the cost of generating and storing the correlation coefficients and makes the method to incorporate global effects into the homogenized parameters more feasible.

As emphasized in the thesis, employing correlations to the infinite lattice homogenized cross sections and the infinite lattice edge-to-average flux ratios from the lattice homogenization code can account for deficiencies in the nodal code flux approximation and ambiguities or uncertainties in the diffusion coefficients. Although correlations relieve apprehensions for the nodal code, it does, unfortunately, elevate worries for the lattice homogenization code. In particular, there are concerns about the

boundary condition used to create a current on a node surface and find correlation coefficients. The shifted circle boundary condition was developed to provide a boundary condition that accurately predicts the flux on the surface of a node and creates a current on the surface.

5.2 Recommendations for Future Work

The results of this thesis open the door to other research avenues in lattice homogenization and nodal diffusion theory. These queries are beyond the limits of the computer codes JTC and NDT and should be investigated using more common production based computer codes.

The shifted circle boundary condition was successfully implemented in the discrete ordinates transport theory code JTC. However, most lattice homogenization codes use integral transport theory; either collision probabilities or the method of characteristics. The shifted circle boundary condition should also be applied to these analysis techniques.

Unlike the analyses in this thesis, lattice homogenization codes used for production analysis employ an energy group structure with twenty to eighty energy groups and then collapse the multigroup structure to two broad groups. Further research should explore how to place currents in a multigroup structure and then collapse the energy group structure (including currents) to two broad groups. For example, three different possibilities may be to i) place a current in only one fine group, ii) place an equal current in each fine group of a broad energy group, or iii) place a current in each fine

group of a broad energy group based on the flux spectrum of the fuel assembly. Although reason warrants the latter example to be the obvious choice, there may be better choices.

Burnup dependencies of the correlations should also require a more thorough examination. Research in this area should concentrate on the intra-nodal burnup shape of the fuel and burnup of burnable absorber pins such as Gadolinium. Although a segment of the thesis touched on an intra-nodal burnup shape, it did not test the correlations to a reference solution. Additionally, the depletion of a strong absorber material in the fuel was not examined in the thesis.

Finally, the method should be applied and benchmarked against experimental data for a full core analysis. These studies should include application of the method to the baffle/reflector regions in the reactor. Also, studies using a three-dimensional model should be performed.

APPENDIX A

JTC BENCHMARK RESULTS

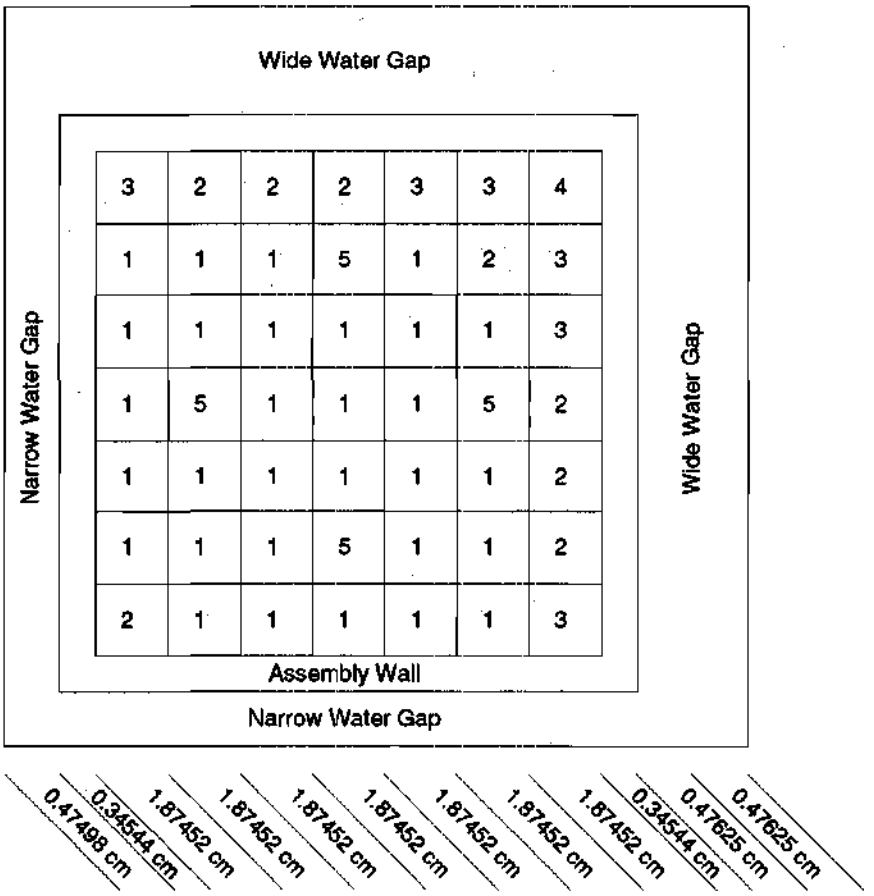

Figure A.1. Geometry Description of the BWR Rod Bundle Benchmark Problem.

Table A.1. Two-Group Material Cross Sections for the BWR Rod Bundle Benchmark Problem. cm^{-1}

Material	Group	Σ_a	Σ_f	$\nu\Sigma_f$	Σ_t	$\Sigma_{1\to2}$
1	1	8.983e-03	2.281e-03	5.925e-03	2.531e-01	1.069e-02
	2	5.892e-02	4.038e-02	9.817e-02	5.732e-01	
2	1	8.726e-03	2.003e-03	5.242e-03	2.536e-01	1.095e-02
	2	5.174e-02	3.385e-02	8.228e-02	5.767e-01	
3	1	8.587e-03	1.830e-03	4.820e-03	2.535e-01	1.112e-02
	2	4.717e-02	2.962e-02	7.200e-02	5.797e-01	
4	1	8.480e-03	1.632e-03	4.337e-03	2.533e-01	1.113e-02
	2	4.140e-02	2.428e-02	5.900e-02	5.837e-01	
5	1	9.593e-03	2.155e-03	5.605e-03	2.506e-01	1.016e-02
	2	1.626e-01	9.968e-03	2.424e-02	5.853e-01	
Assembly Wall	1	1.043e-03	0	0	2.172e-01	9.095e-03
	2	4.394e-03	0	0	4.748e-01	
Water Gap	1	1.983e-04	0	0	2.476e-01	3.682e-02
	2	7.796e-03	0	0	1.123e+00	

Table A.2. Two-Group Fluxes from JTC using 4×4 Mesh Spacing and S_8 Angular Quadrature.

0.1736	0.1741	0.1766	0.1794	0.1796	0.1782	0.1761	0.1726	0.1663	0.1616	0.1602	0.1592
0.1123	0.1108	0.1060	0.0996	0.0958	0.0952	0.0993	0.1069	0.1182	0.1265	0.1296	0.1318
0.1752	0.1760	0.1791	0.1821	0.1822	0.1808	0.1787	0.1752	0.1686	0.1633	0.1614	
0.1089	0.1065	0.1010	0.0942	0.0904	0.0898	0.0940	0.1018	0.1135	0.1225	0.1267	
0.1775	0.1790	0.1828	0.1862	0.1863	0.1848	0.1827	0.1791	0.1720	0.1658		
0.1041	0.1006	0.0945	0.0874	0.0836	0.0830	0.0873	0.0952	0.1074	0.1169		
0.1844	0.1865	0.1925	0.1968	0.1964	0.1942	0.1925	0.1892	0.1808			
0.0939	0.0902	0.0825	0.0746	0.0704	0.0690	0.0743	0.0828	0.0959			
0.1924	0.1949	0.2020	0.2060	0.2049	0.2010	0.2016	0.1984				
0.0810	0.0771	0.0686	0.0604	0.0553	0.0502	0.0587	0.0685				
0.1957	0.1982	0.2047	0.2081	0.2083	0.2069	0.2056					
0.0733	0.0694	0.0606	0.0518	0.0490	0.0481	0.0518					
0.1969	0.1993	0.2051	0.2069	0.2093	0.2092						
0.0697	0.0658	0.0564	0.0446	0.0456	0.0464						
0.1977	0.2001	0.2066	0.2100	0.2104							
0.0707	0.0668	0.0581	0.0493	0.0465							
0.1971	0.1995	0.2065	0.2107				Group 1				
0.0748	0.0709	0.0624	0.0543				Group 2				
0.1930	0.1953	0.2016									
0.0823	0.0785	0.0706									
0.1891	0.1907										
0.0884	0.0850										
0.1880											
0.0909											

Table A.3. Comparison of JTC to the Reference Solution (DOT-III) and the TWOTRAN-II Code. All Solutions used a 4×4 Mesh Spacing and S_8 Angular Quadrature.

		Flux ratio[a]	
	k-eff	maximum	minimum
DOT-III	1.08714	-	-
TWOTRAN-II	1.08727	1.007	0.980
JTC	1.08590	1.012	0.977

[a] The flux ratio is the flux from JTC or TWOTRAN divided by DOT.

APPENDIX B

NDT BENCHMARK RESULTS

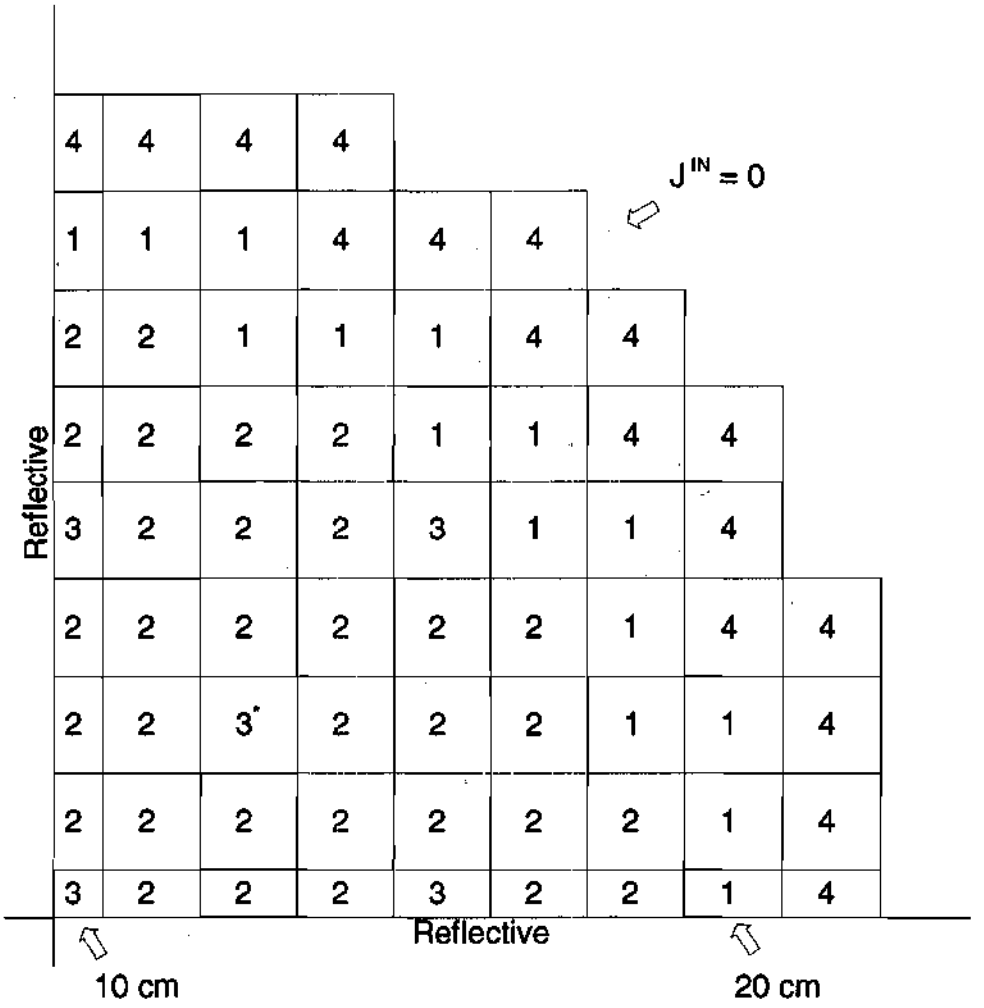

Figure B.1. Radial Geometry Description of the 3-D IAEA Benchmark Problem. Material 3* is a Partially Inserted Control Rod. NDT uses a Zero Scalar Flux Boundary Condition rather than No Incoming Partial Current.

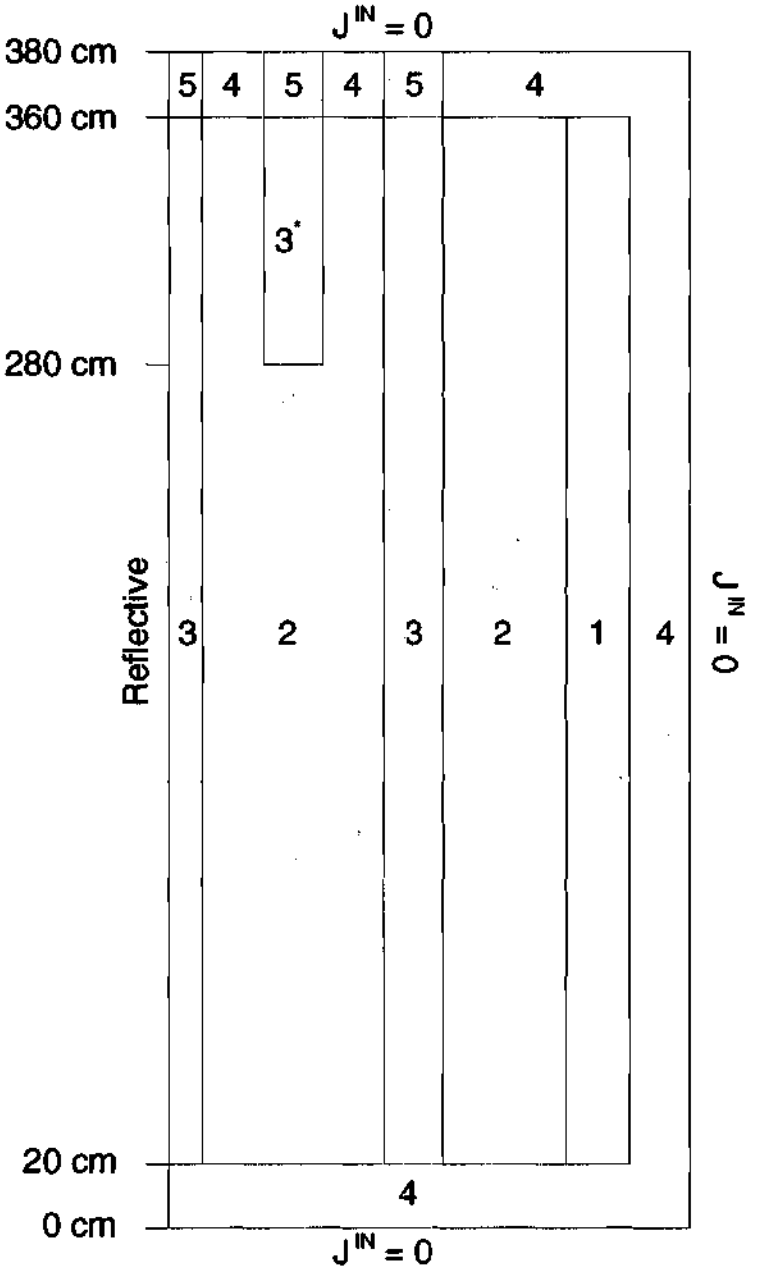

Figure B.2. Axial Geometry Description of the 3-D IAEA Benchmark Problem. Material 3* is a Partially Inserted Control Rod. NDT uses a Zero Scalar Flux Boundary Condition rather than No Incoming Partial Current.

Table B.1. Two-Group Material Cross Sections for the 3-D IAEA Benchmark Problem. cm^{-1}

Material	Group	D (cm)	Σ_a	$\nu\Sigma_f$	$\Sigma_{1\text{-}2}$
1	1	1.500e+00	1.000e-02	0	2.000e-02
	2	4.000e-01	8.000e-02	1.350e-01	
2	1	1.500e+00	1.000e-02	0	2.000e-02
	2	4.000e-01	8.500e-02	1.350e-01	
3	1	1.500e+00	1.000e-02	0	2.000e-02
	2	4.000e-01	1.300e-01	1.350e-01	
4	1	2.000e+00	0	0	4.000e-02
	2	3.000e-01	1.000e-02	0	
5	1	2.000e+00	0	0	4.000e-02
	2	3.000e-01	5.500e-02	0	

Table B.2. Assembly Power Densities for the 3-D IAEA Benchmark Problem.

					0.597		
					0.599		
					0.598		
					0.516		
					0.461		
		Eigenvalue			0.585		
VENTURE		1.02903		0.476	0.700	0.611	
QUANDRY		1.02902		0.475	0.705	0.615	
IQSBOX		1.02911		0.474	0.703	0.611	
NDT F.D.		1.03158		0.364	0.738	0.504	
NDT Quadratic		1.02822		0.447	0.650	0.483	
NDT Quartic		1.02889		0.472	0.697	0.601	
			1.178	0.972	0.923	0.866	
			1.178	0.972	0.924	0.869	
			1.179	0.972	0.926	0.866	
			1.237	1.006	0.921	0.786	
			1.241	1.011	0.888	0.733	
			1.185	0.976	0.919	0.855	
		1.368	1.311	1.181	1.089	1.000	0.711
		1.366	1.311	1.180	1.088	0.999	0.711
		1.366	1.311	1.181	1.087	0.995	0.707
		1.409	1.364	1.188	1.084	1.025	0.577
		1.466	1.396	1.239	1.072	0.922	0.563
		1.378	1.322	1.185	1.087	0.990	0.696
	1.397	1.432	1.291	1.072	1.055	0.976	0.757
	1.392	1.429	1.288	1.071	1.053	0.973	0.754
	1.398	1.431	1.291	1.072	1.054	0.974	0.752
	1.495	1.510	1.371	1.098	1.069	0.943	0.686
	1.546	1.567	1.395	1.137	1.055	0.918	0.653
	1.408	1.443	1.299	1.080	1.053	0.966	0.741
0.729	1.281	1.422	1.193	0.610	0.953	0.959	0.777
0.731	1.276	1.416	1.190	0.611	0.952	0.957	0.772
0.726	1.282	1.423	1.194	0.608	0.953	0.958	0.770
0.658	1.387	1.494	1.302	0.507	0.997	0.928	0.706
0.772	1.443	1.588	1.318	0.610	0.966	0.921	0.687
0.735	1.297	1.433	1.203	0.611	0.956	0.952	0.762

APPENDIX C

ERRORS IN THE ONE-DIMENSIONAL ANALYSIS

Section C.1. Coupling Errors

Section C.2. Boundary Condition Errors

Section C.3. Polynomial Fitting Coefficients and Errors

Section C.1. Coupling Errors

Table C.1. Errors in the Reconstructed Homogenized Parameters due to Energy Group Coupling.

BWR

Group	Σ_a	$\nu\Sigma_f$	$\Sigma_{s\,1\text{-}2}$	
1	-1.29894e-05	8.08371e-06	1.93972e-05	
2	-1.07541e-04	4.42317e-05		
	Flux Discontinuity Factor		Edge-to-Average Flux Ratio	
Group	Left	Right	Left	Right
1	-1.80422e-03	2.55972e-04	-8.27879e-04	9.97523e-04
2	-2.73056e-02	-6.51913e-03	-2.88513e-03	2.95798e-03

PWR

Group	Σ_a	$\nu\Sigma_f$	$\Sigma_{s\,1\text{-}2}$	
1	-1.87684e-05	-1.01935e-06	3.24281e-05	
2	-1.38040e-04	-2.13392e-05		
	Flux Discontinuity Factor		Edge-to-Average Flux Ratio	
Group	Left	Right	Left	Right
1	-1.76736e-03	1.26516e-03	-1.01760e-03	1.14814e-03
2	-1.50626e-02	7.56252e-03	-2.79936e-03	2.66948e-03

Table C.2. Errors in the Reconstructed Homogenized Parameters due to Node Face Coupling.

		BWR		
Group	Σ_a	$\nu\Sigma_f$	$\Sigma_{s\,1\text{-}2}$	
1	-2.01164e-05	-4.00817e-05	1.67031e-05	
2	-3.35163e-05	-1.02004e-04		
	Flux Discontinuity Factor		Edge-to-Average Flux Ratio	
Group	Left	Right	Left	Right
1	-1.69290e-03	-4.33537e-03	8.57928e-04	-5.15076e-04
2	-7.13450e-03	-7.70431e-03	9.23068e-04	-1.33473e-04

		PWR		
Group	Σ_a	$\nu\Sigma_f$	$\Sigma_{s\,1\text{-}2}$	
1	2.08988e-05	3.93179e-06	-3.49225e-05	
2	2.99248e-05	6.40176e-06		
	Flux Discontinuity Factor		Edge-to-Average Flux Ratio	
Group	Left	Right	Left	Right
1	-7.24879e-04	-4.11275e-03	1.33145e-03	-1.08989e-03
2	-1.34768e-02	-1.33253e-02	6.55796e-04	-3.84721e-04

Section C.2 Boundary Condition Errors

Table C.3. Errors in the Reconstructed Homogenized Parameters due to using Albedo Boundary Conditions to Create the Reference Currents.

BWR			
Group	Σ_a	$\nu\Sigma_f$	$\Sigma_{s\,1\text{-}2}$
1	3.14735e-04	3.52483e-04	-3.25981e-04
2	1.52710e-04	3.99891e-04	
Edge-to-Average Flux Ratio			
Group	Left	Right	
1	-2.37042e-02	1.58470e-02	
2	-1.30799e-02	3.90914e-03	

PWR			
Group	Σ_a	$\nu\Sigma_f$	$\Sigma_{s\,1\text{-}2}$
1	-1.93771e-05	-2.81050e-05	2.36974e-05
2	-4.63351e-05	-2.98749e-05	
Edge-to-Average Flux Ratio			
Group	Left	Right	
1	-1.78681e-02	1.30994e-02	
2	-1.47031e-02	1.06456e-03	

Table C.4. Errors in the Reconstructed Homogenized Parameters due to using Shifted Circle Boundary Conditions to Create the Reference Currents.

BWR			
Group	Σ_a	$\nu\Sigma_f$	$\Sigma_{s\,1\text{-}2}$
1	2.33350e-05	2.47564e-05	-2.47853e-05
2	1.74241e-05	1.62484e-05	
Edge-to-Average Flux Ratio			
Group	Left	Right	
1	1.26522e-04	-1.05072e-03	
2	3.24824e-04	-5.34566e-04	

PWR			
Group	Σ_a	$\nu\Sigma_f$	$\Sigma_{s\,1\text{-}2}$
1	-4.36238e-06	-1.23779e-05	3.11808e-06
2	1.83410e-05	-7.11306e-07	
Edge-to-Average Flux Ratio			
Group	Left	Right	
1	7.03570e-04	-5.12517e-03	
2	1.98285e-04	4.25531e-03	

Section C.3 Polynomial Fitting Coefficients and Errors

Table C.5 Polynomial Coefficients Corresponding to the Group 1 Current-to-Flux Ratio on the Left Boundary of the BWR Geometry.

	a_1	a_2	a_3	a_4
$\Sigma_{a\,1}$	-0.09445	-0.06274	0.09178	-0.07591
$\Sigma_{a\,2}$	0.04681	-0.16036	0.17911	-0.06233
$\nu\Sigma_{f\,1}$	-0.16755	0.02701	-0.00269	-0.02464
$\nu\Sigma_{f\,2}$	-0.14129	0.04588	0.01793	-0.05978
$\Sigma_{s\,1\text{-}2}$	0.08128	0.09057	-0.12304	0.10403
ϕ^-_1/ϕ^{ave}_1	5.90235	-4.24340	4.29856	-2.20409
ϕ^-_2/ϕ^{ave}_2	4.30295	-4.42099	3.44129	0.28235
ϕ^+_1/ϕ^{ave}_1	-2.37479	3.51266	-3.89479	2.39307
ϕ^+_2/ϕ^{ave}_2	-2.30869	3.15384	-2.86095	0.27543

Table C.6 Polynomial Coefficients Corresponding to the Group 1 Current-to-Flux Ratio on the Right Boundary of the BWR Geometry.

	a_1	a_2	a_3	a_4
Σ_{a1}	0.20213	0.11055	0.16516	0.31283
Σ_{a2}	0.19948	0.27124	0.50113	1.02689
$\nu\Sigma_{f1}$	0.16953	0.03094	0.01915	0.02800
$\nu\Sigma_{f2}$	0.12596	0.07179	0.07173	0.11955
Σ_{s1-2}	-0.22407	-0.13886	-0.21451	-0.41611
ϕ^-_1/ϕ^{ave}_1	2.17374	3.62489	6.64266	13.10330
ϕ^-_2/ϕ^{ave}_2	2.52156	4.85309	9.95397	21.23110
ϕ^+_1/ϕ^{ave}_1	-5.03891	-3.73229	-6.32901	-12.35860
ϕ^+_2/ϕ^{ave}_2	-3.06169	-4.43969	-8.48237	-17.68940

Table C.7 Polynomial Coefficients Corresponding to the Group 2 Current-to-Flux Ratio on the Left Boundary of the BWR Geometry.

	a_1	a_2	a_3	a_4
$\Sigma_{a\,1}$	0.00129	-0.00207	-0.00107	0.01073
$\Sigma_{a\,2}$	-0.11769	-0.01303	-0.00148	-0.01484
$\nu\Sigma_{f\,1}$	-0.01068	-0.00351	-0.00123	-0.00560
$\nu\Sigma_{f\,2}$	-0.27239	0.00773	0.00299	-0.07771
$\Sigma_{s\,1\text{-}2}$	-0.00454	0.00174	0.00072	-0.00717
ϕ^{-}_1/ϕ^{ave}_1	0.63201	0.09883	0.01726	0.58075
ϕ^{-}_2/ϕ^{ave}_2	5.23383	-0.45630	-0.07374	2.63801
ϕ^{+}_1/ϕ^{ave}_1	-0.43038	-0.04127	0.00077	-0.48436
ϕ^{+}_2/ϕ^{ave}_2	-1.26198	0.29846	0.04384	-1.05128

Table C.8 Polynomial Coefficients Corresponding to the Group 2 Current-to-Flux Ratio on the Right Boundary of the BWR Geometry.

	a_1	a_2	a_3	a_4
Σ_{a1}	0.01999	-0.00466	0.00146	0.00537
Σ_{a2}	0.22511	0.02296	-0.00067	-0.02152
$\nu\Sigma_{f1}$	0.01102	-0.00388	0.00123	-0.00560
$\nu\Sigma_{f2}$	0.26752	0.00623	-0.00060	-0.05380
Σ_{s1-2}	-0.02369	0.00506	-0.00143	0.00000
ϕ^{-}_1/ϕ^{ave}_1	0.41926	-0.03767	0.00361	0.24780
ϕ^{-}_2/ϕ^{ave}_2	1.38968	0.40051	-0.01051	0.43403
ϕ^{+}_1/ϕ^{ave}_1	-0.53582	0.08913	-0.02285	-0.19066
ϕ^{+}_2/ϕ^{ave}_2	-4.21392	-0.36894	0.00105	0.33633

Table C.9 Polynomial Coefficients Corresponding to the Group 1 Current-to-Flux Ratio on the Left Boundary of the PWR Geometry.

	a_1	a_2	a_3	a_4
Σ_{a1}	0.05994	-0.08535	0.10092	-0.08744
Σ_{a2}	0.13923	-0.18099	0.16243	-0.05824
$\nu\Sigma_{f1}$	0.01603	-0.00414	0.00049	0.00291
$\nu\Sigma_{f2}$	0.02962	-0.02691	0.02090	-0.00950
Σ_{s1-2}	-0.09855	0.14701	-0.17521	0.14497
ϕ^-_1/ϕ^{ave}_1	5.57736	-5.41940	6.09532	-5.20818
ϕ^-_2/ϕ^{ave}_2	4.03685	-3.99446	3.23679	-0.79938
ϕ^+_1/ϕ^{ave}_1	-2.67950	4.39067	-5.47837	4.82635
ϕ^+_2/ϕ^{ave}_2	-2.16470	2.92457	-2.72999	0.99927

Table C.10 Polynomial Coefficients Corresponding to the Group 1 Current-to-Flux Ratio on the Right Boundary of the PWR Geometry.

	a_1	a_2	a_3	a_4
$\Sigma_{a\,1}$	0.03589	0.07538	0.14478	0.28468
$\Sigma_{a\,2}$	0.12285	0.22432	0.46659	0.97719
$\nu\Sigma_{f\,1}$	-0.01670	-0.00437	-0.00223	-0.00097
$\nu\Sigma_{f\,2}$	0.00757	0.02789	0.06127	0.12824
$\Sigma_{s\,1\text{-}2}$	-0.06830	-0.13243	-0.25142	-0.509467
ϕ^{-}_1/ϕ^{ave}_1	2.46218	4.47561	8.66217	17.35940
ϕ^{-}_2/ϕ^{ave}_2	2.41831	4.71250	10.02440	21.63910
ϕ^{+}_1/ϕ^{ave}_1	-4.68053	-4.65013	-8.18431	-16.16090
ϕ^{+}_2/ϕ^{ave}_2	-2.77264	-4.04205	-8.14651	-17.36620

Table C.11 Polynomial Coefficients Corresponding to the Group 2 Current-to-Flux Ratio on the Left Boundary of the PWR Geometry.

	a_1	a_2	a_3	a_4
$\Sigma_{a\,1}$	0.01110	-0.00186	0.00047	-0.00474
$\Sigma_{a\,2}$	0.04226	-0.02014	0.00194	-0.01941
$\nu\Sigma_{f\,1}$	0.00234	0.00012	0.00000	0.00000
$\nu\Sigma_{f\,2}$	0.03450	-0.00351	0.00095	-0.01900
$\Sigma_{s\,1\text{-}2}$	-0.01847	0.00336	-0.00083	0.00000
ϕ^{-}_1/ϕ^{ave}_1	0.86980	-0.10045	0.03489	-0.10709
ϕ^{-}_2/ϕ^{ave}_2	5.76812	-0.50424	0.13000	-1.81824
ϕ^{+}_1/ϕ^{ave}_1	-0.50399	0.10646	-0.02269	-0.01260
ϕ^{+}_2/ϕ^{ave}_2	-1.03322	0.31865	-0.06066	0.11062

Table C.12 Polynomial Coefficients Corresponding to the Group 2 Current-to-Flux Ratio on the Right Boundary of the PWR Geometry.

	a_1	a_2	a_3	a_4
Σ_{a1}	0.00758	0.00187	0.00034	-0.00610
Σ_{a2}	0.05376	0.02165	0.00518	-0.03883
$\nu\Sigma_{f1}$	-0.00243	0.00023	0.00000	0.00194
$\nu\Sigma_{f2}$	-0.02309	0.00211	0.00000	0.00950
Σ_{s1-2}	-0.01405	-0.00314	-0.00041	0.012426
ϕ^-_1/ϕ^{ave}_1	0.48322	0.10409	0.01755	-0.24735
ϕ^-_2/ϕ^{ave}_2	1.14604	0.43717	0.10064	-0.57183
ϕ^+_1/ϕ^{ave}_1	-0.73311	-0.06784	-0.01859	0.36864
ϕ^+_2/ϕ^{ave}_2	-4.57186	-0.43706	-0.08595	2.46048

Table C.13. Errors in Homogenized Parameters found by Reconstructing all terms of the Fourth Order Power Series.

BWR

Group	Σ_a	$\nu\Sigma_f$	$\Sigma_{s\,1\text{-}2}$
1	-1.16664e-05	-1.38155e-06	1.37285e-05
2	-8.85129e-05	-1.71746e-05	

Edge-to-Average Flux Ratio

Group	Left	Right
1	-1.52900e-04	-2.41347e-04
2	-1.29092e-03	1.63480e-03

PWR

Group	Σ_a	$\nu\Sigma_f$	$\Sigma_{s\,1\text{-}2}$
1	-1.41551e-05	-9.60762e-06	1.90031e-05
2	-7.51781e-05	-1.50584e-05	

Edge-to-Average Flux Ratio

Group	Left	Right
1	2.85431e-04	-4.12472e-03
2	-1.61748e-03	6.21004e-03

Table C.14. Errors in Homogenized Parameters found by Reconstructing the Quadratic Terms of the Power Series.

BWR			
Group	Σ_a	$\nu\Sigma_f$	$\Sigma_{s\,1\text{-}2}$
1	-7.54204e-06	-1.38949e-06	8.23123e-06
2	-7.92745e-05	-1.61646e-05	
Edge-to-Average Flux Ratio			
Group	Left	Right	
1	-6.63628e-07	-4.49072e-04	
2	-1.14587e-03	1.45896e-03	

PWR			
Group	Σ_a	$\nu\Sigma_f$	$\Sigma_{s\,1\text{-}2}$
1	-1.17642e-05	-9.61671e-06	1.48224e-05
2	-6.95559e-05	-1.43210e-05	
Edge-to-Average Flux Ratio			
Group	Left	Right	
1	4.07032e-04	-4.28176e-03	
2	-1.51952e-03	6.10596e-03	

Table C.15. Errors in Homogenized Parameters found by Reconstructing the Linear Terms of the Power Series.

BWR

Group	Σ_a	$\nu\Sigma_f$	$\Sigma_{s\,1\text{-}2}$
1	-3.84623e-05	3.69566e-05	5.95128e-05
2	-1.63229e-04	5.84802e-05	

Edge-to-Average Flux Ratio

Group	Left	Right
1	-2.67705e-03	2.57943e-03
2	-3.70425e-03	3.72903e-03

PWR

Group	Σ_a	$\nu\Sigma_f$	$\Sigma_{s\,1\text{-}2}$
1	-3.11143e-05	-1.35146e-05	4.74132e-05
2	-8.76080e-05	-1.93027e-05	

Edge-to-Average Flux Ratio

Group	Left	Right
1	-7.28253e-04	-3.43684e-03
2	-1.93870e-03	6.23906e-03

APPENDIX D

TWO-DIMENSIONAL BWR AND PWR HOMOGENIZED PARAMETERS AND CORRELATION COEFFICIENTS

Section D.1. Infinite Lattice Homogenized Parameters

Table D.1. Infinite Lattice Homogenized Parameters for the BWR Fuel Assembly A. (The most reactive BWR assembly.)

BWR without control blade inserted				
Group	D (cm)	Σ_a (cm^{-1})	$\nu\Sigma_f$ (cm^{-1})	$\Sigma_{s\,1\text{-}2}$ (cm^{-1})
1	1.425735e+00	7.785936e-03	5.419602e-03	1.842649e-02
2	3.906145e-01	7.249943e-02	9.348392e-02	
FDF or Edge-to-Average Flux Ratio				
Group	Left	Right	Top	Bottom
1	0.963055	0.863334	0.863334	0.963055
2	1.265587	1.510890	1.510891	1.265588
BWR with control blade inserted				
Group	D (cm)	Σ_a (cm^{-1})	$\nu\Sigma_f$ (cm^{-1})	$\Sigma_{s\,1\text{-}2}$ (cm^{-1})
1	1.423138e+00	8.067234e-03	5.429393e-03	1.763250e-02
2	4.036315e-01	8.313203e-02	1.006144e-01	
FDF or Edge-to-Average Flux Ratio				
Group	Left	Right	Top	Bottom
1	0.993915	0.843372	0.843372	0.993915
2	1.530324	0.901964	0.901963	1.530323

Table D.2. Infinite Lattice Homogenized Parameters for the BWR Fuel Assembly B.

BWR without control blade inserted				
Group	D (cm)	Σ_a (cm^{-1})	$\nu\Sigma_f$ (cm^{-1})	$\Sigma_{s\,1\text{-}2}$ (cm^{-1})
1	1.424528e+00	7.529099e-03	4.923361e-03	1.862690e-02
2	3.898094e-01	6.755748e-02	8.265275e-02	
FDF or Edge-to-Average Flux Ratio				
Group	Left	Right	Top	Bottom
1	0.955802	0.871155	0.871155	0.955802
2	1.243491	1.450460	1.450458	1.243490
BWR with control blade inserted				
Group	D (cm)	Σ_a (cm^{-1})	$\nu\Sigma_f$ (cm^{-1})	$\Sigma_{s\,1\text{-}2}$ (cm^{-1})
1	1.421805e+00	7.813358e-03	4.930959e-03	1.782263e-02
2	4.020903e-01	7.709636e-02	8.810635e-02	
FDF or Edge-to-Average Flux Ratio				
Group	Left	Right	Top	Bottom
1	0.988646	0.848375	0.848375	0.988646
2	1.496791	0.863472	0.863472	1.496793

Table D.3. Infinite Lattice Homogenized Parameters for the BWR Fuel Assembly C. (The least reactive BWR assembly.)

BWR without control blade inserted				
Group	D (cm)	Σ_a (cm^{-1})	$\nu\Sigma_f$ (cm^{-1})	$\Sigma_{s\,1\text{-}2}$ (cm^{-1})
1	1.423612e+00	7.243206e-03	4.368581e-03	1.883679e-02
2	3.880204e-01	6.140771e-02	6.923273e-02	
		FDF or Edge-to-Average Flux Ratio		
Group	Left	Right	Top	Bottom
1	0.955649	0.868517	0.868517	0.955649
2	1.214204	1.385712	1.385713	1.214205
BWR with control blade inserted				
Group	D (cm)	Σ_a (cm^{-1})	$\nu\Sigma_f$ (cm^{-1})	$\Sigma_{s\,1\text{-}2}$ (cm^{-1})
1	1.420907e+00	7.525873e-03	4.375117e-03	1.803560e-02
2	3.996334e-01	7.013191e-02	7.360122e-02	
		FDF or Edge-to-Average Flux Ratio		
Group	Left	Right	Top	Bottom
1	0.988621	0.845818	0.845818	0.988621
2	1.458176	0.822314	0.822314	1.458178

Table D.4. Infinite Lattice Homogenized Parameters for the PWR Fuel Assembly D. (The most reactive PWR assembly.)

PWR without control rod cluster inserted				
Group	D (cm)	Σ_a (cm^{-1})	$\nu\Sigma_f$ (cm^{-1})	$\Sigma_{s\,1\text{-}2}$ (cm^{-1})
1	1.364194e+00	9.326510e-03	6.675741e-03	1.710559e-02
2	4.232055e-01	9.302914e-02	1.341296e-01	
FDF or Edge-to-Average Flux Ratio				
Group	Left	Right	Top	Bottom
1	1.010410	1.010410	1.010410	1.010410
2	0.913214	0.913214	0.913214	0.913214
PWR with control rod cluster inserted				
Group	D (cm)	Σ_a (cm^{-1})	$\nu\Sigma_f$ (cm^{-1})	$\Sigma_{s\,1\text{-}2}$ (cm^{-1})
1	1.363953e+00	9.628238e-03	6.675666e-03	1.635417e-02
2	4.303007e-01	1.019187e-01	1.359635e-01	
FDF or Edge-to-Average Flux Ratio				
Group	Left	Right	Top	Bottom
1	1.015190	1.015190	1.015190	1.015190
2	0.982730	0.982730	0.982730	0.982730

Table D.5. Infinite Lattice Homogenized Parameters for the PWR Fuel Assembly E.

PWR without control rod cluster inserted				
Group	D (cm)	Σ_a (cm^{-1})	$\nu\Sigma_f$ (cm^{-1})	$\Sigma_{s\,1\to2}$ (cm^{-1})
1	1.362365e+00	8.989660e-03	6.018026e-03	1.735948e-02
2	4.198997e-01	8.418949e-02	1.148353e-01	
FDF or Edge-to-Average Flux Ratio				
Group	Left	Right	Top	Bottom
1	1.011197	1.011197	1.011197	1.011197
2	0.921738	0.921738	0.921738	0.921738

Table D.6. Infinite Lattice Homogenized Parameters for the PWR Fuel Assembly F. (The least reactive PWR assembly.)

PWR without control rod cluster inserted				
Group	D (cm)	Σ_a (cm^{-1})	$\nu\Sigma_f$ (cm^{-1})	$\Sigma_{s\,1\to2}$ (cm^{-1})
1	1.361445e+00	8.635555e-03	5.336659e-03	1.762240e-02
2	4.156903e-01	7.500172e-02	9.483869e-02	
FDF or Edge-to-Average Flux Ratio				
Group	Left	Right	Top	Bottom
1	1.012120	1.012120	1.012120	1.012120
2	0.930995	0.930995	0.930995	0.930995

Section D.2. Correlation Coefficients

Table D.7. Correlation Coefficients for the BWR Fuel Assembly A without the Control Blade Inserted.

	J/ϕ^{ave} Effecting the Homogenized Parameter (Boundary and Energy Group)			
	Left 1	Left 2	Top 1	Top 2
	Effected cross section			
Σ_{a1}	-1.08757e-01	8.55787e-04	-2.97352e-01	-2.37569e-02
Σ_{a2}	8.42863e-03	-8.83636e-02	-2.20147e-01	-2.67252e-01
$\nu\Sigma_{f1}$	-1.16166e-01	3.26010e-03	-3.55861e-01	-2.97093e-02
$\nu\Sigma_{f2}$	3.66247e-02	-1.19639e-01	-3.88471e-01	-4.71800e-01
Σ_{s1-2}	2.93738e-02	-8.72185e-03	2.28002e-01	1.88116e-02
Effected Edge-to-Average Flux Ratio (Boundary and Energy Group)				
Left 1	4.80559e+00	7.14579e-01	9.37352e-02	1.12721e-02
Left 2	3.11744e+00	5.59555e+00	-1.43426e-01	-1.73562e-01
Right 1	-1.98108e+00	-5.12519e-01	3.09848e-01	-2.29484e-02
Right 2	-1.87836e+00	-1.42732e+00	2.31551e-02	-2.69872e-01
Top 1	3.63936e-01	1.36465e-02	5.85365e+00	5.89987e-01
Top 2	1.88219e-01	-1.74023e-01	3.62447e+00	5.27790e+00
Bottom 1	6.86386e-02	-1.10078e-02	-2.40292e+00	-4.53316e-01
Bottom 2	-2.54366e-02	-1.07328e-01	-2.70685e+00	-1.63738e+00

Table D.8. Correlation Coefficients for the BWR Fuel Assembly A with the Control Blade Inserted.

	J/ϕ^{ave} Effecting the Homogenized Parameter (Boundary and Energy Group)			
	Left 1	Left 2	Top 1	Top 2
	Effected cross section			
Σ_{a1}	-1.55604e-01	-1.08532e-02	-1.71059e-01	-7.31090e-03
Σ_{a2}	-1.67860e-01	-2.25186e-01	9.63735e-02	9.58112e-02
$\nu\Sigma_{f1}$	-1.30936e-01	-7.18495e-04	-3.55661e-01	-1.73806e-02
$\nu\Sigma_{f2}$	-8.07943e-02	-2.00611e-01	-2.13790e-01	-2.82532e-01
Σ_{s1-2}	9.22175e-02	5.92557e-03	8.62978e-02	3.11844e-03
Effected Edge-to-Average Flux Ratio (Boundary and Energy Group)				
Left 1	4.53430e+00	5.84044e-01	-1.16961e-02	4.66340e-02
Left 2	2.69726e+00	4.41479e+00	1.35414e-01	9.81317e-02
Right 1	-1.88690e+00	-4.27988e-01	4.78463e-01	-4.55870e-02
Right 2	-2.06945e+00	-1.39982e+00	-3.70529e-01	-3.34421e-01
Top 1	5.54477e-01	5.17565e-02	5.73997e+00	3.70218e-01
Top 2	1.01009e+00	3.98560e-01	3.64876e+00	5.37215e+00
Bottom 1	-9.52913e-02	-4.65017e-02	-2.13367e+00	-2.67344e-01
Bottom 2	-3.69942e-01	-3.18656e-01	-1.97798e+00	-9.24231e-01

Table D.9. Correlation Coefficients for the BWR Fuel Assembly B without the Control Blade Inserted.

	J/ϕ^{**} Effecting the Homogenized Parameter (Boundary and Energy Group)			
	Left 1	Left 2	Top 1	Top 2
	Effected cross section			
Σ_{a1}	-1.10109e-01	1.00671e-03	-2.75749e-01	-2.46229e-02
Σ_{a2}	-9.30016e-03	-1.01621e-01	-1.49686e-01	-2.26036e-01
$\nu\Sigma_{f1}$	-1.26860e-01	1.05915e-03	-3.16216e-01	-2.82279e-02
$\nu\Sigma_{f2}$	8.28639e-03	-1.45865e-01	-2.81021e-01	-4.24078e-01
Σ_{s1-2}	2.67541e-02	-9.63754e-03	2.08841e-01	1.97294e-02
Effected Edge-to-Average Flux Ratio (Boundary and Energy Group)				
Left 1	4.85963e+00	7.55514e-01	1.03818e-01	-6.22768e-04
Left 2	3.06499e+00	5.81576e+00	-8.05305e-02	-1.47861e-01
Right 1	-1.99450e+00	-5.43909e-01	3.04998e-01	-3.70688e-03
Right 2	-1.89521e+00	-1.52806e+00	1.78834e-02	-2.55071e-01
Top 1	3.12959e-01	-1.83499e-03	5.43237e+00	6.19646e-01
Top 2	1.60379e-01	-1.81465e-01	3.13729e+00	5.34459e+00
Bottom 1	1.06476e-01	-2.80237e-04	-2.07036e+00	-4.79029e-01
Bottom 2	-8.21574e-03	-1.03279e-01	-2.20756e+00	-1.60520e+00

Table D.10. Correlation Coefficients for the BWR Fuel Assembly B with the Control Blade Inserted.

	J/ϕ^{ave} Effecting the Homogenized Parameter (Boundary and Energy Group)			
	Left 1	Left 2	Top 1	Top 2
	Effected cross section			
Σ_{a1}	-1.59652e-01	-1.21782e-02	-1.58381e-01	-6.66829e-03
Σ_{a2}	-1.77786e-01	-2.40452e-01	1.40663e-01	1.34091e-01
$\nu\Sigma_{f1}$	-1.40136e-01	-2.52070e-03	-3.37866e-01	-1.65250e-02
$\nu\Sigma_{f2}$	-9.48347e-02	-2.19531e-01	-1.71181e-01	-2.70480e-01
Σ_{a1-2}	9.11702e-02	6.31049e-03	7.92786e-02	2.73571e-03
Effected Edge-to-Average Flux Ratio (Boundary and Energy Group)				
Left 1	4.56772e+00	6.18300e-01	-2.08520e-03	4.24002e-02
Left 2	2.64683e+00	4.60821e+00	1.80528e-01	1.21772e-01
Right 1	-1.89412e+00	-4.55605e-01	4.76336e-01	-3.69565e-02
Right 2	-2.06427e+00	-1.49411e+00	-4.19471e-01	-3.46080e-01
Top 1	5.17903e-01	4.40518e-02	5.95336e+00	3.86650e-01
Top 2	9.90963e-01	4.39334e-01	3.83413e+00	5.68549e+00
Bottom 1	-6.93890e-02	-4.23893e-02	-2.36089e+00	-2.82463e-01
Bottom 2	-3.53142e-01	-3.27053e-01	-2.10750e+00	-9.71102e-01

Table D.11. Correlation Coefficients for the BWR Fuel Assembly C without the Control Blade Inserted.

	J/ϕ^{ave} Effecting the Homogenized Parameter (Boundary and Energy Group)			
	Left 1	Left 2	Top 1	Top 2
	Effected cross section			
Σ_{a1}	-1.10955e-01	1.31497e-03	-2.83504e-01	-2.57649e-02
Σ_{a2}	-1.12466e-02	-1.00751e-01	-1.38513e-01	-2.17977e-01
$\nu\Sigma_{f1}$	-1.28597e-01	1.41951e-03	-3.26986e-01	-2.97000e-02
$\nu\Sigma_{f2}$	6.36280e-03	-1.50975e-01	-2.86224e-01	-4.47727e-01
Σ_{s1-2}	2.60508e-02	-1.02219e-02	2.11201e-01	2.03528e-02
	Effected Edge-to-Average Flux Ratio (Boundary and Energy Group)			
Left 1	4.84597e+00	8.00628e-01	9.77686e-02	-9.32130e-04
Left 2	2.96433e+00	6.10437e+00	-8.37793e-02	-1.46023e-01
Right 1	-1.97048e+00	-5.81445e-01	3.21763e-01	-3.17555e-03
Right 2	-1.86268e+00	-1.64542e+00	3.90988e-02	-2.51646e-01
Top 1	3.22176e-01	-1.19132e-03	5.72395e+00	6.63063e-01
Top 2	1.61662e-01	-1.78437e-01	3.42597e+00	5.88990e+00
Bottom 1	1.05988e-01	-6.30980e-04	-2.32255e+00	-5.17160e-01
Bottom 2	-1.17109e-02	-1.02089e-01	-2.46621e+00	-1.78015e+00

Table D.12. Correlation Coefficients for the BWR Fuel Assembly C with the Control Blade Inserted.

	J/ϕ^{ave} Effecting the Homogenized Parameter (Boundary and Energy Group)			
	Left 1	Left 2	Top 1	Top 2
	Effected cross section			
Σ_{a1}	-1.63817e-01	-1.28786e-02	-1.50316e-01	-6.51104e-03
Σ_{a2}	-1.91541e-01	-2.52390e-01	1.47852e-01	1.70663e-01
$\nu\Sigma_{f1}$	-1.39412e-01	-2.18640e-03	-3.28342e-01	-1.71949e-02
$\nu\Sigma_{f2}$	-9.26842e-02	-2.27182e-01	-1.54664e-01	-2.67946e-01
$\Sigma_{s1\to2}$	9.02151e-02	6.39879e-03	7.41560e-02	2.60058e-03
Effected Edge-to-Average Flux Ratio (Boundary and Energy Group)				
Left 1	4.80964e+00	6.51184e-01	-8.50719e-03	4.47398e-02
Left 2	2.83359e+00	4.88080e+00	1.57645e-01	1.36598e-01
Right 1	-2.11226e+00	-4.86653e-01	4.85361e-01	-3.88936e-02
Right 2	-2.31235e+00	-1.64409e+00	-3.43236e-01	-3.42193e-01
Top 1	5.70108e-01	4.84446e-02	5.67083e+00	4.05644e-01
Top 2	1.09834e+00	5.09118e-01	3.51564e+00	5.88516e+00
Bottom 1	-1.07661e-01	-4.63285e-02	-2.10313e+00	-2.96692e-01
Bottom 2	-4.04043e-01	-3.46350e-01	-1.85592e+00	-9.88262e-01

Table D.13. Correlation Coefficients for the PWR Fuel Assembly D without the Control Rod Cluster Inserted.

	J/ϕ^{ave} Effecting the Homogenized Parameter (Boundary and Energy Group)	
	Left 1	Left 2
	Effected cross section	
Σ_{a1}	1.95973e-02	3.50736e-03
Σ_{a2}	1.02145e-02	2.35306e-02
$\nu\Sigma_{f1}$	2.20165e-02	3.94226e-03
$\nu\Sigma_{f2}$	1.58419e-02	3.65152e-02
Σ_{a1-2}	-1.96876e-02	-3.51366e-03
Effected Edge-to-Average Flux Ratio (Boundary and Energy Group)		
Left 1	6.81531e+00	1.35069e+00
Left 2	4.93461e+00	6.31864e+00
Right 1	-3.22142e+00	-7.90438e-01
Right 2	-3.02291e+00	-1.20513e+00
Top 1	-1.36733e-02	-1.13905e-03
Top 2	8.35435e-03	3.82427e-02
Bottom 1	-1.35948e-02	-9.11243e-04
Bottom 2	8.47373e-03	3.85116e-02

Table D.14. Correlation Coefficients for the PWR Fuel Assembly D with the Control Rod Cluster Inserted.

	J/ϕ^{ave} Effecting the Homogenized Parameter (Boundary and Energy Group)	
	Left 1	Left 2
	Effected cross section	
Σ_{a1}	1.35801e-02	2.31633e-03
Σ_{a2}	2.00956e-03	-4.81990e-05
$\nu\Sigma_{f1}$	2.15350e-02	3.64252e-03
$\nu\Sigma_{f2}$	1.58970e-02	3.15991e-02
Σ_{s1-2}	-1.29299e-02	-2.20775e-03
	Effected Edge-to-Average Flux Ratio (Boundary and Energy Group)	
Left 1	6.86038e+00	1.24913e+00
Left 2	5.07806e+00	5.83164e+00
Right 1	-3.29699e+00	-7.32380e-01
Right 2	-3.12397e+00	-1.13688e+00
Top 1	-2.09688e-02	1.76619e-03
Top 2	2.13577e-02	2.54384e-02
Bottom 1	-2.09688e-02	1.76619e-03
Bottom 2	2.13577e-02	2.54384e-02

Table D.15. Correlation Coefficients for the PWR Fuel Assembly E without the Control Rod Cluster Inserted.

	J/ϕ^{ave} Effecting the Homogenized Parameter (Boundary and Energy Group)	
	Left 1	Left 2
	Effected cross section	
Σ_{a1}	1.94006e-02	3.74954e-03
Σ_{a2}	9.16032e-03	2.30376e-02
$\nu\Sigma_{f1}$	2.18969e-02	4.22842e-03
$\nu\Sigma_{f2}$	1.50999e-02	3.79686e-02
Σ_{s1-2}	-1.89775e-02	-3.66032e-03
	Effected Edge-to-Average Flux Ratio (Boundary and Energy Group)	
Left 1	6.80452e+00	1.47654e+00
Left 2	4.85324e+00	6.62846e+00
Right 1	-3.22305e+00	-8.73821e-01
Right 2	-3.00927e+00	-1.33125e+00
Top 1	-1.52450e-02	-1.43629e-03
Top 2	6.03175e-03	3.72158e-02
Bottom 1	-1.50588e-02	-1.07722e-03
Bottom 2	6.28130e-03	3.76852e-02

Table D.16. Correlation Coefficients for the PWR Fuel Assembly F without the Control Rod Cluster Inserted.

	J/ϕ^{avg} Effecting the Homogenized Parameter (Boundary and Energy Group)	
	Left 1	Left 2
	Effected cross section	
Σ_{a1}	1.91797e-02	4.02982e-03
Σ_{a2}	7.96073e-03	2.21616e-02
$\nu\Sigma_{f1}$	2.17609e-02	4.56948e-03
$\nu\Sigma_{f2}$	1.42464e-02	3.96635e-02
Σ_{s1-2}	-1.82487e-02	-3.82752e-03
	Effected Edge-to-Average Flux Ratio (Boundary and Energy Group)	
Left 1	6.79144e+00	1.62973e+00
Left 2	4.75633e+00	7.00487e+00
Right 1	-3.22480e+00	-9.77200e-01
Right 2	-2.99127e+00	-1.48906e+00
Top 1	-1.71088e-02	-1.90407e-03
Top 2	3.56291e-03	3.58585e-02
Bottom 1	-1.67755e-02	-1.24497e-03
Bottom 2	4.03152e-03	3.66944e-02

Table D.17. Correlation Coefficients for the BWR Fuel Assembly B with the Control Blade Inserted and the Fuel Temperature Increased.

	J/ϕ^{ave} Effecting the Homogenized Parameter (Boundary and Energy Group)			
	Left 1	Left 2	Top 1	Top 2
	Effected cross section			
Σ_{a1}	-1.59167e-01	-1.19594e-02	-1.62351e-01	-6.88622e-03
Σ_{a2}	-1.78316e-01	-2.40294e-01	1.41356e-01	1.34441e-01
$\nu\Sigma_{f1}$	-1.40039e-01	-2.49312e-03	-3.37843e-01	-1.65441e-02
$\nu\Sigma_{f2}$	-9.47569e-02	-2.18640e-01	-1.71772e-01	-2.70070e-01
Σ_{s1-2}	9.26919e-02	6.37985e-03	8.20562e-02	2.86813e-03
Effected Edge-to-Average Flux Ratio (Boundary and Energy Group)				
Left 1	4.56868e+00	6.19451e-01	-2.17617e-03	4.24558e-02
Left 2	2.65020e+00	4.59756e+00	1.80632e-01	1.20148e-01
Right 1	-1.89632e+00	-4.56745e-01	4.75730e-01	-3.71098e-02
Right 2	-2.06878e+00	-1.49549e+00	-4.22182e-01	-3.47964e-01
Top 1	5.18333e-01	4.41710e-02	5.95502e+00	3.87537e-01
Top 2	9.92134e-01	4.35716e-01	3.83937e+00	5.66853e+00
Bottom 1	-7.04395e-02	-4.26879e-02	-2.36242e+00	-2.83177e-01
Bottom 2	-3.55457e-01	-3.29345e-01	-2.11152e+00	-9.71918e-01

Table D.18. Correlation Coefficients for the BWR Fuel Assembly B with the Control Blade Inserted and 40% Water Void.

	J/ϕ^{ave} Effecting the Homogenized Parameter (Boundary and Energy Group)			
	Left 1	Left 2	Top 1	Top 2
	Effected cross section			
Σ_{a1}	-1.39489e-01	-6.13984e-03	-1.30793e-01	-3.14052e-03
Σ_{a2}	-1.56548e-01	-2.36947e-01	1.38617e-01	1.33462e-01
$\nu\Sigma_{f1}$	-1.15245e-01	3.20623e-04	-2.81611e-01	-8.90055e-03
$\nu\Sigma_{f2}$	-4.53713e-02	-1.45989e-01	-1.24800e-01	-2.14402e-01
Σ_{s1-2}	7.19988e-02	1.26890e-03	1.20412e-01	3.44420e-03
Effected Edge-to-Average Flux Ratio (Boundary and Energy Group)				
Left 1	3.61938e+00	3.29424e-01	3.11061e-02	2.78298e-02
Left 2	1.93780e+00	3.54716e+00	1.21561e-01	1.02221e-01
Right 1	-1.54059e+00	-2.43181e-01	3.69176e-01	-2.50705e-02
Right 2	-1.60648e+00	-1.34160e+00	-2.54883e-01	-3.41277e-01
Top 1	4.22583e-01	1.90082e-02	4.45380e+00	2.08407e-01
Top 2	6.26034e-01	2.58863e-01	2.65030e+00	4.32716e+00
Bottom 1	-2.17901e-02	-1.94735e-02	-1.89672e+00	-1.66445e-01
Bottom 2	-2.63927e-01	-2.77391e-01	-1.61680e+00	-9.29075e-01

Table D.19. Correlation Coefficients for the BWR Fuel Assembly B with the Control Blade Inserted and a Linear Gradient for the Fuel Cross Sections.

	J/ϕ^{ave} Effecting the Homogenized Parameter (Boundary and Energy Group)			
	Left 1	Left 2	Top 1	Top 2
	Effected cross section			
Σ_{a1}	-8.13728e-02	6.30496e-03	-1.66744e-01	-5.80100e-03
Σ_{a2}	-1.09044e-01	-1.84586e-01	1.29999e-01	1.33111e-01
$\nu\Sigma_{f1}$	-5.80471e-01	1.67441e-02	-3.38304e-01	-1.55679e-02
$\nu\Sigma_{f2}$	-1.74796e-02	-1.55470e-01	-1.69141e-01	-2.64482e-01
Σ_{s1-2}	9.14660e-02	6.71024e-03	7.90999e-02	2.96814e-03
	Effected Edge-to-Average Flux Ratio (Boundary and Energy Group)			
Left 1	4.49116e+00	6.13736e-01	-5.58387e-02	4.03997e-02
Left 2	2.69929e+00	4.69651e+00	1.27426e-01	1.23620e-01
Right 1	-1.85303e+00	-4.46654e-01	5.30033e-01	-3.46115e-02
Right 2	-1.96320e+00	-1.42073e+00	-3.25423e-01	-3.34942e-01
Top 1	5.16860e-01	4.49617e-02	5.68784e+00	3.91735e-01
Top 2	1.01562e+00	4.55838e-01	3.61040e+00	5.65058e+00
Bottom 1	-6.76669e-02	-4.20949e-02	-2.12676e+00	-2.84887e-01
Bottom 2	-3.30645e-01	-3.08014e-01	-1.91835e+00	-9.49860e-01

LIST OF REFERENCES

1. Smith, K. S. (1979). An analytic nodal method for solving the two-group, multidimensional, static and transient neutron diffusion equations. Engineers Thesis, Department of Nuclear Engineering, M.I.T., Cambridge, MA, March.

2. Lawrence, R. D. (1981). A nodal interface current method for multigroup calculations in hexagonal geometry. *Trans. Am. Nucl. Soc.*, Vol. **39**, p. 461.

3. Lawrence, R. D. & Dorning, J. J. (1980). A nodal Green's function method for multidimensional neutron diffusion calculations. *Nuclear Science and Engineering*, Vol. **76**, p. 218.

4. Smith, K. S., Ver Planck, D. M. & Edenius, M. (1985). QPANDA: An advanced nodal method for LWR analyses. *Trans. Am. Nucl. Soc.*, Vol. **50**, p. 532.

5. Lawrence, R. D. (1986). Progress in nodal methods for the solution of the neutron diffusion and transport equations. *Progress in Nuclear Energy*, Vol. **17**, p. 271.

6. Delp, D. L., Fisher, D. L., Harriman, J. M. & Stedwell, M. J. (1964). FLARE, A three-dimensional boiling water reactor simulator. GEAP-4598, General Electric Company.

7. Henry, A. F. (1975). Nuclear-Reactor Analysis. The MIT Press, Cambridge, MA.

8. Koebke, K. (1981). Advances in homogenization and dehomogenization. *International Topical Meeting on Advances in Mathematical Methods for the Solution of Nuclear Engineering Problems*, Vol. **2**, p. 59, Munich, April 27-29.

9. Wagner, M. R. & Koebke, K. (1983). Progress in nodal reactor analysis. *A Topical Meeting on Advances in Reactor Computations*, Vol **2**, p. 941, Salt Lake City, March 28-31.

10. Smith, K. S. (1980). Spatial homogenization methods for light water reactor analysis. PhD Thesis, Department of Nuclear Engineering, M.I.T., Cambridge, MA., June.

11. Smith, K. S. (1986). Assembly homogenization techniques for light water reactor analysis. *Progress in Nuclear Energy*, Vol. **17**, p. 303.

12. Koebke, K. & Hetzelt, L. (1985). On the reconstruction of local homogenous neutron flux and current distributions of light water reactors from nodal schemes. *Nuclear Science and Engineering*, Vol. **91**, p. 123.

13. Smith, K. S. & Rempe, K. R. (1988). Testing and applications of the QPANDA nodal model. *Nuclear Science and Engineering*, Vol. **100**, p. 324.

14. Rempe, K. R., Smith, K. S. & Henry, A. F. (1989). SIMULATE-3 pin power reconstruction: Methodology and benchmarking. *Nuclear Science and Engineering*, Vol. **103**, p. 334.

15. Smith, K. S., Henry, A. F. & Loretz, R. A. (1980). The determination of homogenized diffusion theory parameters for coarse mesh nodal analysis. *Proceedings of the Conference on Advances in Reactor Physics and Shielding*, p. 294, Sun Valley, September 14-19.

16. Davis, H. F. & Snider, A. D. (1988). Introduction to Vector Analysis. Wm. C. Brown Publishers, Dubuque, IA.

17. Cheng, A. Y., Hoxie, C. L. & Henry, A. F. (1981). A method for determining equivalent homogenized parameters. *International Topical Meeting on Advances in Mathematical Methods for the Solution of Nuclear Engineering Problems*, Vol. **2**. p. 3. Munich, April 27-29.

18. Smith, K. S., Rempe, K. R., Rhodes, J. D. & Stevens, J. G. (1992). Enhancements of the Studsvik Core Management System (CMS). *Topical Meeting on Advances in Reactor Physics*, Vol. **1**, p. 117, Charleston, March 8-11.

19. Hughes, R. P. (1978). A unified derivation of the various definitons of lattice cell diffusion coefficients. *Nuclear Science and Engineering*, Vol. **67**, p. 85.

20. Stamm'ler, R. J. J. & Abbate, M. J. (1983). Methods of Steady-State Reactor Physics in Nuclear Design. Academic Press, London, Great Britain.

21. Rahnema, F. (1989). Boundary condition perturbation theory for use in spatial homogenization methods. *Nuclear Science and Engineering*, Vol. **102**, p. 183.

22. Rahnema, F. (1990). Influence of flux gradients on local and global reactivities in BWR's. *International Conference on the Physics of Reactors: Operation, Design, and Computation*, Vol. **8**, p. 47, Marseille, April 23-27.

23. Halsall, M. J. (1993). Neutron transport in WIMS by the characteristics method. *Trans. Am. Nucl. Soc.*, Vol. **68**, p. 454.

24. Knott, D. & Edenius, M. (1993). The two-dimensional transport solution within CASMO-4. *Trans. Am. Nucl. Soc.*, Vol. **68**, p. 457.

25. Jonsson, A. & Loretz, R. A. (1993). Integral transport theory methods in the DIT code. *Trans. Am. Nucl. Soc.*, Vol. **68**, p. 461.

26. Grimesey, R. A., Nigg, D. W. & Curtis, R. L. (1990). COMBINE/PC - A portable ENDF/B Version 5 neutron spectrum and cross-section generation program. (EGG-2589), Idaho National Engineering Laboratory.

27. Nigg, D. W., Grimesey, R. A. & Curtis, R. L. (1990). COMBINE/PC - A portable neutron spectrum and cross-section generation program. *Trans. Am. Nucl. Soc.*, Vol. **61**, p. 19.

28. Larsen, E. W. & Miller, W. F., Jr. (1986). A two-step acceleration method for transport problems. *Trans. Am. Nucl. Soc.*, Vol. **52**, p. 416.

29. Ames, W. F. (1977). Numerical Methods for Partial Differential Equations. Academic Press, Inc., Orlando, FL.

30. Press, W. H., Teukolsky, S. A., Vetterling, W. T. & Flannery, B. P. (1992). Numerical Recipes in FORTRAN: The Art of Scientific Computing. Cambridge University Press, New York, NY.

31. Argonne Code Center: Benchmark Problem Book (1977). ANL-7416. Suppl. 2, Argonne National Laboratory.

32. Zolotar, B. A. & Nero, R. A. (1976). BWR rod bundle benchmark problem. *Trans. Am. Nucl. Soc.*, Vol. **23**, p. 214.

33. Dodds, H. L. Jr. (1977). Computational benchmark problems - A review of recent work within the American Nuclear Society Mathematics and Computation Division. *Nuclear Science and Engineering*, Vol. **64**, p. 64.

34. Parsons, K. D., (1988). ANISN/PC, Multigroup one-dimensional discrete ordinates transport code system with anisotropic scattering (CCC-514), Oak Ridge National Laboratory.

35. Rhoades, W. A., & Childs, R. L., (1982). An updated version of the DOT 4 one- and two-dimensional neutron/photon transport code (CCC-532), Oak Ridge National Laboratory.

36. Alcouffe, R. E., Brinkley, F. W., Marr, D. R., & ODell, R. D., (1992). TWODANT-SYS: One- and two-dimensional, multigroup, discrete-ordinates transport code system (CCC-547), Oak Ridge National Laboratory.

37. Bell, G. I., & Glasstone, S., (1985). Nuclear Reactor Theory. Robert E. Krieger Publishing Company, Malabar, FL..